NORTHWESTERN UNIVERSITY

Continental Rifting and Precambrian Tectonics:

Insights from Gravity Modeling and Apparent Polar Wander Paths

A DISSERTATION

SUBMITTED TO THE GRADUATE SCHOOL

IN PARTIAL FULFILLMENT OF THE REQUIREMENTS

for the degree

DOCTOR OF PHILOSOPHY

Field of Earth and Planetary Sciences

By

Reece Phillip Elling

EVANSTON, ILLINOIS

June 2022

ABSTRACT

Continental Rifting and Precambrian Tectonics:

Insights from Gravity Modeling and Apparent Polar Wander Paths

Reece Phillip Elling

Failed continental rifts provide unique opportunities to study aspects of plate tectonic evolution frozen in time. North America contains three major failed rifts: The Midcontinent Rift (MCR), Southern Oklahoma Aulacogen (SOA), and the Reelfoot Rift (RR). To understand why some rifts fail and why others might succeed to seafloor spreading, this thesis explores details of these rifts and their interactions within the framework of Laurentia's tectonic history.

First, in Chapter 2, I explored aspects of the ~1100 Ma MCR. Although it is exposed along Lake Superior, it is primarily delineated by gravity, magnetic, and seismic data through the central United States. Its structures and evolution, defined by gravity modeling, seismic, and geologic data, tell a story of a sequence of extension, volcanism, subsidence, sedimentation, and subsequent inversion. Near the MCR's eastern arm also lie orogenic facies related to the Grenville Orogeny, a series of discrete collisions between Laurentia and Amazonia that culminated in the assembly of the supercontinent of Rodinia. I examined the interaction of these juxtaposing tectonic events using their gravity signatures and determined that the lineated gravity highs in the eastern U.S. appear similar to those along the remainder of the MCR, and unlike those along any portion of the Grenville Front (GF) where it is exposed and identified by seismic and potential field data in

Canada. However, thrust sheet structures, like those of the southern Canadian GF, are likely present along the MCR's east arm, as implied by recent seismic data.

Next, in Chapter 3, I investigated the similarities and differences of North America's three major failed rifts – the MCR, SOA, and RR – to gain insight into the rifting process. All three rifts formed in similar tectonic settings as part of Laurentia's interactions within Rodinia, and followed similar evolutionary paths of extension, magmatism, subsidence, and inversion by later compression, leading to similar widths and architecture. However, differences between the rifts reflect the extent to which these processes occurred.

Because no sea floor older than a few hundred million years exists, understanding the tectonics of the Precambrian requires the use of paleomagnetic data to constrain plate motions and model global tectonics. Part of this research, described in Chapters 4 and 5, involved consistent collection and compilation of over 15,000 published paleomagnetic poles to support global plate modeling efforts. The compilation supported a 1.5 Ga plate model that I used to create apparent polar wander (APW) paths for Laurentia, Amazonia, and eleven other major plates. Because cusps in APW paths have long been proposed to be caused by continental rifts or major collisional orogenies, I analyzed this hypothesis by determining the timing of directional changes in the motion of each plate and correlating them to the timing of major tectonic events. Preliminary investigations show promising statistical correlations between the two. This approach can be useful in defining tectonic events in time periods during which paleomagnetic data may be the only constraints.

Acknowledgements

Many people in my life deserve acknowledgement for the roles they've played in supporting my journey to becoming the person and researcher I am today. First and foremost, I would like to thank my graduate committee: Seth Stein, Christopher Scotese, and Donna Jurdy. Their constant guidance, encouragement, and trust in me during my time at Northwestern has been so important in allowing me to explore research opportunities and ask scientific questions. Specifically, I thank Seth Stein for his unshakeable support and patience as I learned how to navigate the academic world, and for always encouraging me to think about the bigger picture. His passion for adventure and the outdoors filled my time at Northwestern with exciting discussions and experiences (like completing the Des Plaines River Kayak marathon together). Additionally, I owe many thanks to Christopher Scotese, who fostered my interest in paleomagnetic data and plate modeling. His willingness to share his expertise and savvy in global tectonic modeling allowed me to participate some amazing projects and even travel across the world to share and present them. I'm grateful for his friendship through the years. To have been a part of a committee who never stopped asking questions, broadening their scientific horizons, and supporting and advocating on behalf of myself and other students, I consider myself truly fortunate.

It wouldn't feel complete to thank my committee and not acknowledge the massive role that Carol Stein played in advising me as well. Her kindness and patience in our myriad of conversations throughout my projects were pivotal in getting to this point. She constantly probed the boundaries of our research projects to find new and exciting questions to be asked, and I'm grateful for her guidance and generosity as a de facto committee member.

I would also like to thank two important mentors that introduced and fostered my passion for geology early in my career: Chris Bolhuis and John Weber. Chris Bolhuis is a high school earth science teacher in West Michigan who leads an annual geology field camp in the western U.S. that I was lucky enough to join in 2012. It was my first experience with geology and exploring scientific questions out in the field. His enthusiasm for the outdoors, geology, and encouraging students to wonder about and explore nature sparked my interest in the forces and features that formed our planet. Furthermore, he introduced me to John Weber at Grand Valley State University, who taught me how to do research and was my undergraduate advisor. He found interesting ways to challenge me in my undergraduate classes and allowed me to join in exciting research that we did together in Trinidad. John also encouraged me to consider graduate school as a possibility, and introduced me to Seth Stein, which sparked the relationship that has gotten me to this point today. I'm forever grateful for these teachers who truly care about their students and chose to mentor and encourage my curiosity when I was still learning how to apply it in my life.

Thanks also to John Mariano for offering me the opportunity to intern with the Geophysical Applications team at ExxonMobil, an experience that drastically shaped my outlook on utilizing my graduate research in industry applications. I'm grateful for the mentorship and guidance you provided during that incredible experience.

I would like to thank several additional people from the Department of Earth and Planetary Sciences at Northwestern, whose help should be acknowledged. Thank you to the more senior graduate students who helped me prepare for and overcome my qualifying exams, in particular Amir Salaree and Eddie Brooks. I'm also pleased to have been in a research group with Leah Salditch, Boris Rösler, Molly Galahue, and Jamie Neely, and thank them for their friendship and

comradery. Thanks also to Trish Beddows for her advice and encouragement as I explored other aspects of academia, such as expeditions to the Yucatan Peninsula, or restoring a climate monitoring station on campus. I'd also like to thank Matt Hurtgen, whose guidance as department chair and mentor through uncertain and difficult situations kept me and other students feeling supported and heard.

To my family and friends, thank you for your unwavering belief in me from the beginning and support of this endeavor. Without you all, none of this would have been possible. I'm forever grateful for my parents' love and generosity, and for them encouraging me to pursue my passions. And for my brothers, who have provided relief from the academic world when I needed it. I'm so thankful for your friendship. I'd also like to acknowledge my gratitude for the Schrams, whose kindness and encouragement during this time has been so important.

Finally, I would like to thank my wife Hayley, who has been by my side through some of the most stressful times. Thank you for filling my life with joy and happiness when I need it the most. Your faithful love, constant support, and unfaltering encouragement has kept me sane as I've been working to finish my thesis. You overflow my cup with laughter, peace, and optimism (and coffee!). Most of all, thank you for being my best friend.

Above all else, I give thanks to God, who has gifted me with a spirit of curiosity, knowledge, love, power, sound judgement, and self-discipline. I owe it all to Him.

Contents

Abstract 3

Acknowledgements 5

Contents 8

Chapter 1. Thesis Overview 15

1.1. Introduction 16

1.2. Chapter 2: Tectonic Implications of the Gravity Signatures of the Midcontinent Rift and Grenville Front 17

1.3. Chapter 3: Three Major Failed Rifts in Central North America: Similarities and Differences 18

1.4. Chapter 4: The PALEOMAP Paleopole Compilation: A Paleomagnetic Database for use in Global Plate Modeling 19

1.5. Chapter 5: What does the Shape of Apparent Polar Wander (APW) Paths Tell Us About Global Plate Motions? 20

1.6. Chapter 6: Conclusion 20

Chapter 2. Tectonic Implications of the Gravity Signatures of the Midcontinent Rift and Grenville Front 22

2.1. Summary 23

2.2. Introduction 24

2.3. Comparison of Gravity Data for the Rift and Front 27

2.4. Midcontinent Rift Models 30

2.5. Grenville Front Models 33

2.6. Tectonic Implications 34

2.7. Conclusions 36

Chapter 3. Three Major Failed Rifts in Central North America: Similarities and Differences 37

3.1. Summary 38

3.2. Introduction 38

3.3. Midcontinent Rift 42

3.4. Southern Oklahoma Aulacogen 45

3.5. Reelfoot Rift 47

3.6. Similarities and Differences 48

3.6.1. Tectonic Setting 48

3.6.2. Spatial Scale and Architecture 50

3.6.3. Igneous Rock Volumes 52

3.7. Conclusions 54

Chapter 4. The PALEOMAP Paleopole Compilation: A Paleomagnetic Database for use in Global Plate Modeling 55

4.1. Summary 56

4.2. Introduction 56

4.3. Data Compilation 59

4.4. Global Mean Pole (GMP) Calculation for use in APW Path Analyses 63

4.5. Comparison With Recently Published Data 75

4.6. Conclusions 76

Chapter 5. What does the shape of Apparent Polar Wander Paths Tell Us About Global Plate Motions? 77

5.1. Summary 78

5.2. Introduction 79

5.3. Methodology – Major Tectonic Events and Construction of APW Paths 82

5.4. Analysis of Apparent Polar Wander Paths 85

5.5. Results and Implications 103

5.6. Conclusions 105

Chapter 6. Conclusion 107

References 113

List of Tables

4.1. Documentation of the attributes provided in the database of compiled paleopoles 62

4.2. Phanerozoic Global Mean Poles calculated for the PALEOMAP Paleopole Compilation with a 45° cutoff and rotated into the model reference frame of Scotese and Elling (2017) 66

4.3. Precambrian Global Mean Poles calculated for the PALEOMAP Paleopole Compilation with a 45° cutoff and rotated into the model reference frame of Scotese and Elling (2017) 67

4.4. Precambrian Global Mean Poles for the paleomagnetic data from Evans et al. (2022), rotated into the model reference frame of Scotese and Elling (2017) 68

5.1. Catalogue of major tectonic events 86

List of Figures

2.1. (a) ~1.1 Ga reconstruction of major blocks and Grenville-age orogenic belts and (b) complete Bouguer anomaly gravity map of the Midcontinent Rift and Grenville Front 25

2.2. Mean gravity anomalies of the Midcontinent Rift and Grenville Front 29

2.3. Gravity models across the east and west arms of the Midcontinent Rift and north and south sections of the GF 31

3.1. Topographic map of central North America 40

3.2. Bouguer gravity anomaly map for central North America and average gravity profiles across the Midcontinent Rift, Southern Oklahoma Aulacogen, and Reelfoot Rift 42

3.3. Gravity models across the east and west arms of the Midcontinent Rift, Southern Oklahoma Aulacogen, and Reelfoot Rift, including inversion tests 44

3.4. Schematic reconstruction of the tectonic origins of each rift, along with the associated cusps in Laurentia's apparent polar wander path 49

3.5. Gravity anomalies expected at various stages in rift evolution 51

4.1. Schematic timeline of truncated paleopoles ages for use in GMP Calculations 65

4.2. Phanerozoic Global Mean Poles (GMPs) for 0 to 160 Ma 69

4.3. Phanerozoic Global Mean Poles (GMPs) for 180 to 340 Ma 70

4.4. Phanerozoic Global Mean Poles (GMPs) for 360 to 500 Ma 71

4.5. Precambrian Global Mean Poles (GMPs) for 550 to 900 Ma 72

4.6. Precambrian Global Mean Poles (GMPs) for 950 to 1200 Ma 73

4.7. Precambrian Global Mean Poles (GMPs) for 950 to 1200 Ma 74

5.1. Apparent polar wander (APW) path of Laurentia between 1200 and 500 Ma 80

5.2. Continental blocks used in analysis of timing of cusps and tectonic events 82

5.3. Number of paleopoles in the PALEOMAP Paleopole Compilation (PPC) used to constrain the global plate model of Scotese and Elling (2017) 83

5.4. Apparent polar wander (APW) path of Laurentia from 1200 Ma to 1000 Ma, with GMPs plotted every 50 million years 83

5.5. Analysis of the directional changes in Laurentia's apparent polar wander path from 1.5 Ga to present day, including the timing of major tectonic events 90

5.6. Analysis of the directional changes in Amazonia's apparent polar wander path from 1.5 Ga to present day, including the timing of major tectonic events 91

5.7. Analysis of the directional changes in Baltica's apparent polar wander path from 1.5 Ga to present day, including the timing of major tectonic events 92

5.8. Analysis of the directional changes in Siberia's apparent polar wander path from 1.5 Ga to present day, including the timing of major tectonic events 93

5.9. Analysis of the directional changes in India's apparent polar wander path from 1.5 Ga to present day, including the timing of major tectonic events 94

5.10. Analysis of the directional changes in North China's apparent polar wander path from 1.5 Ga to present day, including the timing of major tectonic events 95

5.11. Analysis of the directional changes in South China's apparent polar wander path from 1.5 Ga to present day, including the timing of major tectonic events 96

5.12. Analysis of the directional changes in the Congo craton's apparent polar wander path from 1.5 Ga to present day, including the timing of major tectonic events 97

5.13. Analysis of the directional changes in West Africa's apparent polar wander path from 1.5 Ga to present day, including the timing of major tectonic events 98

5.14. Analysis of the directional changes in Australia's apparent polar wander path from 1.5 Ga to present day, including the timing of major tectonic events 99

5.15. Analysis of the directional changes in Antarctica's apparent polar wander path from 1.5 Ga to present day, including the timing of major tectonic events 100

5.16. Analysis of the directional changes in Rio de la Plata's apparent polar wander path from 1.5 Ga to present day, including the timing of major tectonic events 101

5.17. Analysis of the directional changes in the Kalahari craton's apparent polar wander path from1.5 Ga to present day, including the timing of major tectonic events 102

5.18. Observed vs. randomized averages of ΔT of Laurentia for five cutoff angles between 30° and 90° 104

5.19. Average ΔTs for observed and randomized simulations of each of the 13 tectonic plates, using a cutoff angle of 60° 104

CHAPTER 1

Thesis Overview

1.1. Introduction

Over roughly the past decade, there has been a renewal of interest in the Midcontinent Rift (MCR), as useful insights into rift evolution can be obtained from studying it. Although for some cases, the fate of continental rifting events is to evolve to passive continental margins, many others fail to develop into seafloor spreading. Such failed rifts become an important part of the fabric of the continents and preserve fossil features of the rifting process that can be difficult to observe elsewhere. The MCR represents one of the world's most impressive failed rifts, and remains buried beneath the central United States as a 3000-km-long horseshoe-shaped band of igneous and sedimentary rocks. Its formation at ~1.1 Ga is seemingly juxtaposed against the collisional orogenesis of the Elzeverian, Shawinigan, and Grenville Orogenies that culminated in the assembly of Rodinia. How the MCR formed during these compressive series of events remains a long-standing question. In this thesis, I use gravity and paleomagnetic data to model its structure and tectonic history to gain insights into several questions related to its formation and evolution.

In Chapter 2, I first investigate the differences between the east and west arms of the MCR to estimate variations in magma volume, extensional regimes, and inversion amounts. Differences between the gravity anomalies of the east and west arms also allow me to establish the extent of the east arm, which has been shrouded by the traditional views of the Grenville Front's (GF) location in the eastern United States. While the Front is observed in SE Canada from surface geology and reflection seismic data, it has traditionally been assumed to extend southward into the eastern U.S. based on linear gravity and magnetic anomalies. I examine the gravity signatures of the MCR and GF away from the disputed area in the eastern U.S. and find vastly differing gravity anomalies, owing to their different tectonic natures.

This thesis also investigates in Chapter 3 how the MCR is related to other major failed rifts in central North America: the ca. 600 Ma Southern Oklahoma Aulacogen (SOA) and Reelfoot Rift (RR). I explore how their structures differ and what insights they can provide about their evolution and tectonic origins. One interesting aspect of these three rifts is that cusps, or hairpins, have been identified in the apparent polar wander (APW) path of Laurentia concurrent with the timing of their formation. In the final chapters of this thesis, I review the usefulness of Precambrian and Phanerozoic paleomagnetic data in constraining the tectonic events of these time periods. I create APW paths for 13 major tectonic plates back to 1.5 Ga from a global plate model and present an analysis of the timing of cusps and major tectonic events in an attempt to answer the long-standing question of their correlation.

1.2. Chapter 2: Tectonic Implications of the Gravity Signatures of the Midcontinent Rift and Grenville Front

In Chapter 2, I investigate two Precambrian features of central North America that record opposite ends of the Wilson cycle: the Midcontinent Rift (MCR) and Grenville Front (GF). The MCR is a 3000-km long horseshoe-shaped band of more than 2.6 million km^3 of buried igneous and sedimentary rocks that outcrops near Lake Superior but is buried by younger sediments to the south. The GF, on the other hand, is the observed continentward boundary of deformation from the Grenville Orogeny, the sequence of discrete collisional events from ~1.3–0.98 Ga culminating in the assembly of the supercontinent Rodinia. While its location in southeast Canada is generally accepted based on exposed metamorphic facies and seismic and potential field data, its extension

into the eastern U.S. has largely been inferred based on linear gravity and magnetic anomalies extending southward from Michigan to Alabama.

I distinguish between these two major tectonic events by examining the gravity signatures of the MCR and GF away from the disputed area in the eastern U.S. The two features have quite different gravity signatures, which I combine with observations from seismic data to model their structures and suggest the extent to which their locations can be defined.

This chapter has been published as Elling, R., Stein, S., Stein, C., and Keller, G., 2020, Tectonic implications of the gravity signatures of the Midcontinent Rift and Grenville Front: Tectonophysics, v. 778, p. 1–6.

1.3. Chapter 3: Three Major Failed Rifts in Central North America: Similarities and Differences

Chapter 3 takes what I have learned from the MCR and investigates how its structure and tectonic origin are related to the other major failed rifts in central North America. Similar to the MCR, the Southern Oklahoma Aulacogen (SOA) shows a prominent gravity anomaly due to the large volumes of igneous rocks which fill the rift basin. The Reelfoot Rift (RR), on the other hand, is obscure in gravity data but of interest due to its seismicity. Comparative study of these rifts using geophysical and geological data reveals intriguing similarities and differences. These three failed rifts are grossly similar, with similar tectonic origins and structural features, but their interesting differences highlight contrasting aspects of their evolution. Together they provide insight into how rifts evolve and are useful when studying other failed or active rifts elsewhere around the world.

This chapter has been published as Elling, R., Stein, S., Stein, C., and Gefeke, K., 2022, Three major failed rifts in Central North America: Similarities and Differences: GSA Today, v. 32, 8 pp.

1.4. Chapter 4: The PALEOMAP Paleopole Compilation: A Paleomagnetic Database for use in Global Plate Modeling

With the recent interest in global paleogeographic modeling for Precambrian times, researchers are trying to determine which paleomagnetic poles to use in their kinematic reconstructions. Chapter 4 describes my compilation of over 15,000 global paleomagnetic poles from the Precambrian to the Phanerozoic. State of the art modeling software, such as GPlates, is essential for creating such models but requires consistent data formats of paleopoles. While previous reconstructions focus on single databases, it is increasingly important to provide researchers with as much data as possible. Although some studies limit their data on the basis of reliability, I believe that even the least reliable poles can be useful in filling in gaps in time periods during which other data may not exist. I also calculate Global Mean Poles (GMP) at 20-million-year intervals in the Phanerozoic and 50-million-year intervals in the Precambrian that are useful in constraining accurate APW paths for major continents. Analyzing the temporal and spatial constraints on plate movement via paleomagnetic data will allow the paleomagnetic research community to further constrain the robustness of global Precambrian plate models.

This chapter will be submitted in part to the Earth-Science Reviews special volume “Plate Tectonics, the Last 2 Billion Years” as “A Global Plate Tectonic Model for the Mesoproterozoic and early Neoproterozoic (1500 – 720 Ma)” by Elling, R. P., and Scotese, C. R.

1.5. Chapter 5: What does the Shape of Apparent Polar Wander (APW) Paths Tell Us About Global Plate Motions?

Chapter 5 explores the hypothesis that there is a distinct correlation between cusps in apparent polar wander (APW) paths and major tectonic events such as rifts or orogenies. Recent continental breakups, such as the rifting of Gondwana from Laurasia, or of Europe from North America, as well as Precambrian tectonic events such as the Midcontinent Rift and Grenville Orogeny, are accompanied by a change in plate boundary configuration and rapid changes in the direction of North America motion. APW paths are simple representations of the motion of continents with respect to Earth's spin axis. Using a global plate model back to 1.5 Ga that was constrained by the paleomagnetic pole compilation from Chapter 4, I invert synthetic APW paths for 13 major tectonic plates. I analyze directional changes in APW paths and correlate them in time to major global tectonic events in the history of each plate, testing multiple criteria for defining directional changes or cusps, and calculating the delay in time between the cusps and the tectonic events.

This chapter will be submitted to the Earth-Science Reviews special volume "Plate Tectonics, the Last 2 Billion Years" as "What does the Shape of Apparent Polar Wander (APW) Paths tell us about Global Plate Motions?" by Elling, R. P., Scotese, C. R., Stein, S., and Stein, C.

1.6. Chapter 6: Conclusion

Chapter 6 summarizes thesis results, outlining the gravity analyses of the Midcontinent Rift and how it relates in space and time to the Grenville Front, Southern Oklahoma Aulacogen, and Reelfoot Rift. I find useful insight from the comparisons, delineating the east arm of the MCR and the Grenville Front in the eastern United States, and expanding our understanding of rift formation

and features that form early in passive margin evolution. A primary constraint on the tectonics of the Precambrian interactions between Laurentia and Amazonia comes from paleomagnetic data and their use in constraining global plate models. Compiling available paleomagnetic poles in one consistently formatted dataset will allow paleogeographic modelers the flexibility to decide which poles to use in their studies. My analysis supports the hypothesis that cusps in apparent polar wander paths are concurrent with major rifting or collisional events, and an analysis of the timing of such occurrences reveals strong correlations between them. These results motivate future work which I also suggest in the conclusion.

CHAPTER 2

Tectonic Implications of the Gravity Signatures of the Midcontinent Rift and Grenville Front

2.1. Summary

North America's Midcontinent Rift (MCR) and Grenville Front (GF) jointly record aspects of the complex history of the assembly of Rodinia. The ~1100 Ma MCR, remaining from a failed major rifting event, is exposed along Lake Superior and well defined by gravity, magnetic, and seismic data. The GF, which results from collisions with Laurentia, is exposed in and identified by seismic and potential field data in Canada. In the eastern U.S., lineated gravity highs extending southward from Michigan to Alabama, along the trend of the front in Canada, have been interpreted either as a buried Grenville Front or as part of the MCR's east arm. I explore this issue by examining the gravity signatures of the MCR and GF. Both the MCR's arms have pronounced gravity highs, with the west arm's greater than the east arm's. Combining the gravity observations with seismic data suggests that the west arm contains 20–25 km thickness of volcanics, whereas the east arm contains 10–15 km of volcanics. Along the Grenville Front in Canada, thickened crust along the northern portion causes a broad gravity low, whereas the stacked thrusts along the southern portion cause essentially no gravity signature. Hence the lineated gravity highs in the eastern U.S. appear similar to those along the remainder of the MCR, and unlike those on either portion of the GF. These data favor the gravity anomalies traditionally interpreted as the Grenville Front in the eastern U.S. as instead being part of the MCR's east arm. A thrust sheet structure like that of the southern Canadian Grenville Front – which would have essentially no gravity effect – could also be present along the MCR's east arm, as implied by recent EarthScope seismic data.

2.2. Introduction

Two prominent Precambrian features of central North America (Figure 2.1) record opposite ends of the Wilson cycle. One, the Midcontinent Rift (MCR), is a 3000-km long horseshoe-shaped band of more than 2 million km^3 of buried igneous and sedimentary rocks that outcrop near Lake Superior (Ojakangas et al., 2001; S. Stein et al., 2018). To the south, it is buried by younger sediments, but easily traced because the rift-filling volcanic rocks are dense and highly magnetized (Merino et al., 2013). The western arm extends at least through Oklahoma, and perhaps Texas and New Mexico, as evidenced by similar-age diffuse volcanism (Adams and Keller, 1994, 1996; Bright et al., 2014). The eastern arm extends southward through lower Michigan and probably to Alabama (Lyons, 1970; Keller et al., 1982; Dickas et al., 1992; Stein et al., 2014).

The MCR likely formed as part of the rifting of the Amazonia craton (now in northeastern South America) from Laurentia, the Precambrian core of North America (Stein et al., 2014, 2016). Surface exposures, seismic data, and gravity data delineate a rift basin filled by inward-dipping flood basalt layers, underlain by thinned and underplated crust. These features are suggestive of those at volcanic passive margins, which are characterized by thick sequences of volcanic rocks yielding magnetic anomalies landward of and sometimes larger than the oldest spreading anomalies. Seaward-dipping reflectors, packages of volcanic flows interbedded with volcanoclastic sediments and tuff, mostly occur on thinned continental crust landward of the oldest oceanic crust and are frequently underplated by high velocity lower crustal bodies (HVLC). That the MCR shows many features common to rifted volcanic margins suggests that it came close to continental breakup before it failed and illustrates how passive margins may form prior to breakup (S. Stein et al., 2018).

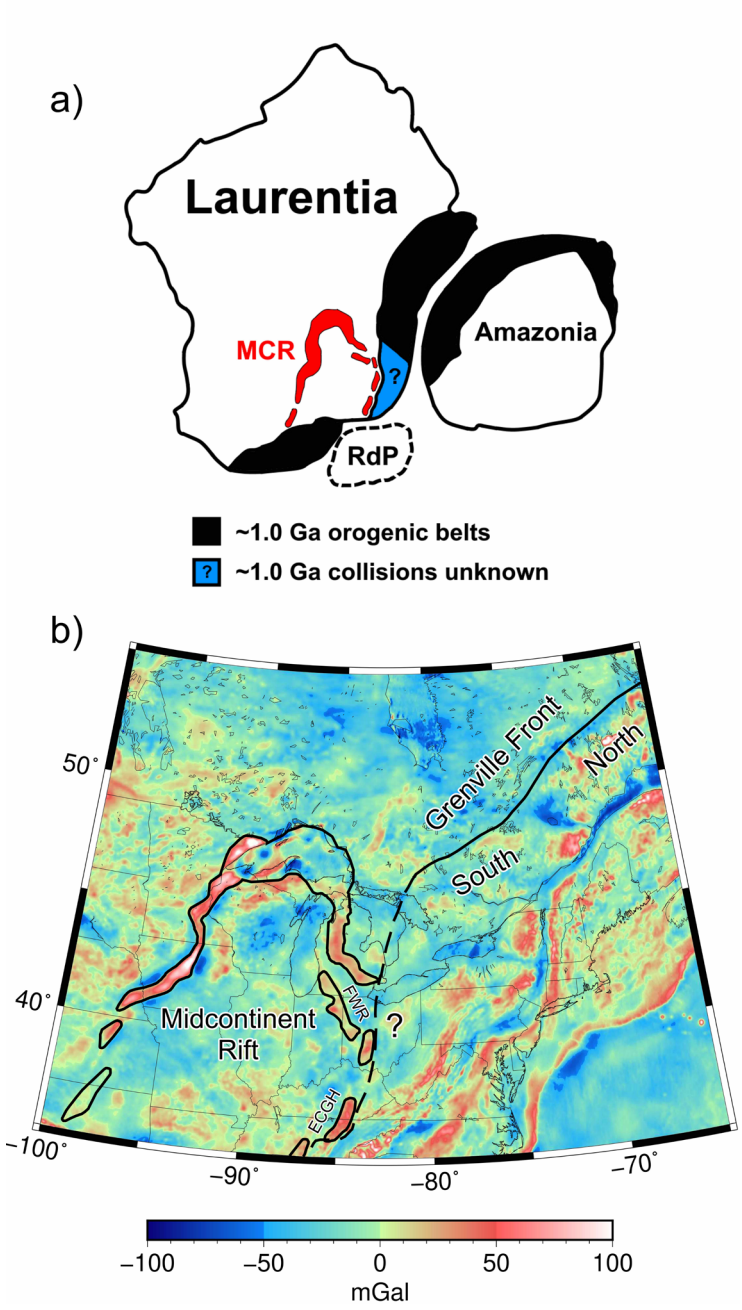

Figure 2.1. (a) Reconstruction showing commonly assumed locations of major blocks and Grenville-age orogenic belts, in present-day orientation, associated with the accretion of the Amazonia and Rio de la Plata (RdP) blocks to Laurentia, the core of Precambrian North America (after Li et al., 2008). (b) Complete Bouguer anomaly gravity map, showing locations of the MCR, East Continent Gravity High (ECGH), Fort Wayne Rift (FWR), and the Grenville Front in Canada. Dashed segment shows the traditionally assumed continuation of the GF in the eastern United States, adapted from Whitmeyer and Karlstrom (2007).

The second major feature, east of the MCR, is the Grenville Front (GF). The front is the observed continentward boundary of deformation from the Grenville orogeny, the sequence of orogenic events from ~1300–980 Ga culminating in the assembly of the supercontinent of Rodinia from blocks including Amazonia and Laurentia (Li et al., 2008). Studies in SE Canada, where Grenville rocks are exposed, find that the orogeny involved discrete contractional phases, notably the Shawinigan from ~1200–1140 Ma, Ottawan from ~1090–1030 Ma, and Rigolet from ~1010–980 Ma (Rivers, 2012; McLelland et al., 2013). In SE Canada from ~54°N to Lake Ontario, erosion has exposed deformed rocks from these orogenic events.

The orogeny's phases presumably reflect a series of continental blocks and arcs colliding with and accreting to Laurentia at various locations along its eastern margin. However, the specifics of the plate interactions remain unresolved because the limited paleomagnetic data allow a range of possible scenarios. A common aspect of many reconstructions during this time period is that Amazonia collided, rifted, and re-collided with Laurentia during multiple phases (Tohver et al., 2002, 2006), but the inferred southern extent of this collision varies between reconstructions (Li et al., 2008, 2013; Cawood and Pisarevsky, 2017; Merdith et al., 2017). The MCR likely formed between compressional phases of the Grenville Orogeny, involving the rifting of Amazonia from Laurentia, where it was left behind as a failed rift, with extension ending in ~1096 Ma (Stein et al., 2014, 2015).

The locations of the Grenville Front in Canada and of the MCR's east arm from Lake Superior to southern Michigan are generally accepted. However, questions remain as to their locations further south in the eastern U.S. Lineated gravity highs (Figure 2.1b), known as the East Continent Gravity High (ECGH) and Fort Wayne Rift (FWR), extend southward from Michigan to Alabama.

Based on the similarity of their trend to that of the Grenville Front in Canada, these have been interpreted as indicating a southward extension of the front (Zietz et al., 1966; Hoffman, 1988; Whitmeyer and Karlstrom, 2007; Baranoski et al., 2009; Bartholomew and Hatcher, 2010). Alternatively, based on the anomalies' similarities to those along the MCR, they have been interpreted as part of the MCR's eastern arm (Lyons, 1970; Keller et al., 1982; Dickas et al., 1992; C.A. Stein et al., 2014, 2018). The traditionally assumed front's location near southeast Michigan implies that the MCR's east arm ended there, presumably because propagation of the rift extension and volcanism were stopped by the preexisting front (Cannon et al., 1989). However, it now appears that the MCR formed before the presently observed Grenville Front (Malone et al., 2016; S. Stein et al., 2018).

In this chapter, I explore this issue by examining the gravity signatures of the MCR and GF away from the disputed area in the eastern U.S. The two features have quite different gravity signatures, owing to their different tectonic natures. I find that the lineated gravity highs in the eastern U.S. appear similar to those along the remainder of the MCR, and unlike those on either portion of the GF, favoring the gravity anomalies reflecting a southward part of the MCR's east arm. In addition, a thrust sheet structure like that of the southern Canadian Grenville Front – which would have a minimal gravity signature – could also be present along the MCR's east arm, as implied by recent EarthScope seismic data (Long et al., 2019).

2.3. Comparison of Gravity Data for the Rift and Front

I analyzed gravity data to compare and contrast the differences between four features: the west and east arms of the MCR and the northern and southern portions of the Grenville Front in Canada.

Profiles were grouped into MCR west, MCR east, GF south, and GF north. Using a combination of the PACES gravity database jointly developed by the University of Texas at El Paso and the U.S. Geological Survey (Keller et al., 2006) and the TOPEX satellite-derived free-air gravity data (Sandwell et al., 2013) over the lakes, profiles 150 km long and approximately 50 km apart were extracted (Figure 2.2a). The gravity anomalies used to derive the models in this paper reflect the complete Bouguer anomalies from the PACES database. These attempt to correct for the mass of the material between each gravity station and Earth's geoid, which if left uncorrected, would cause a variation of gravity with elevation. I then calculated a mean gravity profile and its standard deviation for each feature (Figure 2.2b).

The mean profiles show differences between the features, reflecting their structure and origin. The Grenville Front in Canada exhibits two decidedly different gravity signatures. Along its northern portion, the front appears as a broad negative anomaly of ~−40 mGal. Along the front's southern section, it exhibits essentially no anomaly, positive or negative. Hence the two portions of the front differ, with one showing a low and the other showing essentially no anomaly.

In contrast, the rift appears as a large positive anomaly along its entire length. This anomaly, which has been used to map the MCR, reflects the fact that the MCR combines the geometry of a rift and the huge igneous rock volume of a Large Igneous Province (Green, 1983; Stein et al., 2015). Some differences appear between the east and west arms of the MCR. The west arm is characterized by large gravity highs (~80 mGal) bounded by ~−20 mGal lows on either side of the rift basin. The east arm has smaller (~40 mGal) gravity highs and lacks the bounding lows. Thus, the anomalies over the two arms are generally similar, in that both are highs, but with differing amplitudes. These differ noticeably from the anomalies over the Grenville Front.

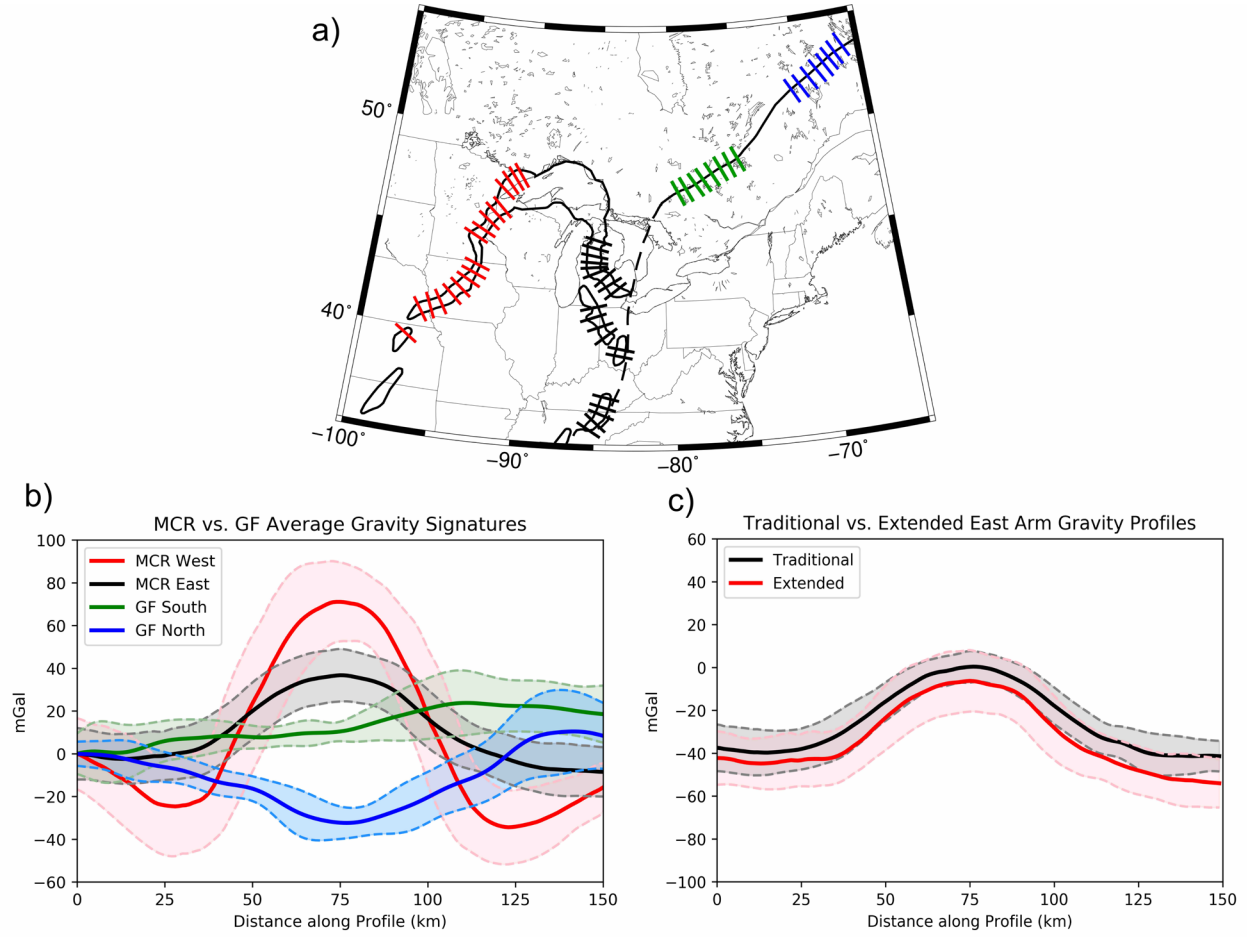

Figure 2.2. (a) Locations of gravity profiles across each of the regions considered. Colors correspond to those for profiles in parts b and c, with black corresponding to the traditionally mapped east arm in Michigan (north of 42°N) and grey to its southward extension through Alabama (south of 42°N). (b) Mean gravity anomalies for west and east arms of the MCR and south and north sections of the Grenville Front in Canada. The mean for the MCR East anomaly includes both the black and grey plotted profiles. Solid lines indicate average anomalies, and dashed lines indicate 1σ range from the mean. For graphic purposes, all four profiles are set to zero on the left side. (c) Mean gravity anomalies for the nine profiles across the traditionally mapped east arm are plotted in black and the eleven other profiles across its southward extension are plotted in grey, matching the profile map. Solid lines are averages and dashed lines indicate 1σ range from the mean.

I divided the profiles across the east arm into nine crossing the traditionally mapped east arm in Michigan and eleven crossing its proposed southward extension (Figure 2.2c). As shown, the mean profiles of the two sets are almost identical in shape and overlap in amplitude. Hence this larger dataset supports C.A. Stein et al.'s (2018) analysis, based on individual profiles, that the gravity anomalies of the East Continent Gravity High and Fort Wayne Rift, traditionally interpreted as a southward extension of the Grenville Front, are instead part of the MCR's east arm.

2.4. Midcontinent Rift Models

The gravity signatures of the features reflect their different subsurface structures. The Midcontinent Rift's present structure results from the combined effects of a sequence of rifting, volcanism, sedimentation, subsidence, compression, erosion, and any later effects (Stein et al., 2015; S. Stein et al., 2018). The large positive gravity anomalies along the MCR primarily reflect the large volume of high-density igneous rocks filling the rift basins. Modeling this for each arm provides a useful comparison of the effects of magma volume and position. Merino et al. (2013) produced a generalized model, inspired by a COCORP reflection line in Kansas (Serpa et al., 1984; Woelk and Hinze, 1991), in which the intrusions were modeled simply, as trapezoids of uniform density. Here, I developed more detailed models for the average structure along each arm (Figure 2.3). I began with structural results from the Great Lakes International Multidisciplinary Program on Crustal Evolution (GLIMPCE) seismic reflection profiles of the rift across Lake Superior (Green et al., 1989). I also considered other 2-D gravity models across the MCR (Mayhew et al., 1982; Van Schmus and Hinze, 1985; Chandler et al., 1989; Hinze et al., 1992; Shay and Tréhu, 1993), and new seismic data from the Superior Province Rifting EarthScope Experiment (SPREE)

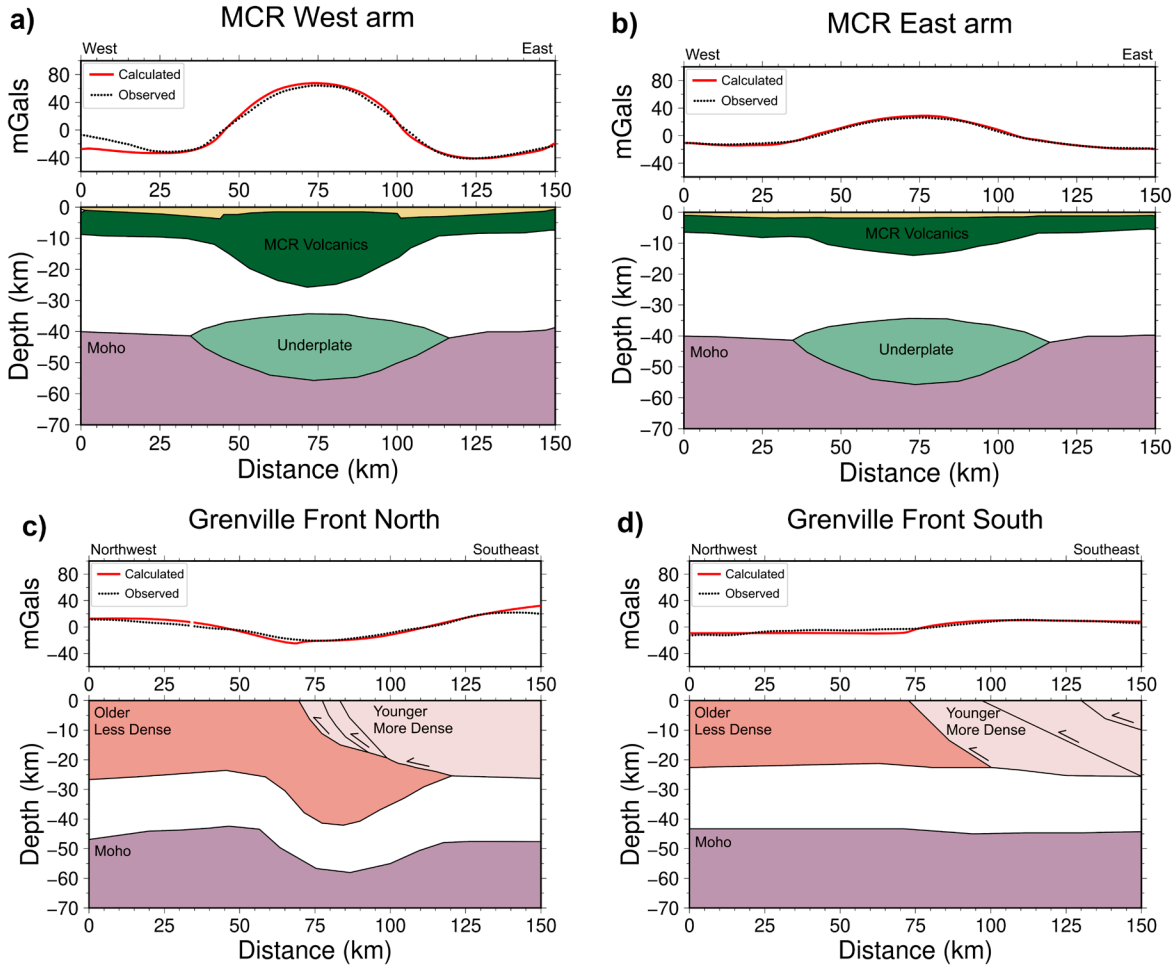

Figure 2.3. Gravity models matching the mean anomalies across the west (a) and east (b) arms of the MCR. Densities, in g/cm^3: sediments – yellow – 2.45, Keweenawan Volcanics – dark green – 2.95, lower crust – white – 2.67, underplate – light green – 3.10, upper mantle – purple – 3.30. Gravity models for the north (c) and south (d) sections of the Grenville Front in Canada. North model assumes strong crustal thickening of the Laurentian crust. South model assumes no crustal thickening, with the front expressed only as stacked thrusts. Densities, in g/cm^3: Laurentian Crust – dark pink – 2.70, Grenvillian Crust – light pink – 2.75, lower crust – white – 2.85, upper mantle – purple – 3.30.

(Zhang et al., 2016). The SPREE data show structure below the west arm similar to that below Lake Superior, suggesting that the structure along the entire MCR is similar.

Hence in our models, the rift arms have similar structures. The largest difference between the arms is the thickness of the rift-filling volcanics. Based on the SPREE seismic data, the west arm model has 20–25 km of volcanics filling the rift basin, producing an 80 mGal positive anomaly that closely matches the actual data. On either side of the rift basin, sedimentary basins roughly 5 km thick resulting from post-rift sedimentation produce the bounding gravity lows. The sediments are much thinner over the basin as a result of inversion, uplift, and erosion after rifting ended. These events stripped off much of the overlying sediments, leaving only the bounding basins. The east arm's comparatively moderate gravity high, however, is modeled assuming significantly less (10–15 km) volcanics. Because the data do not show bounding gravity lows, the model does not include bounding sedimentary basins. The models for both arms assume similar Moho depth and underplating, presumably the dense lower residuum from the magma extraction (Vervoort et al., 2007; S. Stein et al., 2018). The ratio of the cross-sectional area of rift-filling volcanics to that of underplated material is 1.55 in the west arm of the MCR and 0.97 in the east arm.

I modeled the underplated bodies as similar in depth and volume for both arms, as seismic reflection data constraining its location have lower resolution at these depths, and gravity modeling alone cannot constrain its location well. Receiver function data from the SPREE profiles reveal a consistent Moho beneath regions away from the MCR (Zhang et al., 2016). However, its depth elsewhere along the rift remains less clear owing to the lack of detailed studies, which should improve as additional EarthScope data are analyzed. While exploring possible thicknesses of the rift-filling volcanics and underplated structures, it became clear that the volume of the highly dense

igneous rocks which fill the rift basin affects the overall gravity anomaly much more than changing the depth or volume of the underplate. Hence, while the subsurface model of the west arm was largely constrained by the available seismic data, the geometry of the volcanics in the east arm was only adjusted within the rift basin itself to match the average gravity profiles. Past modeling of seismic and gravity profiles has yielded estimates of the total magma volume within the MCR. Hutchinson et al. (1990) analyzed the available seismic data and calculated a total volume of more than 1.3×10^6 km^3. This estimation was based on the traditionally drawn MCR with a truncated east arm, leading to an estimate that likely did not capture the total extent of the rift. Using the new geometry to recalculate the values, Stein et al. (2015) estimated the total magma volume to be ~2.1×10^6 km^3. Our new average models for the west and east arms of the MCR provide hopefully better estimates for the cross-sectional area of volcanics within the rift basin along both arms. Along the west arm, the average cross-sectional area is roughly 1200 km^2, while along the east arm it is 740 km^2. This adds up to ~2.0×10^6 km^3 of magma in the arms alone. Accounting for the magma volumes inferred from the GLIMPCE surveys across Lake Superior (Cannon et al., 1989), the total magma volume estimated based on our new average models is increased to 2.6×10^6 km^3. The models are schematic, in that they seek to characterize an average structure of the two arms. Nonetheless, they show clear differences between the MCR and Grenville Front, discussed next.

2.5. Grenville Front Models

COCORP and Lithoprobe seismic reflection studies have imaged the crustal structure of the Grenville Front in Canada, showing southeast-dipping structures throughout preserved sections of the orogen (Culotta et al., 1990; Ludden and Hynes, 2000; Hynes and Rivers, 2010). Using these,

I modeled schematic subsurface structures to fit the negative gravity anomaly in the northern section and the lack of a gravity anomaly in the south (Figure 2.3).

The northern section of the front is characterized by a pronounced Bouguer gravity low that likely reflects progressive thickening of the older and less dense northwestern Laurentian crust with continued orogenic thrusting, consistent with studies of analogous mountain-building events such as the Himalayan-Tibetan orogen (Pilkington, 1990; Hynes, 1994; Hynes and Rivers, 2010). In our models, thickening of the Laurentian crust by roughly 10 km at the front replicates the ~−40 mGal gravity anomaly.

In contrast, gravity data across the southern section show essentially no gravity anomaly, positive or negative. This observation accords with the fact that seismic data along the southern section show no crustal thickening (Culotta et al., 1990). Our model is consistent with Lithoprobe reflection and refraction lines along this section that show a relatively well-defined Moho at about 40 km which deepens slightly to about 45 km to the southeast (Ludden and Hynes, 2000; Rivers, 2014). Most of the present-day preserved structure is likely related to the last major episode of orogeny in this area, during which the shear zones soled (became sub-horizontal) into the present-day middle crust no deeper than 25 km (White et al., 2011). The thrust faulting has only a minor gravity signature. In our model, denser younger crust to the southeast stacked against an older less dense Laurentian crust leads to a small anomaly that becomes more negative to the northwest.

2.6. Tectonic Implications

The analysis here confirms our previous conclusion that the lineated positive gravity anomalies along the FWR and ECGH are consistent with their being due to igneous rocks filling part of the

MCR's east arm. Moreover, these positive gravity anomalies are unlike those on either portion of the Grenville Front in Canada.

Given that the gravity highs likely reflect the MCR's east arm, the question remains whether a Grenville Front-type structure could also exist nearby. Because the northern Grenville Front in Canada has a pronounced negative anomaly associated with crustal thickening, it seems implausible that such a structure could exist along the MCR's east arm. However, the gravity data do not exclude GF South-type structures, in which thrust faulting produces only a minor gravity anomaly. Deformation interpreted as Grenville age has been identified in Ohio and Kentucky in seismic reflection data and geology (Drahovzal, 1997; Baranoski et al., 2009; Moecher et al., 2018). Recent seismic data support this possibility, as EarthScope projects in the last decade have provided us with a wealth of new data on crustal structure in the eastern United States. Schmandt et al. (2015) used multimode receiver function stacking and Rayleigh wave tomography data to investigate crustal thicknesses across the U.S. and revealed an overall thickened crust along segments of the MCR. P-to-S receiver function data for the Mid-Atlantic Geophysical Integrative Collaboration (MAGIC) array just north of the gravity high beneath central Ohio similarly imaged local crustal thicknesses ~100–200 km from the west end of the transect as high as ~58 km (Long et al., 2019). These observations are consistent with the base of the underplated high velocity lower crustal body in our models. They also imaged southeastward dipping structures extending to the east of the positive gravity lineaments that I associate with the east arm of the MCR. This has been interpreted as the main deformation front of the Grenville orogen in the eastern United States. I believe this interpretation to be consistent with the location of the MCR in this region. If stacked thrust sheets similar to those seen in the south GF continued southward into the United States, it

makes sense that they should be found to the east of the positive gravity anomalies our models aim to match. This view is also consistent with the deformation related to the Grenville Front having occurred primarily in the upper ~30 km of the crust, rather than deeply seated near the Moho.

2.7. Conclusions

In summary, the gravity data favor the traditionally inferred position of the “Grenville Front” in the eastern U.S. being part of the MCR's east arm. However, a thrust sheet structure like that of the southern Canadian Grenville Front - which would have essentially no gravity effect - could also be present in the area. In our view, modern high-quality seismic reflection surveys combined with additional geological studies would be the best way to address this question.

CHAPTER 3

Three Major Failed Rifts in Central North America: Similarities and Differences

3.1. Summary

The North American craton preserves nearly two billion years of geologic history, including three major rifts that failed rather than evolving to continental breakup and seafloor spreading. The Midcontinent Rift (MCR) and Southern Oklahoma Aulacogen (SOA) show prominent gravity anomalies due to large volumes of igneous rift-filling rock. The Reelfoot Rift (RR), though obscure in gravity data, is of interest due to its seismicity. The ca. 1.1 Ga MCR records aspects of the assembly of Rodinia, whereas the ca. 560 Ma SOA and RR initiated during the later breakup of Rodinia and were inverted during the assembly of Pangea. Comparative study of these rifts using geophysical and geological data shows intriguing similarities and differences. The rifts formed in similar tectonic settings and followed similar evolutionary paths of extension, magmatism, subsidence, and inversion by later compression, leading to similar width and architecture. Differences between the rifts reflect the extent to which these processes occurred. Further study of failed rifts would give additional insight into the final stages of continental rifting and early stages of seafloor spreading.

3.2. Introduction

Plate tectonics shapes the evolution of the continents and oceans via the Wilson cycle, in which continents rift to form new oceans. Many rifts evolve to passive continental margins. However, some rifts fail before continental breakup and remain as fossil features within continents, which are largely buried beneath the surface and studied primarily with gravity and seismic surveys. Failed rifts preserve a snapshot of the rifting process before the beginning of seafloor spreading

and thus give insight into late stages of continental rifting and formation of passive continental margins (S. Stein et al., 2018; Stein et al., 2022).

North America contains multiple impressive, failed rifts (Figure 3.1), preserving important aspects of the fabric of nearly two billion years of geologic history in Laurentia, its Precambrian core (Whitmeyer and Karlstrom, 2007; Marshak and van der Pluijm, 2021). I focus on three major failed rifts, covering ~10% of central North America (defined for these purposes as the area shown in Figure 3.1). One, the Midcontinent Rift (MCR), is a prominent feature in geophysical maps of the region. Due to its size and the availability of geophysical and geological data, the MCR has been the focus of many studies giving insight into its evolution, role in the assembly of Rodinia, and processes of rifting and passive margin evolution (e.g., Green et al., 1989; C. Stein et al., 2018; Swanson-Hysell et al., 2019). Two other failed rifts, the Southern Oklahoma Aulacogen (SOA) and Reelfoot Rift (RR), have also been subjects of much interest. Parts of the SOA lie within the basement near and below the Anadarko Basin, a major oil- and gas-producing basin. Thus, its oil-bearing upper crust is well studied (Brewer et al., 1983; Keller and Stephenson, 2007; Hanson et al., 2013), but the deeper structures in the lower crust and uppermost mantle are rarely the primary target of study. The RR and its northern extensions, on the other hand, have little interest for the energy industry but are of interest due to their active seismicity (Hildenbrand and Hendricks, 1995; Calais et al., 2010).

These three failed rifts are grossly similar, with similar tectonic origins and structural features, but with interesting differences highlighting aspects of their evolution. These are shown by gravity data that are uniformly sampled across the central U.S. (Figure 3.2). In contrast, other data

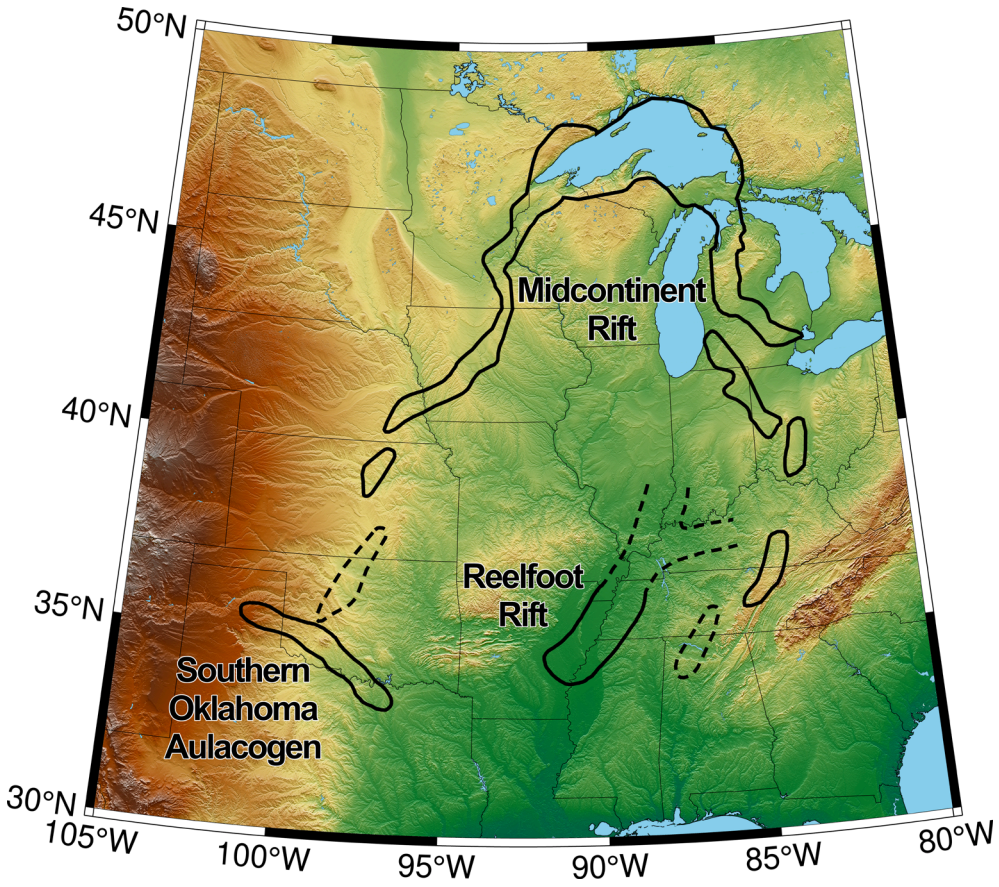

Figure 3.1. Topographic map of central North America outlining the extent of its three major failed rifts: the Mesoproterozoic Midcontinent Rift, and the Ediacaran-Cambrian Southern Oklahoma Aulacogen and Reelfoot Rift. Dashed lines indicate possible extensions of rift arms.

available differ from area to area. In particular, high-quality seismic reflection data giving detailed structure at depth that allows modeling of the rift's evolution are available only across the part of the MCR below Lake Superior. Conversely, EarthScope local seismic array data showing structure beneath the rift are available only across parts of the MCR's west arm and the RR.

Using gravity data from the PACES (Keller et al., 2006) and TOPEX data sets (Sandwell et al., 2013), I extracted profiles 150 km long and ~50 km apart across each rift (Figure 3.2B). Figure 3.2 shows each rift's mean Bouguer anomaly and standard deviation. The mean profiles show

differences between rifts, reflecting their tectonic origin and subsurface structure. The MCR's west arm shows large gravity highs (~80 mGal) bounded by ~20 mGal lows on either side of the rift basin. In contrast, the MCR's east arm has a positive anomaly half that of the west arm and lacks bounding lows. The Southern Oklahoma Aulacogen has an ~60 mGal positive anomaly, similar to the MCR, whereas the RR shows only a minor (~10–15 mGal) positive anomaly despite forming about the same time as the SOA.

The profiles are generally similar in width and form, but differ in amplitude, suggesting general similarities in crustal and uppermost mantle structure between the rifts. I use the mean gravity profiles augmented with seismic and other data, combined with results from earlier studies, to model the rifts' general subsurface structures. I start with the hypothesis that the rifts are similar, and so when needed use inferences from one rift to gain insight into the others, to the extent that the data permit. Although models from gravity data alone are non-unique, augmenting them with information from seismic, aeromagnetic, surface mapping, and drill-hole data lets us characterize average structure along the rifts and illustrate similarities and differences between them. The similarities and differences reflect the combined effects of a sequence of rifting, volcanism, sedimentation, subsidence, compression, erosion, and later effects (Stein et al., 2015; Elling et al., 2020). They give insight into how rifts evolve and are useful when studying other failed or active rifts elsewhere.

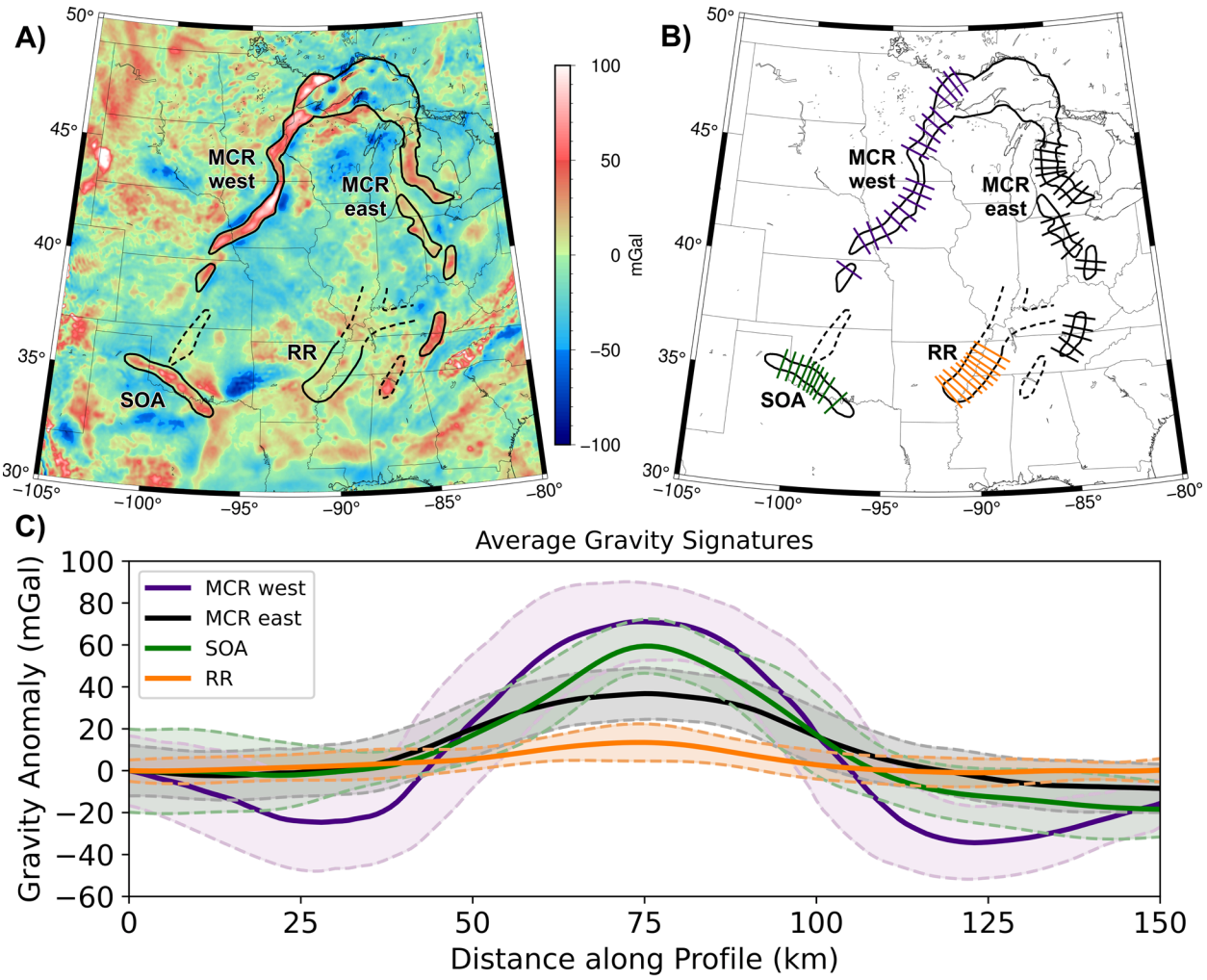

Figure 3.2. (A) Bouguer gravity anomaly map for central North America. Anomalies related to the Midcontinent Rift (MCR), Southern Oklahoma Aulacogen (SOA), and Reelfoot Rift (RR) are outlined. Dashed lines outline possible extensions of rift arms not included in analysis. (B) Profiles used in calculating the average gravity anomalies. (C) Mean anomalies and standard deviations for rifts.

3.3. Midcontinent Rift

The Midcontinent Rift (MCR), a 3000-km-long band of more than 2 million km^3 of buried igneous and sedimentary rocks that outcrop near Lake Superior, has been extensively studied, as reviewed by Ojakangas et al. (2001) and S. Stein et al. (2018). To the south, it is buried by younger

sediments, but easily traced because the rift-filling volcanic rocks are dense and highly magnetized. The western arm extends southward to Oklahoma, as shown by positive gravity anomalies and similar-age diffuse volcanism (Bright et al., 2014). The eastern arm extends southward to Alabama (Keller et al., 1983; C. Stein et al., 2014, 2018; S. Stein et al., 2018; Elling et al., 2020). The MCR likely formed as part of rifting of the Amazonia craton (now in northeastern South America) from Laurentia, the Precambrian core of North America at 1.1 Ga, after the Elzeverian and Shawinigan orogenies and before the Grenville Orogeny (C. Stein et al., 2014, 2018; S. Stein et al., 2018). Surface exposures, seismic data, and gravity data delineate rift basins filled by thick basalt layers and sediments, underlain by thinned crust and an underplate unit, presumably the dense residuum from the magma extraction (Vervoort et al., 2007; S. Stein et al., 2018). The rift was later massively inverted by regional compression, uplifting the volcanic rocks so that some are exposed at the surface today. The MCR has little seismicity along most of its length, but portions in Kansas and Oklahoma experienced seismicity and Phanerozoic deformation (Burberry et al., 2015; Levandowski et al., 2017).

I developed models for each arm (Figure 3.3A and Figure 3.3B), following Elling et al. (2020), because the west arm's larger gravity anomaly indicates differences in magma volume and tectonic evolution. For simplicity, the models use average densities of the sediment, igneous rift fill, underlying crust, underplate, and mantle. I began with GLIMPCE seismic reflection profiles across Lake Superior that give the best available image of structure at depth in the MCR (Green et al., 1989) and permit detailed modeling of its evolution (Stein et al., 2015). I also considered prior gravity models across parts of the MCR (Mayhew et al., 1982; Shay and Trehu, 1993). EarthScope data (Zhang et al., 2016) provided values for the depth and thickness of the volcanics

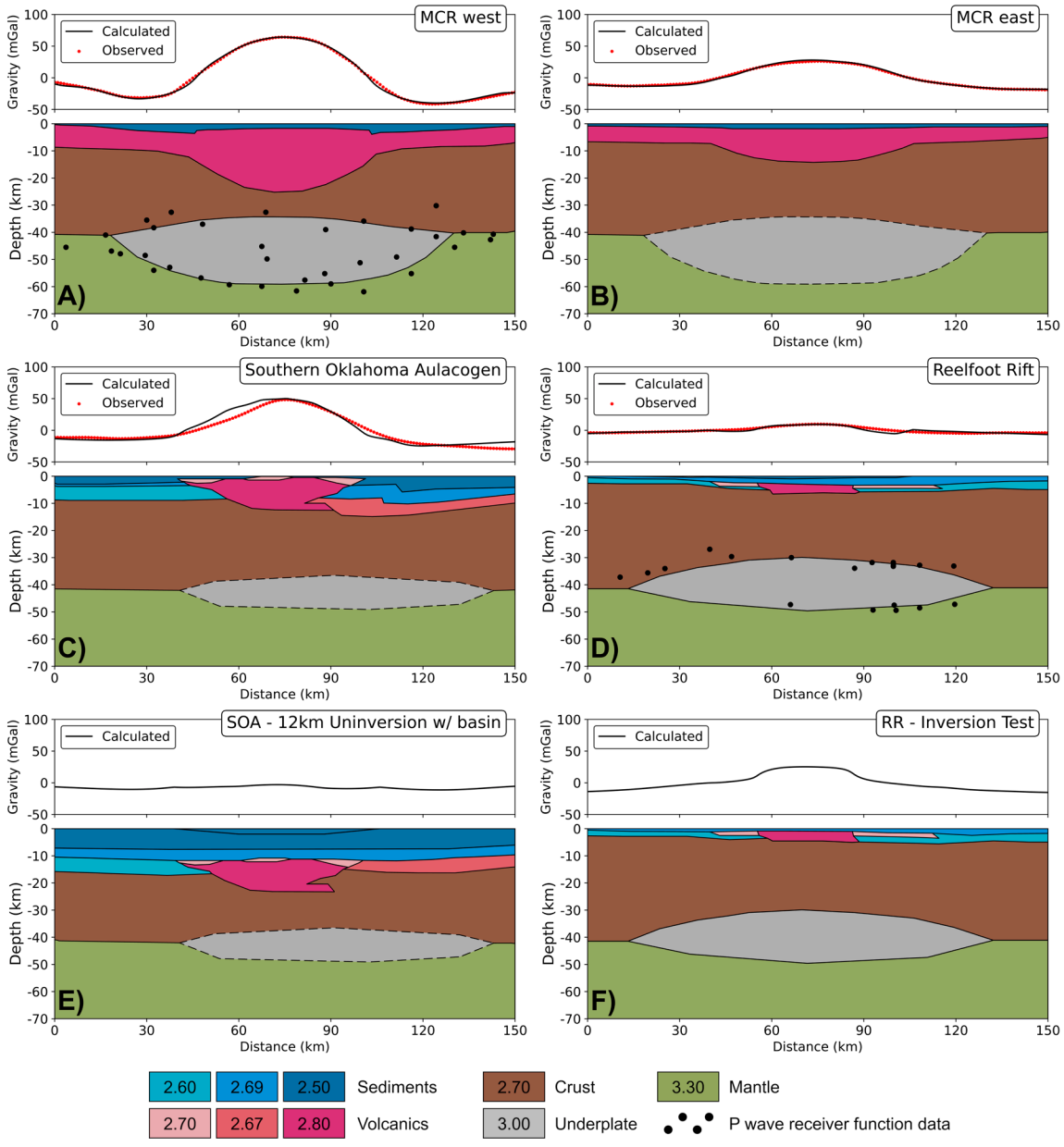

Figure 3.3. Gravity data and rift models. (A) West Midcontinent Rift (MCR) arm, with underplate based on receiver function data (dots). (B) East MCR arm, modeled with underplate like the west arm's, dashed given its uncertainty. (C) Southern Oklahoma Aulacogen (SOA), with proposed underplate dashed given its uncertainty. (D) Reelfoot Rift (RR), with underplate based on receiver function data (dots). (E) Model for the SOA if it had not been inverted, eliminating the positive anomaly. (F) Model for the RR if it had been inverted, producing a positive anomaly. Densities in g/cm^3.

and underplate along the west arm that were used to update the models. These data showed that structure below the west arm resembles that below Lake Superior, suggesting that the structure along the entire MCR is similar. On either side of the central rift basin, basins ~5 km thick resulting from post-rift sedimentation produce bounding gravity lows. The sediments are much thinner over the central basin as a result of inversion, uplift, and erosion after rift failure.

I model the east arm as similar to the west. Because the east arm does not show bounding gravity lows, the model does not include bounding basins. I include an underplate like that below the west arm, although seismic data needed to resolve it are lacking, because such underplates are also seen below the RR, have been proposed below the SOA, are common in rifts worldwide (Thybo and Artemieva, 2013; Rooney et al., 2017), and are expected given the igneous rift fill (Vervoort et al., 2007). The largest difference between the models is the thickness of rift-filling volcanics; the west arm contains 20–25 km of volcanics, whereas the east arm contains 10–15 km. The dense igneous rocks affect the gravity anomaly much more than the underplate, so the geometry of the volcanics in the east arm was adjusted to match the gravity profiles.

3.4. Southern Oklahoma Aulacogen

The Southern Oklahoma Aulacogen (SOA) (Walper, 1977) is a linear alignment of extensively inverted rift structures perpendicular to the southern tip of the MCR's west arm. Its main structures are the Wichita uplift (and associated igneous provinces) and Anadarko Basin. Both the SOA and RR (discussed shortly) initiated as the Cuyania block, also known as the Argentine Precordillera, rifted away from Laurentia (Thomas, 2011; Whitmeyer and Karlstrom, 2007). Rifting is thought

to have begun in latest Precambrian, but the oldest dates come from SOA igneous rocks dated at ca. 540 Ma (Wall et al., 2021).

The SOA's geologic and tectonic history has three major phases. The first involved emplacement of the Wichita Igneous Province during development of a rift beginning in the Ediacaran to mid-Cambrian (Brewer et al., 1983; Perry, 1989; Wall et al., 2021). Extensional and transtensional tectonism within the SOA developed during the latest Precambrian–Cambrian opening of the southern Iapetus Ocean as part of Rodinia's breakup (Robert et al., 2021). Following rift failure, thermal subsidence allowed deposition of thick sedimentary sequences, marking the onset of the Anadarko Basin formation (Perry, 1989; Johnson, 2008). Finally, Late Mississippian through Pennsylvanian compression inverted the SOA and formed a NE-trending fold-thrust belt containing the Wichita and Arbuckle Mountains (Keller and Stephenson, 2007). The compression is believed to be related to North America's collision with Africa and South America during the Alleghenian Orogeny (Kluth and Coney, 1981) or tectonic activity along North America's western and southwestern margins (Lawton et al., 2017; Leary et al., 2017). The SOA exposes only a fraction of its extent in the Wichita Mountains and contains more than 210,000 km3 of buried mafic rocks up to 10 km thick along the entire rift (Hanson et al., 2013), along with a large volume of felsic igneous rocks, including granitic intrusions and interbedded rhyolites. Emplacement and subsequent inversion of the igneous rocks yielded a positive gravity anomaly of ~60 mGal, similar to the average of the MCR arms.

Our SOA model is modified from Keller and Stephenson's (2007) model based on gravity, seismic, aeromagnetic, surface mapping, and drilling data. Seismic reflection data were used to constrain the location and thicknesses of the gabbroic and felsic intrusions producing the large

positive anomaly. I simplified their model for comparison with the other rifts. Sedimentary basin rocks were averaged into a few units, and bodies within the gabbroic intrusion that increased in density with depth in the original model were averaged to a single density. Keller and Baldridge (1995) proposed the presence of an underplate, which is consistent with the gravity data and included in our model, though seismic data adequate to confirm (or disprove) its presence are not available.

3.5. Reelfoot Rift

The Reelfoot Rift (RR) underlies the Upper Mississippi Embayment, a broad trough with a complex history of rifting and subsidence (Catchings, 1999). The NE-trending graben of the RR is 70 km wide and more than 300 km long. Reflection profiles and mafic alkalic plutons suggest several episodes of faulting and intrusive activity (Mooney et al., 1983). The RR is believed to have experienced multiple phases of subsidence (Ervin and McGinnis, 1975), with the earliest rifting in the Ediacaran associated with widespread rifting along North America's margins during the breakup of Rodinia. The rift basin primarily developed during this Cambrian event. Later subsidence, perhaps as late as the Cretaceous, is associated with emplacement of mafic igneous intrusives inside the rift and deposition of several kilometers of sediments that bury them (Hildenbrand and Hendricks, 1995; Cox and Van Arsdale, 2002). Relative to the MCR and SOA, the RR experienced significantly less volcanic activity during rifting, and its subsidence influenced the sedimentation and subsequent development of the drainage basins of major rivers, such as the Mississippi. Climate-controlled erosion and unloading of sediments that fill the rift basin have

been proposed to have triggered the present seismicity (New Madrid seismic zone) on faults remaining from the rifting (Calais et al., 2010).

I developed my model by modifying one by Liu et al. (2017) based on their work and earlier models constrained by seismic refraction, gravity, and magnetic data (Mooney et al., 1983; Braile et al., 1986; Nelson and Zhang, 1991). Earlier studies identified an underplate, or "rift pillow", whose location is constrained by Liu et al.'s (2017) results. An underplate has also been observed along the RR's northeastern extension (Aziz Zanjani et al., 2019). A feature of our model, required to replicate the lack of a large gravity anomaly, is that the RR contains far less high-density volcanics than the other rifts, perhaps because it extended less. Low-density Quaternary sediments of the Mississippi River basin overlying the rift rocks also contribute to the minimal anomaly.

3.6. Similarities and Differences

Comparing the three rifts' average gravity profiles and subsurface structures inferred in part from them illustrates similarities and differences between the rifts.

3.6.1. Tectonic Setting

All three formed during rifting associated with Laurentia's interactions within the supercontinent of Rodinia. The MCR formed after the Elzeverian and Shawinigan orogenies and before the Grenville Orogeny that assembled Rodinia (e.g., Hynes and Rivers, 2010). Its formation was likely associated with rifting between Laurentia and Amazonia during a plate boundary reorganization (S. Stein et al., 2014, 2018) (Figure 3.4A), although details of Amazonia's location and motion are not well constrained at this time because of limited paleomagnetic data (Tohver et al., 2006; Li et al., 2008).

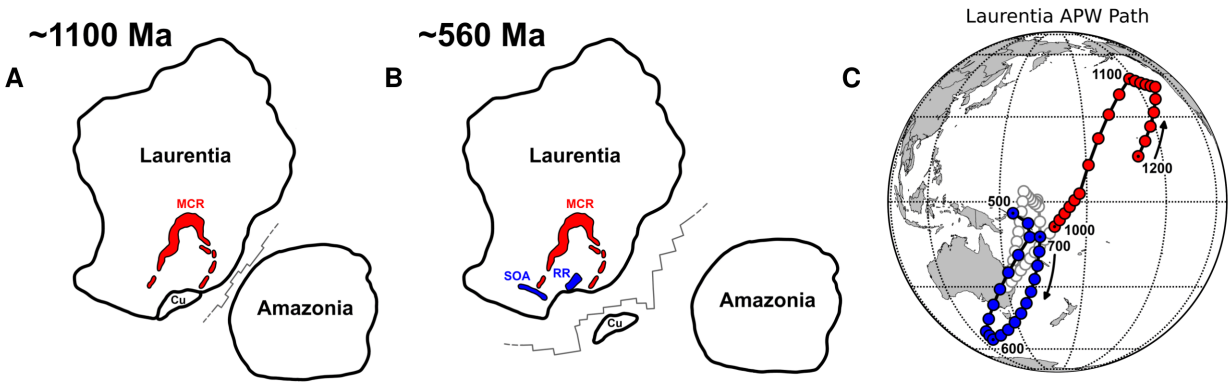

Figure 3.4. (A) Schematic reconstruction of plate positions relative to Laurentia ca. 1100 Ma during formation of Rodinia. After the Elzeverian and Shawinigan orogenies, but before the Grenville orogeny, spreading likely initiated between the major plates. Following failure of the Midcontinent Rift (MCR), Amazonia shifted north along the margin before recolliding. (B) Similar reconstruction at ca. 560 Ma as Rodinia was breaking up. Cuyania (Cu) block rifted off Laurentia, leaving the Southern Oklahoma Aulacogen (SOA) and Reelfoot Rift (RR) as failed arms. (C) Apparent polar wander (APW) path of Laurentia, plotted in present-day coordinates, at 10-m.y. increments. Red cusp (1200–1000 Ma) is related to formation of the MCR, and blue cusp (700–500 Ma) is related to initial rifting of the SOA and RR. Path between these events plotted in gray.

Additional evidence for this view comes from a change in Laurentia's absolute plate motion around the time of the formation of the MCR. A global plate model (Scotese and Elling, 2017), updated with a global compilation of paleomagnetic poles (McElhinny and Lock, 1996; Torsvik et al., 2008, 2012; Merdith et al., 2017; Scotese and Van der Voo, 2017; Veikkolainen et al., 2017), was inverted to generate synthetic apparent polar wander (APW) paths that match the plate model. Comparison with Global Mean Poles (GMP) revealed these synthetic APW paths produce a good fit within the α95 error of the GMPs. Laurentia's APW path has a major cusp, called the Logan Loop, recorded in part by the MCR's volcanic rocks (Figure 3.4C). Cusps in APW paths have been observed elsewhere when continents rift apart (Gordon et al., 1984). A similar cusp appears ca. 600 Ma in this model (Figure 3.4C), during opening of the Iapetus Ocean as the Argentine

Precordillera microcontinent rifted from the Wichita embayment on Laurentia's SE margin (Whitmeyer and Karlstrom, 2007; Thomas, 2011). Both the SOA and RR opened as arms of this triple junction but ultimately failed (Figure 3.4B).

3.6.2. Spatial Scale and Architecture

The three rifts have similar spatial scales and structures that seem to characterize failed rifts. Their central grabens, filled with volcanic and sedimentary rocks, are bounded by faults that presumably had normal fault motion during extension. Despite structural differences, all three rifts are ~60–80 km wide, suggesting that failed rifts are consistent with observations that presently spreading rifts had initial widths controlled by crustal thickness rather than the extension history (Allemand and Brun, 1991).

For the MCR and SOA, the rifting faults were reactivated as reverse faults during subsequent inversion. The SOA's gravity high reflects structural inversion of basaltic and gabbroic material in the Wichita Mountains, but significant amounts of rift-fill remain buried beneath the Anadarko Basin (Keller and Stephenson, 2007). Although the RR looks similar overall, it was not significantly reactivated by later inversion. This left its rift-filling volcanics deeper in the subsurface, causing the absence of a positive gravity anomaly. This effect is illustrated by a model showing the gravity anomaly at different stages in the MCR's evolution (Figure 3.5), derived from cross-section–balanced reconstructions from GLIMPCE data (Stein et al., 2015). During rifting, dense volcanics near the surface would have caused a large positive anomaly. Subsequent deposition of low-density sediments and subsidence that depressed the volcanics would have caused a gravity low. Eventually, inversion of the rift and erosion and removal of low-density

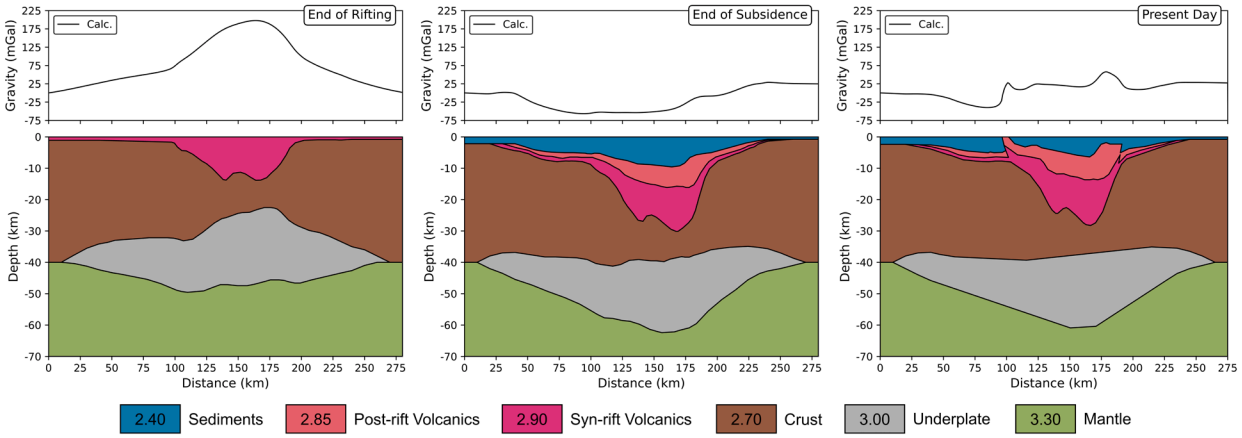

Figure 3.5. Gravity anomalies expected at various stages in rift evolution, based on model for the Midcontinent Rift under Lake Superior. During rifting, dense volcanics cause a large positive anomaly. Subsequent deposition of low-density sediments and associated subsidence cause a gravity low. Inversion of the rift and erosion of low-density sediments cause the high observed today. Densities in g/cm^3. (After Elling et al., 2020).

sediments brought the volcanics closer to the surface, causing today's gravity high. Without this inversion, a positive anomaly would not have developed.

I explored the hypothesis that inversion is crucial for producing a positive gravity anomaly using the SOA and RR. The SOA experienced up to 15 km of inversion in the late Paleozoic (Keller and Stephenson, 2007). "Uninverting" the rift by re-burying the gabbroic fill 12 km below a sedimentary basin eliminates the positive anomaly (Figure 3.3E). Hence the SOA's gravity high largely reflects the inversion. Conversely, because the RR did not experience significant inversion, its rift basin is buried beneath low-density sediments. Inverting the RR by 3 km and removing sediments overlying the basin (Figure 3.3F) produces a positive anomaly due to the high-density igneous rift fill being much nearer to the surface.

3.6.3. Igneous Rock Volumes

There are interesting differences in the volumes of rift volcanics. The MCR is ~3000 km long and contains more than 2 million km^3 of buried igneous rocks, while the SOA and RR are both roughly 1/10 the length of the MCR and contain significantly less volcanics. Although the SOA's volcanic package produces a large positive gravity anomaly, it contains only ~1/10 as much volcanics as the MCR (Hanson et al., 2013).

The differences appear in the cross sections. Volcanics in MCR's west and east arms have average cross-sectional areas of 1100 km^2 and 680 km^2, the SOA has an average cross-sectional area of 470 km^2, whereas the RR's cross-sectional area is much smaller (160 km^2). How these differences arose is unclear. The volumes of igneous rocks produced in rifting can reflect two effects. The first is passive rifting in which extension due to far-field forces causes lithospheric thinning and inflow of hot asthenosphere, such that greater extension produces more melt (Koptev et al., 2015). The second, active rifting, involves an upwelling thermal plume, such that melt is generated by elevated mantle temperatures beneath the lithosphere (Burov and Gerya, 2014). The relative roles of these and other possible rifting processes (King, 2007) are extensively debated but remain unclear (Foulger, 2010). Both active and passive rifting have been invoked to explain the volumes of volcanic rocks at rifted continental margins (White and McKenzie, 1989; Richards et al., 1989; van Wijk et al., 2001). Gallahue et al. (2020) find evidence for both processes on continental margins, with passive rifting having a stronger effect.

A plume contribution for the MCR has been inferred from petrologic and geochemical data (Nicholson et al., 1997; White, 1997; Davis et al., 2021), consistent with the enormous volume of volcanic rocks making it a Large Igneous Province (Green, 1983; Stein et al., 2015). The large

volume of MCR rocks also likely reflects Precambrian mantle temperatures higher than today's (Korenaga, 2013). The difference between the west and east arms likely reflects a difference in the amount of extension during rifting (Merino et al., 2013; Elling et al., 2020). The smaller cross-sectional areas of volcanics in the SOA and RR probably do not require assuming a plume. Hence, in our view, the simplest explanation of the differences between the SOA and RR, which formed about the same time in similar events, is that the RR had less extension and inversion.

Although models without underplates could fit the gravity data, I include underplates because seismic data both from the MCR (below Lake Superior and on its west arm) and RR show them, and underplates are typically observed at presently spreading rifts. Furthermore, underplates are thought to form from residual melt after extraction of low-density lavas and would be expected given the volume of volcanic material in these rifts. I expect their size to be proportional to the volume (cross-sectional area) of volcanics, as observed for rifted continental margins (Gallahue et al., 2020). Hence, the similar underplates beneath the western MCR and RR are surprising, given that the MCR has roughly ten times more volcanics in cross section. One possible explanation is that in addition to the volcanics in our RR model, another volcanic unit, a mafic high-density upper crustal layer, also exists. Liu et al. (2017, p. 4581) suggest this possibility while noting that such a layer is not required by the data and would be "rare, if not previously unrecognized, for continental rifts." Another possibility is that during the mid-Cretaceous, as the area passed over the Bermuda plume (Cox and Van Arsdale, 2002), plume-derived material may have augmented the underplate. An improved understanding of the relation between the volcanics and underplate would be helpful in understanding the transition between the final stages of continental rifting and early stages of seafloor spreading.

3.7. Conclusions

Traditionally, studies have considered the major failed rifts in central North America separately. However, it is useful to consider them as similar although not identical entities and to view them in the context of both failed and active rifts worldwide. Although they are grossly similar, with similar tectonic origins and structural features, interesting differences between them reflect the extent to which extension, magmatism, subsidence, and inversion by later compression occurred. Further study of these and other failed rifts would provide additional insight into how many rifts transition from the final stages of continental rifting to the early stages of seafloor spreading.

CHAPTER 4

The PALEOMAP Paleopole Compilation:

A Paleomagnetic Database for use in Global Plate Modeling

4.1. Summary

Models of plate motions in the distant past are less constrained than modern day motions, because no sea floor exists older than a few hundred million years. For example, many uncertainties remain about the complex tectonic interaction between Amazonia and Laurentia during the Grenville Orogeny, or for time intervals like the Ediacaran (~635–441 Ma), when paleopoles are widely dispersed. I compiled publicly available paleomagnetic data from the PALEOMAGIA, Global Paleomagnetic Database (GPMDB), and compilations of Torsvik and Van der Voo databases to produce the most complete database to date of Phanerozoic and Precambrian paleomagnetic data available, the PALEOMAP Paleopole Compilation (PPC). Two important features of this compilation are: 1) all data have been recast into a uniform format, and 2) the data were reformatted so that they could be combined with state-of-the-art software (GPlates) to test and produce new plate tectonic models. For example, apparent polar wander (APW) paths can be easily calculated for any tectonic element and diverse paleomagnetic data can be combined into Global Mean Poles (GMPs) that describe the past location of Earth's axial geocentric magnetic dipole, which is assumed to be coincident with the spin axis. Recently published highly reliable poles agree well with the PPC, validating its usefulness. I use this database in Chapter 5 to test whether the shapes of APW paths reflect the timing of important plate tectonic events such as rifting and continental collision.

4.2. Introduction

Since the proposal of continental drift in the early twentieth century, the idea of large-scale motions of rigid sections of Earth's crust has been a fundamental principle in the geosciences.

After the widespread acceptance of plate tectonics in in the 1960's, paleomagnetic data have allowed us to reposition the continental and oceanic plates and reconstruct their interactions through time. One recurring feature of global plate motions is the formation and breakup of supercontinents. Plate tectonics is also fundamental to the diversification and divergence of environments and life-forms. For example, the late Precambrian supercontinent Rodina, first recognized by Valentine and Moores (1970) and named from the Russian word "rodit" meaning "to beget" or "to give birth", was considered to have been the antecedent of all subsequent continents and its shallow seas were postulated to be "the cradles of the earliest animals" (McMenamin and McMenamin, 1990). The concept of Rodinia quickly gained traction and three key papers published nearly simultaneously in 1991 reviewed the geological evidence supporting the assembly and break-up of this supercontinent (Moores, 1991; Dalziel, 1991; Hoffman, 1991). A key feature of the Rodinia model is the SWEAT fit, which links the Southwest U.S. and East Antarctica.

Another important connection established by these early reconstructions of Rodinia was the collision of Amazonia (cratonic South America) with the east coast of Laurentia during the Elzeverian, Shawinigan, and Grenville orogenies, a sequence of collisions that took place over hundreds of millions of years and culminated with the assembly of Rodinia. Metamorphic and igneous rocks as well as a complex deep crustal root provided evidence for a mountain-forming collisional event (Goodwin, 1996; McLelland et al., 2013). Grenville-aged rocks found in coastal Labrador and southwest Texas indicate that these orogenies may have occurred in a series of discrete contractional phases as continental blocks and island arcs collided with and accreted to eastern Laurentia (Tohver et al., 2002, 2006; Rivers et al., 2012; McLelland et al., 2013).

Seemingly inconsistent with this collisional environment, the Midcontinent Rift (MCR) began extending during this time. The MCR has been proposed to have formed as part of a tectonic readjustment between Laurentia and Amazonia (King and Zietz, 1971; Hinze et al., 1997; Tohver et al., 2002, 2006) after the Elzeverian and Shawinigan orogenies but before the onset of the Grenville Orogeny (C. Stein et al., 2018; S. Stein et al., 2018; Elling et al., 2022). The MCR did not form a new ocean basin and rifting in the system ended ca. 1.096 Ga (Stein et al., 2014, 2015), leaving a failed rift surrounded by the collisional traces of the Grenville Orogeny.

While modern and recent plate motion is becoming easier to model with GPS, marine magnetic anomalies, hotspot tracks, and active deformation, the complex interactions that occurred hundreds of millions of years ago in the Precambrian, such as those between Laurentia and Amazonia during the assembly of Rodinia, remain contested and unresolved due to limited constraints. Paleomagnetic data offer the primary information that can constrain the motion of continents for times when we no longer have hotspot tracks or evidence from seafloor spreading. Combining high quality paleomagnetic data with software that allows us to reconstruct the motion of tectonic plates back through the Precambrian, Scotese and Elling (2017) built a computer simulation describing the evolution of global plate boundaries back to 1.5 Ga. This global plate model utilized the Precambrian paleomagnetic database PALEOMAGIA (Veikkolainen et al., 2017) to constrain the global plate motions. In this chapter, I present how a new compilation of over 15,000 global paleomagnetic poles (see Supplemental Material) was assembled, reformatted for use with GPlates, and used to calculate Global Mean Poles and APW paths for major tectonic blocks during the late Precambrian.

4.3. Data Compilation

Researchers have recently begun extending continuous global paleogeographic models back into the Precambrian (e.g., Li et al., 2008; Pisarevsky et al., 2014; Pehrsson et al., 2016; Merdith et al., 2017, 2021; Scotese and Elling, 2017). These models of Precambrian plate motion have been made possible by the systematic compilation of paleomagnetic poles (or paleopoles) from around the globe. Most studies rely on few paleopoles that have been deemed to be reliable (e.g., Gordon and Van der Voo, 1995; Merdith et al., 2017, 2021; Evans et al., 2022). Scotese and Elling (2017) took an alternate approach which began with an unbiased look at all the data and chose not to reject paleopoles solely based on reliability factors such as the Q number (Van der Voo, 1990). Having more data allows the modeler to consider all the possible evidence for a plate's location at any given time. Furthermore, using an ensemble of poles from all plates rather a single plate encourages a view of the bigger picture during supercontinent cycles.

To facilitate the construction of the Precambrian plate tectonic model, I merged paleomagnetic pole data from four paleomagnetic datasets into a standard data format so that the data could be used with the plate-modeling software, GPlates. Duplicate poles were identified based on their reference numbers and consolidated where possible. The best-known dataset, the Global Paleomagnetic Database (GPMDB) was established in 1991 (McElhinny and Lock, 1996) and has been updated every two years since then, with the current version being GPMDBv4.6b (Pisarevsky, 2005). The GPMDB database utilizes Microsoft Access. Its most recent version was released in 2011 and includes all published data up to December 2004. Recent addenda include Australian data published up to January 2011, and additional data published between 2005 and

2010. The next update will be released in the near future (Evans, et al., 2022). In its current form, the database contains over 9,500 paleopoles.

A second database, the PALEOMAGIA database (Veikkolainen et al., 2017), was jointly assembled by paleomagnetists at the University of Helsinki and Yale University. The goal of the project was to offer easy access to Precambrian paleomagnetic data for use in the geo- and paleomagnetic research communities. PALEOMAGIA was used to constrain the global Precambrian reconstructions of Scotese and Elling (2017). While PALEOMAGIA was built primarily from data in the Global Paleomagnetic Database (GPMDB) (Pisarevsky, 2005), it has been updated frequently with new data gathered from peer-reviewed journals as well as archival data. It currently contains 3,799 paleomagnetic poles from over 1,000 individual studies and provides an unprecedented resource for Precambrian plate reconstructions.

For completeness of the compilation, and to provide paleomagnetic constraints for the assessment of the relationship between Phanerozoic APW paths and tectonic events described in Chapter 5, two additional Phanerozoic paleomagnetic datasets were included in the PALEOMAP Paleopole Compilation. These are the databases of Van der Voo (1993) and Torsvik et al. (2008, 2012). Van der Voo (1993) compiled 1,637 Phanerozoic paleomagnetic poles for several well-studied cratons. Torsvik et al. (2008) assembled up-to-date paleomagnetic data from original sources and graded the poles according to Van der Voo's quality or "Q" classification system (Van der Voo, 1990, 1993). This early version of the Torsvik dataset contained 419 paleomagnetic poles dating back to the Late Carboniferous. In 2012, Torsvik updated the compilation with new and expanded results to provide a robust database of paleomagnetic poles from the Late Cambrian to

the Paleogene (Torsvik et al., 2012). Combined, the Torsvik datasets provide 942 robust and graded Phanerozoic paleopoles.

These four paleomagnetic datasets contain over 15,000 paleomagnetic poles from the Archean to present-day. Unfortunately, the original datasets have slightly different formats. Some variables present in one database are absent in another (i.e., declination and inclination) and all databases were missing paleomagnetic information useful for the evaluation of plate tectonic models (i.e., paleolatitude). To be effectively used with state-of-the-art plate modeling software (GPlates), all data needed to be reformatted, standardized, and missing information needed to be recalculated where missing. Documentation of new fields is provided in Table 4.1, which lists and describes the 18 "standard" fields for each paleomagnetic record. The fields – Description, SiteLatitude, SiteLongitude, PoleLatitude, PoleLongitude, QSum, OldAge, YoungAge, Alpha95, and AuthorYear – were obtained from the original databases. In some cases, Declination and Inclination needed be calculated because they are absent in the original databases. In all cases, Paleolatitude and MeanAge needed to be calculated. The paleolatitude (λ) is a function of the inclination (the angle between the vertical component of magnetism and the horizontal) following the dipole equation (van Hinsbergen et al., 2015):

$$\tan I = 2 \tan \lambda \tag{4.1}$$

The poles were then sorted by tectonic element so that each pole could be assigned a PlateID required by the GPlates software to apply the correct plate rotation parameters.

Table 4.1. Documentation of the attributes provided in the database of compiled paleopoles.

Field	Description
URN	The unique reference number of the entry in the database. Reference numbers have been assigned in sequence based on the database the pole was derived from.
Description	Descriptive column, often providing the rock from where the samples were gathered, as listed in the original databases.
PlateID	The unique ID number of the plate that each pole is assigned to for rotation calculations done using the GPlates software.
SiteLatitude, SiteLongitude	The latitude (°N) and longitude (°E) of the sampling site in decimal degrees.
PoleLatitude, PoleLongitude	The latitude (°N) and longitude (°E) of the mean paleomagnetic pole in decimal degrees.
PaleoLatitude	The latitude that the sample would have been at during initial magnetization. Paleolatitude is calculated using the inclination and the dipole equation (4.1).
Declination, Inclination	Declination and inclination of the characteristic component of the natural remanent magnetization in decimal degrees.
Qsum	Sum of the 6 quality parameters from Van der Voo (1990). N/A where not provided.
OldAge, YoungAge	Estimated lower and upper limits of the age of the magnetization (age interval) as determined using the isotopic results or geological information, denoted in million years (Ma).
MeanAge	Average between the old and young ages of magnetization.
Alpha95	The 95% confidence circle of the pole in degrees and decimals in cases where site mean poles have been used to obtain the pole.
AuthorYear	Primary reference where the paleomagnetic data has been obtained.
Database	Reference database where this pole was compiled from.
DatabaseResNo	Unique result number of the pole in the original database for reference.

Once PlateIDs were assigned and paleolatitudes were calculated, PaleoPolePlotter (https://www.earthbyte.org/a-paleomagnetic-database-for-gplates-paleopoles-declination-arrows-and-paleolatitudes/) and PaleoDataPlotter (https://www.earthbyte.org/paleomap-paleoatlas-for-gplates/) were used to build the paleopole symbology such as declination arrows and paleolatitude numerals that would assist in visualizing and constraining plate motions.

Finally, it is important to realize that although some polarity sequences have been recognized and are well-defined during the Precambrian, the absolute polarities of paleomagnetic poles are generally unknown. Hence, it is difficult to know whether an individual paleopole represents the north or south magnetic pole. To deal with this uncertainty, both north and south paleopoles were created for each paleomagnetic record by calculating antipoles using:

$$\text{Antipole Latitude} = (-1) \times \text{Latitude} \tag{4.2}$$

$$\text{Antipole Longitude} = \text{Longitude} + 180° \tag{4.3}$$

4.4. Global Mean Pole (GMP) Calculation for use in APW Path Analyses

Apparent polar wander (APW) is the motion of Earth's spin axis relative to a fixed reference frame, often a tectonic plate or stable interior of a continent (Gordon and Van der Voo, 1995). APW paths offer simple ways to visualize the motion of continents back through time. Assuming that the Earth's magnetic field can be approximated by a geocentric axial dipole, it is possible to estimate the location of the spin axis by combining individual paleopoles into a Global Mean Pole (GMP) for a specific time. Various methods can be used to select the paleopoles that are to be included in the GMP. A simple approach is to average the individual poles that occur over a selected time interval (Schettino and Scotese, 2005). In this study, a slightly different approach

was taken. GMPs were calculated by combining paleopoles whose age ranges intersected fixed time intervals (Figure 4.1). I used a 20-million-year sampling interval for the Phanerozoic and 50-million-year sampling for the Precambrian. This approach guarantees that a statistically significant number of poles (>30) were available to calculate each mean pole. On average, 76 paleopoles were used to calculate each GMP (Table 4.2). This far exceeds the number of poles usually considered in paleomagnetic studies.

This approach, however, can be confounded by low-quality, poorly dated paleopoles that have long durations (i.e., 100 million years or more), and as a result may be sampled by multiple time intervals. To assure that each paleopole in the PPC was only sampled once when calculating the GMPs, I truncated the age ranges of suspect paleopoles so that they only fell within one sampling interval (Figure 4.1). For the Phanerozoic, these new age ranges were defined as the mean age ± 10 million years, and in the Precambrian the new age ranges were defined as the mean age ± 25 million years.

The revised paleopoles with truncated age ranges were then reconstructed into the model reference frame using the Scotese Precambrian Global Plate Model (Scotese and Elling, 2017) and GMPs were calculated back to 1.5 Ga. After reconstruction, some paleopoles were still located well away from Earth's spin axis. There are many reasons why this might be, the most likely being due to poor age-dating, low quality numbers, complex or poorly understood tectonics, or remagnetization. I did not want to include these poor-quality data in the calculations of GMPs and subsequent APW paths, so poles more than 45° from the spin axis were rejected. This technique of trimming paleopoles that do not meet a 45° cutoff is a common practice. Unlike other studies

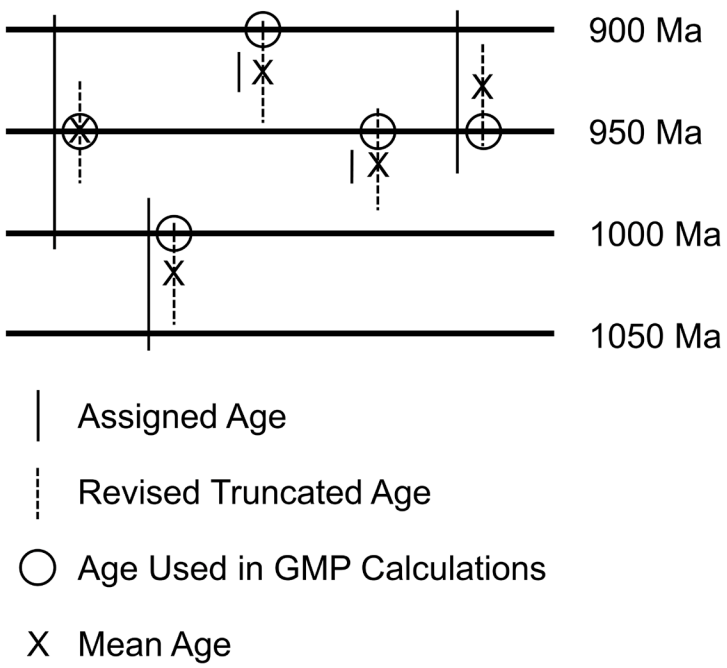

Figure 4.1. Schematic timeline of truncated ages reassigned to the paleopoles for use in GMP Calculations.

(e.g., Gordon and Van der Voo, 1995; Merdith et al., 2017; Evans et al., 2022), I tentatively accepted paleopoles that have low quality (Q) or reliability scores. After applying these selection criteria, roughly 30% of the total database was used, or 3893 of the 13,216 total poles between 1500 and 0 Ma. The GMPs were calculated using standard Fisherian statistics, along with the associated precision parameters (κ, a measure of precision; R, the magnitude of a vector sum of unit vectors having the directions of the poles at each time interval) and cone of confidence (A_{95}) (Table 4.2) (Fisher, 1953). The distribution of poles used to calculate each GMP, as well as the GMPs and their associated A_{95} values, are plotted in reference to the present-day north pole in Figure 4.2–Figure 4.7. While presented in the model reference frame, GMPs can be useful in analyzing the motion of plates by rotating them into the plate's reference frame.

Table 4.2. Phanerozoic Global Mean Poles calculated for the PALEOMAP Paleopole Compilation with a 45° cutoff and rotated into the model reference frame of Scotese and Elling (2017).

Age (Ma)	N	Lon (°)	Lat (°)	κ	R	A_{95}
0	52	138.58	88.77	70.75	51.28	2.36
10	70	149.64	85.16	26.34	67.38	3.37
20	75	-161.31	84.30	19.24	71.15	3.83
30	71	175.93	83.16	18.95	67.31	3.97
40	101	-174.43	83.01	18.75	95.67	3.34
50	134	-176.56	83.77	22.43	128.07	2.63
60	158	-162.49	84.61	29.40	152.66	2.10
70	121	-164.97	86.56	35.78	117.65	2.18
80	87	-68.97	88.43	28.85	84.02	2.87
90	91	-38.62	86.60	29.17	87.91	2.79
100	73	-26.27	84.91	29.56	70.56	3.10
120	81	-61.78	86.91	35.07	78.72	2.69
140	43	3.06	88.83	19.65	40.86	5.04
160	104	-39.95	87.95	18.79	98.52	3.28
180	94	25.93	88.63	35.07	91.35	2.50
200	62	84.41	87.46	47.48	60.72	2.64
220	84	115.71	88.76	26.44	80.86	3.06
240	105	6.73	88.25	22.29	100.34	2.99
260	108	-81.86	88.92	21.71	103.07	2.99
280	129	29.62	87.69	34.70	125.31	2.14
300	137	40.54	87.08	52.46	134.41	1.68
320	42	28.64	88.63	22.00	40.14	4.81
340	28	-130.46	88.63	11.85	25.72	8.27
360	22	-103.04	77.77	17.84	20.82	7.55
380	35	21.76	84.86	11.22	31.97	7.58
400	32	24.56	79.48	12.58	29.54	7.46
420	65	66.82	80.71	16.70	61.17	4.44
440	33	-112.83	85.11	21.86	31.54	5.47
460	52	-60.73	77.93	10.19	47.00	6.51
480	31	-72.72	72.49	14.58	28.94	7.01
500	34	-55.99	71.84	20.19	32.37	5.62

Table 4.3. Precambrian Global Mean Poles calculated for the PALEOMAP Paleopole Compilation with a 45° cutoff and rotated into the model reference frame of Scotese and Elling (2017).

Age (Ma)	N	Lon (°)	Lat (°)	κ	R	A_{95}
550	116	48.51	82.33	7.90	101.44	4.99
600	79	64.25	83.32	7.93	69.16	6.05
650	27	-73.50	64.87	10.73	24.58	8.90
700	48	-124.31	79.11	12.57	44.26	6.04
750	65	-88.23	84.05	16.26	61.06	4.50
800	59	-20.43	80.05	11.90	54.12	5.60
850	39	0.39	81.80	8.30	34.42	8.47
900	70	-70.40	83.90	9.60	62.81	5.78
950	102	-68.39	82.47	13.01	94.24	4.04
1000	82	17.24	85.35	7.94	71.80	5.93
1050	84	-14.56	83.51	10.81	76.32	4.93
1100	250	43.81	81.24	16.52	234.93	2.26
1150	67	-77.62	79.51	13.85	62.24	4.83
1200	54	-145.26	81.63	8.81	47.98	6.92
1250	110	-158.41	73.08	12.72	101.43	3.93
1300	54	-60.02	89.21	12.59	49.79	5.69
1350	11	-156.38	82.60	10.38	10.04	14.88
1400	61	-122.14	74.96	16.74	57.42	4.58
1450	103	-110.76	87.20	21.81	98.32	3.05
1500	58	21.14	82.93	11.26	52.94	5.82

Table 4.4. Precambrian Global Mean Poles for the paleomagnetic data from Evans et al. (2022), rotated into the model reference frame of Scotese and Elling (2017).

Age (Ma)	N	Lon (°)	Lat (°)	κ	R	A_{95}
550	18	85.51	65.72	3.00	12.34	24.26
600	13	-72.61	63.12	3.67	9.73	25.22
650	8	-32.10	60.55	3.63	6.07	33.88
700	2	-86.78	43.67	3.89	1.74	N/A
750	10	-136.93	60.99	3.13	7.13	32.76
800	8	173.80	75.98	4.64	6.49	28.86
850	3	-73.15	68.80	3.45	2.42	80.29
900	8	-4.22	68.19	6.35	6.90	23.84
950	5	-157.56	60.52	6.11	4.35	33.70
1000	6	155.98	53.06	3.79	4.68	39.77
1050	10	-24.32	56.90	2.57	6.50	38.04
1100	22	39.00	70.61	4.42	17.25	16.71
1150	7	-123.24	84.32	4.46	5.65	32.25
1200	6	-161.97	66.48	7.00	5.29	27.23
1250	6	-134.57	75.26	14.25	5.65	18.37
1300	6	-10.21	70.03	28.02	5.82	12.88
1350	0	N/A	N/A	N/A	N/A	N/A
1400	9	-133.94	54.14	7.00	7.86	20.94
1450	13	-99.15	87.31	15.43	12.22	10.90
1500	9	8.19	82.00	3.69	6.83	31.17

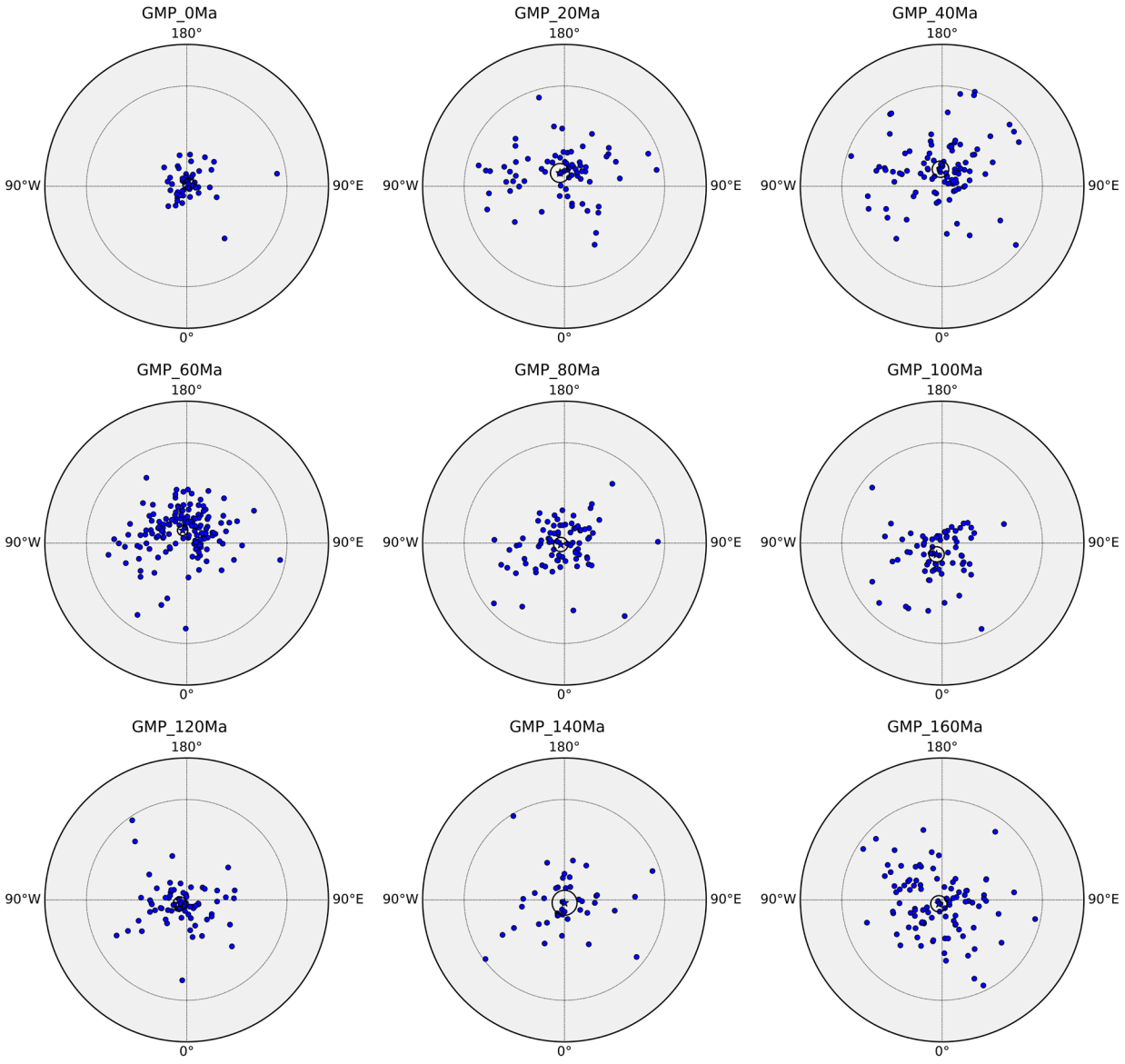

Figure 4.2. Phanerozoic Global Mean Poles (GMPs) for 0 to 160 Ma. Solid blue circles are the paleopoles used to calculate each respective GMP, and blue stars are the locations of the GMPs with their 95% confidence intervals.

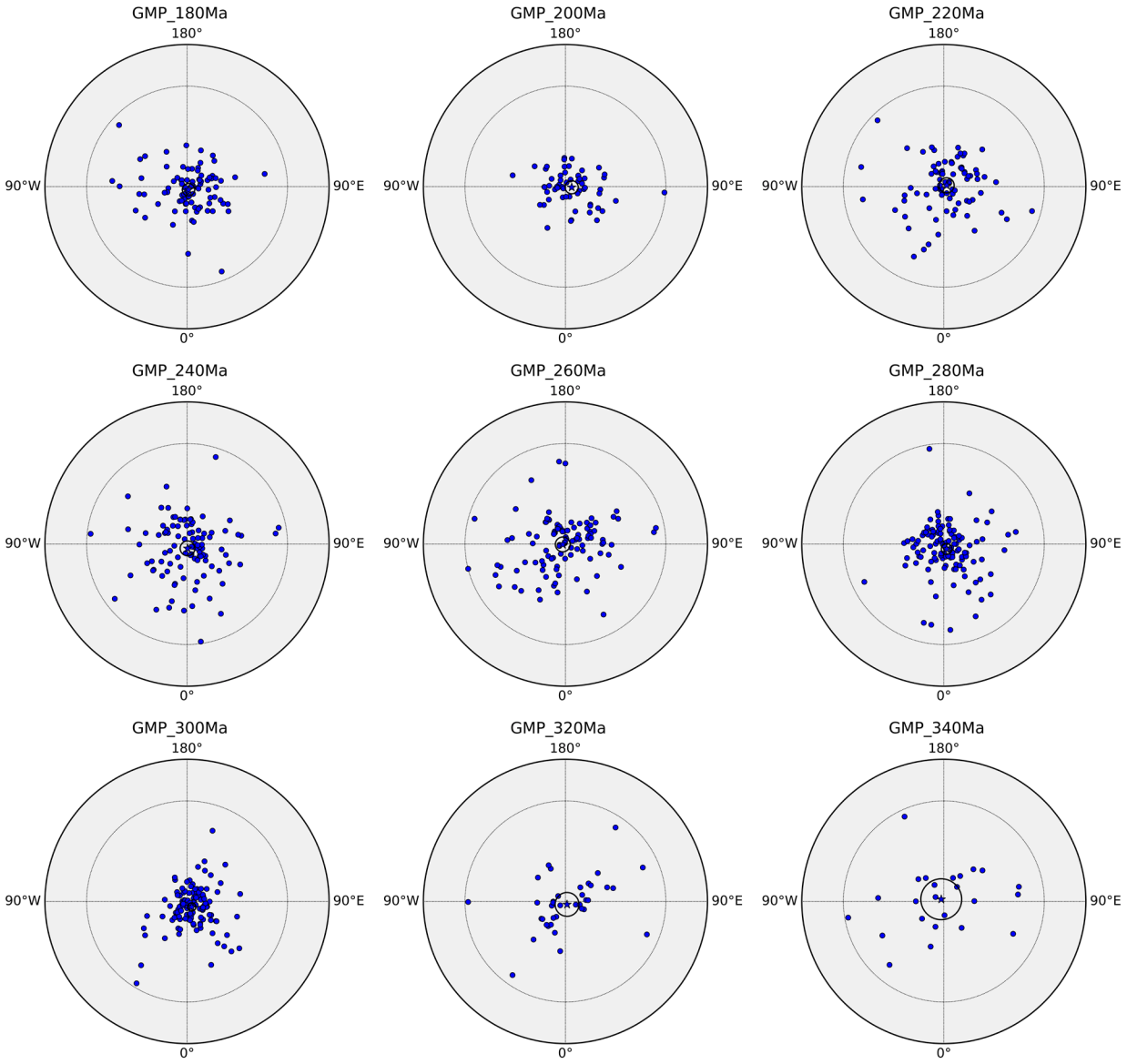

Figure 4.3. Phanerozoic Global Mean Poles (GMPs) for 180 to 340 Ma. See Figure 4.2 caption above for description.

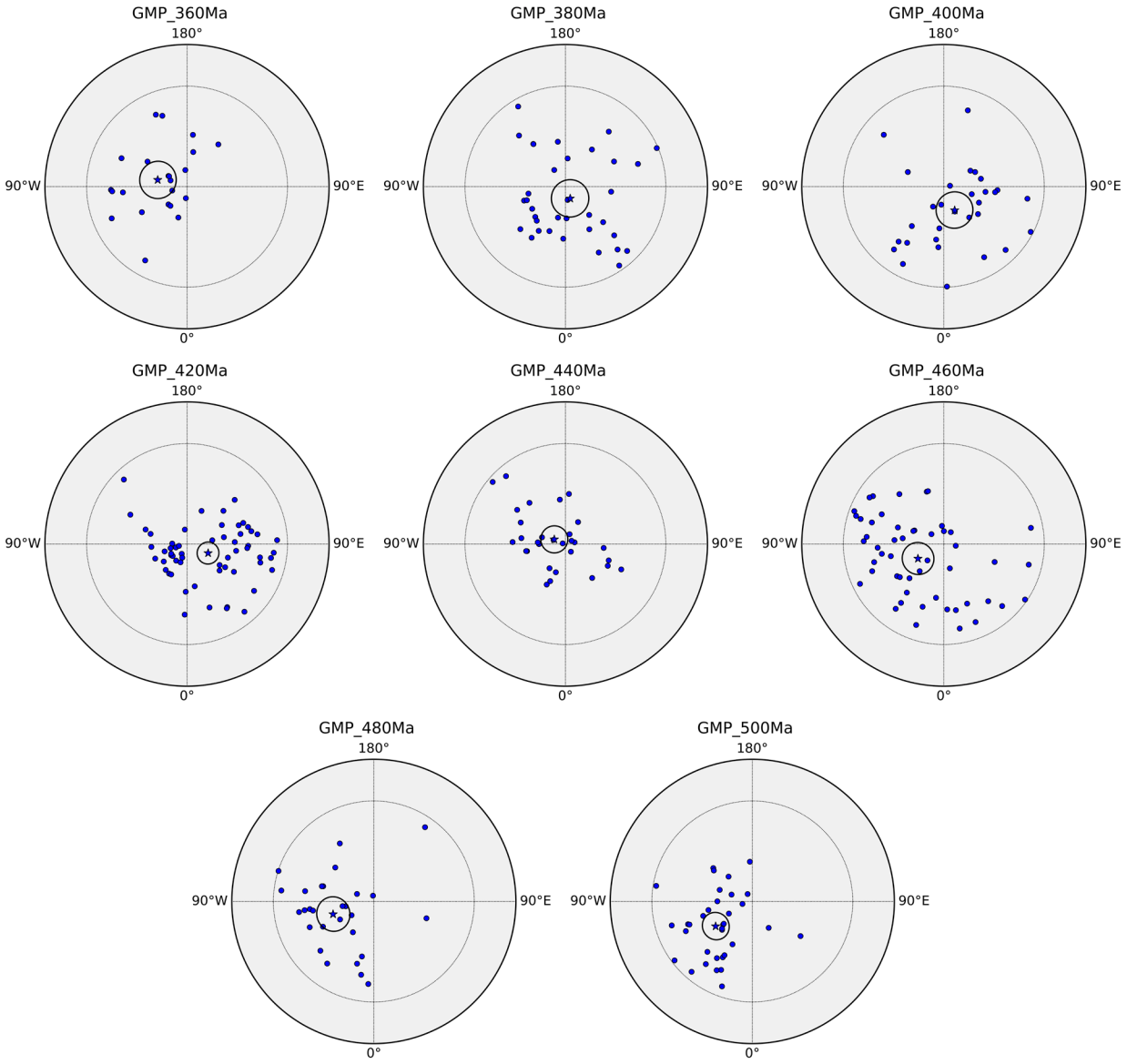

Figure 4.4. Phanerozoic Global Mean Poles (GMPs) for 360 to 500 Ma. See Figure 4.2 caption above for description.

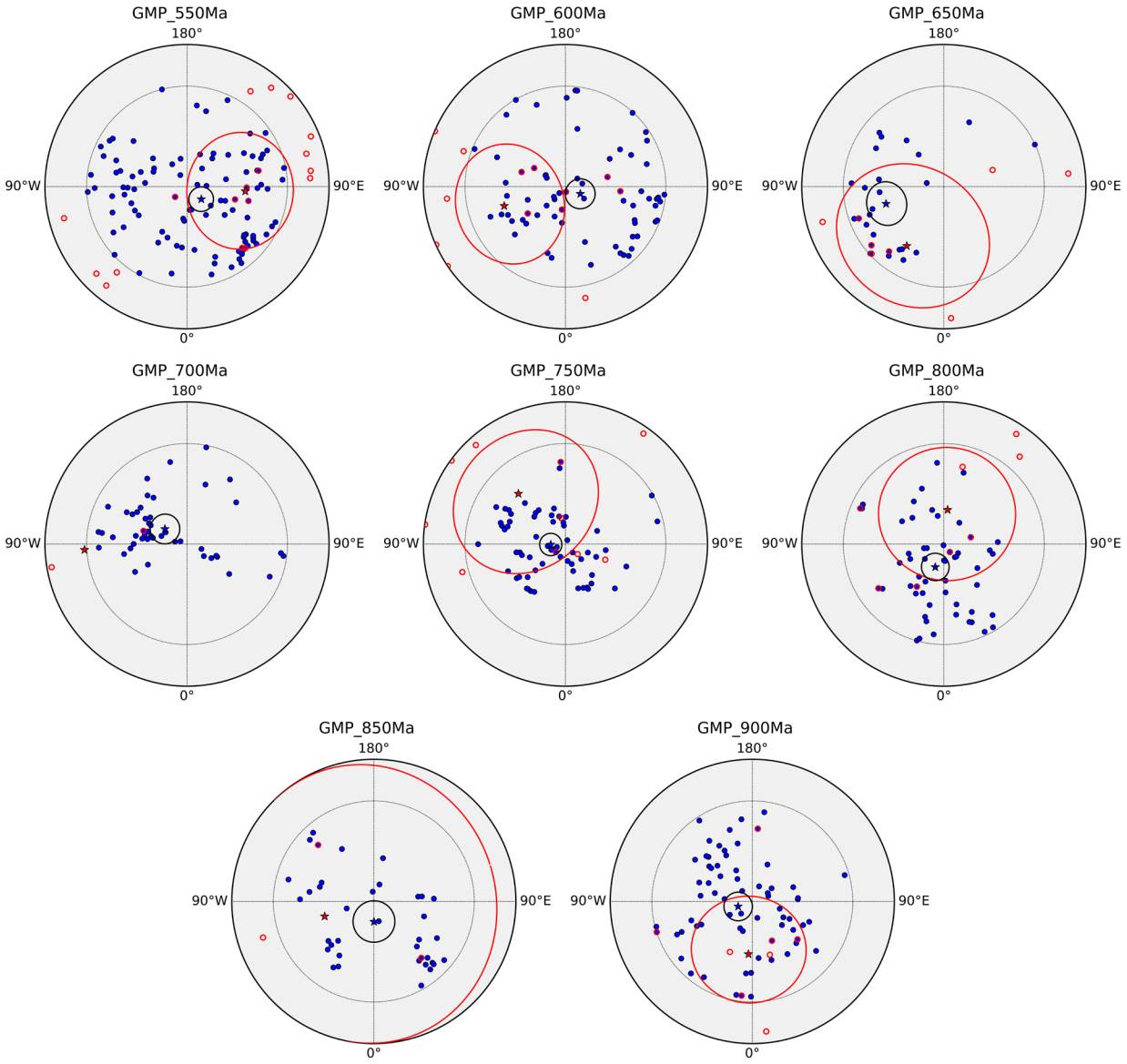

Figure 4.5. Precambrian Global Mean Poles (GMPs) for 550 to 900 Ma. Solid blue circles are the paleopoles used to calculate each respective GMP, and blue stars are the locations of the GMPs and their 95% confidence intervals. Red outlined paleopoles are from Evans et al. (2022), and red stars are the locations of GMPs with their respective 95% confidence intervals.

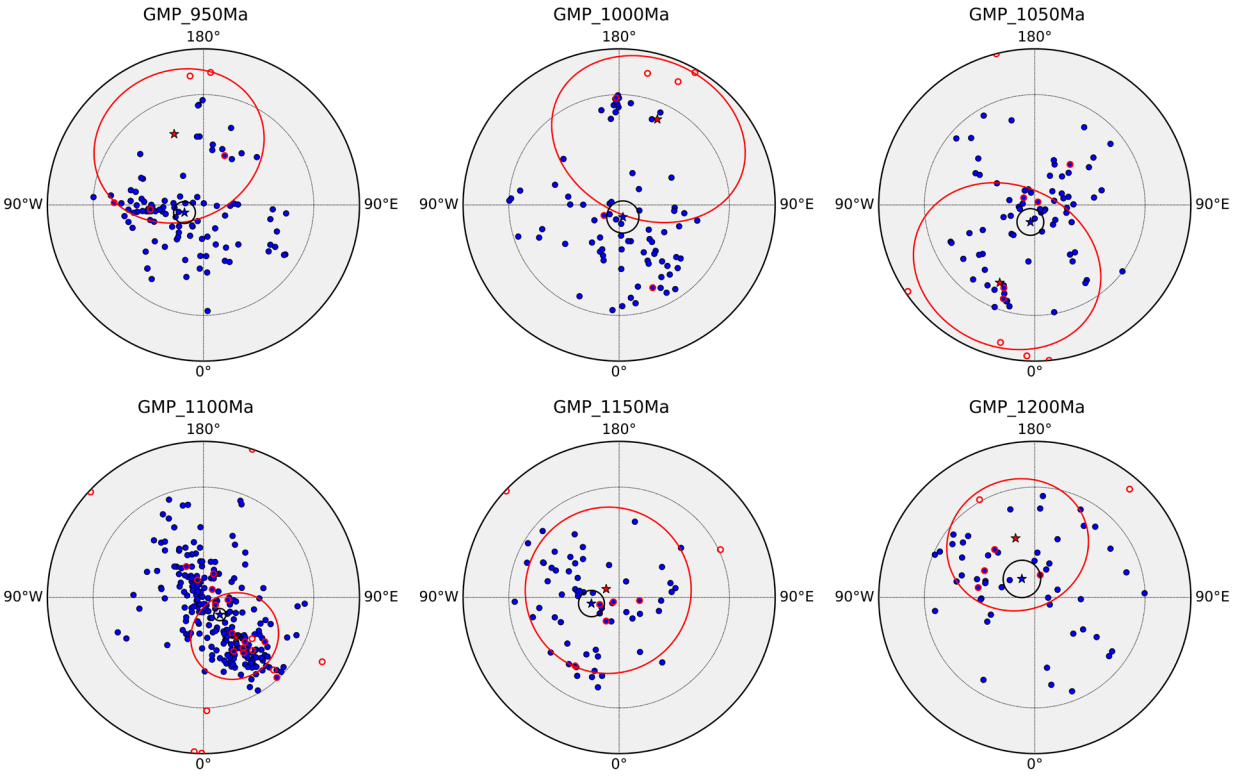

Figure 4.6. Precambrian Global Mean Poles (GMPs) for 950 to 1200 Ma. See Figure 4.5 caption above for description.

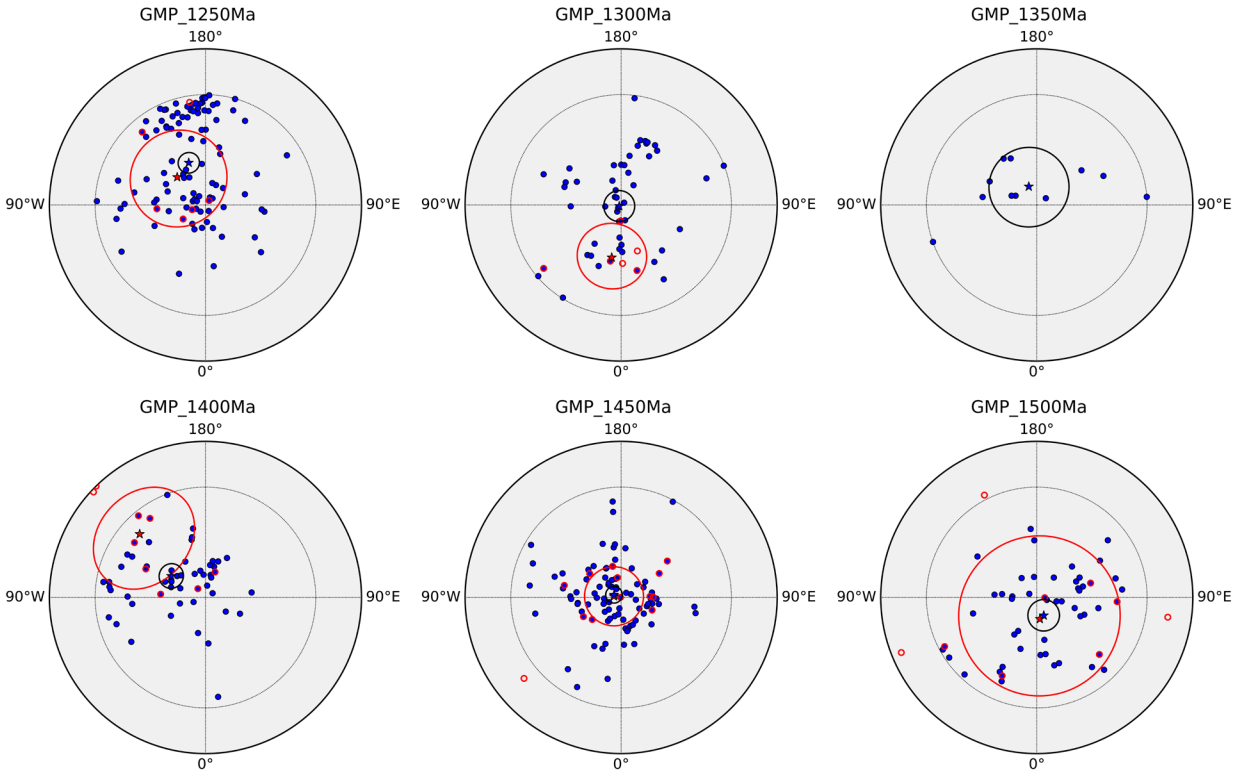

Figure 4.7. Precambrian Global Mean Poles (GMPs) for 1250 to 1500 Ma. See Figure 4.5 caption above for description.

4.5. Comparison With Recently Published Data

After I compiled the original version of the PALEOMAP Paleopole Compilation and calculated the GMPs, a new compilation of Precambrian paleomagnetic poles was published. Evans et al. (2022) compiled what they deemed to be the most "reliable" Precambrian paleopoles. Two classes of poles were recognized: 123 "Grade-A" poles that are of the highest quality, confirmed to be primary magnetizations, and essential constraints on tectonic reconstructions, and 175 "Grade-B" poles that are high-quality but have not yet been confirmed to be primary magnetizations.

In Figure 4.5–Figure 4.7, I compare these high-quality paleopoles with the paleopoles used in my study. All paleopoles were rotated into the reference frame of the Scotese and Elling (2017) global plate model. The paleopoles from the PPC are plotted in blue circles; the highest quality poles of Evans et al. (2022) are plotted in red circles. The Global Mean Poles for both compilations are plotted as blue and red stars, respectively. For many time periods (e.g., 1150 Ma, 1250 Ma, 1450 Ma) the two sets of paleopoles are in good agreement and their respective GMPs are in close proximity. However, in a few instances, the highest quality poles fall well outside the 45° cutoff, indicating that for these time periods the plate tectonic model needs to be reevaluated. At other times, no consensus can be reached, probably due to poor paleomagnetic control. For example, paleopoles for 550 Ma are widely distributed, plotting nearly everywhere on the globe, and many of Evans' paleopoles are far from the north pole. This makes sense, as the Ediacaran period is known to have widely disparate paleopoles (Abrajevitch and Van der Voo, 2010; Meert, 2013) and plate tectonic models for this time period are often regarded as poorly constrained or contentious. At other times, such as 800 Ma or 1000 Ma, the high-quality paleopoles defined by

Evans et al. (2022) are grouped to one side of the north pole. This indicates that small corrections should be made to the global plate model to bring the two data sets into alignment. In general, however, the “Grade-A” and “Grade-B” paleopoles from Evans et al. (2022) agree well with the much larger dataset compiled in this study.

4.6. Conclusions

Revising and compiling the PALEOMAGIA, GPMDB, Torsvik, and Van der Voo paleomagnetic datasets for use with the GPlates software allowed calculation of GMPs at 20-million-year intervals in the Phanerozoic and 50-million-year intervals in the Precambrian. Although many poles in this dataset are excluded from some recent studies on the basis of poor quality or reliability, I believe they may be useful in filling in gaps where other data might not exist, such as 1350 Ma, where Evans et al. (2022) define no high-quality data. These GMPs can also be used in constraining accurate APW paths. The GPlates software allows the creation of synthetic APW paths corresponding to any tectonic element, and in the following chapter I compare these APW paths with the history of major tectonic events to provide insight into the relationship between cusps in APW paths and rifting or collisional events. Analyzing the temporal and spatial constraints on plate movement via paleomagnetic data will allow us to further constrain a more robust model of Precambrian plate tectonics.

CHAPTER 5

What does the shape of Apparent Polar Wander Paths Tell Us About Global Plate Motions?

5.1. Summary

Directional changes, known as cusps and hairpins, in apparent polar wander (APW) paths have long been proposed to be correlated in time with continental rifting or major collisional orogenies. Some evidence for this view comes from a change in the absolute plate motion of Laurentia (the Precambrian core of North America) during the time of the formation of the Midcontinent Rift and the Grenville Orogeny. To test this hypothesis, I analyzed APW paths for 13 major continental blocks from 1200 Ma to present day, calculating the timing of directional changes based on synthetic apparent polar wander paths. Using these data, I compared the timing of directional changes in the APW paths to the timing of major collisions and rifting events throughout the history of each plate as well as adjacent plates during supercontinent cycles. These data reveal a statistically significant correlation between the changes in shape of APW paths and major tectonic events. This approach may be useful in defining tectonic events for time periods when paleomagnetic data exist, but few geologic or geographic constraints are known.

5.2. Introduction

Apparent polar wander (APW) paths are simple representations of the motion of continents with respect to Earth's spin axis. Cusps, or hairpins (Irving and Park, 1972), in APW paths have been observed in the past where continents rift apart (Gordon et al., 1984). Two recent cusps in North America's APW path have been proposed to correspond to major rifting events: a cusp near 180 Ma near the time of the rifting of Gondwana from Laurasia (Bartolini and Larson, 2001; Veevers, 2004), and a cusp around 80–60 Ma near the time of the rifting of Europe from North America (Kristoffersen, 1978; Hallam, 1981). Both of these recent continental breakups were accompanied by a change in plate boundary configuration and a rapid change in the direction of North American motion.

Additional evidence for this view comes from a change in the absolute plate motion of Laurentia (the Precambrian core of North America) during the time of the formation of the Midcontinent Rift (MCR). Laurentia's APW path has a major cusp (Figure 5.1), called the Logan Loop (Robertson and Fahrig, 1971; Pesonen, 1979; Ernst and Buchan, 1993), recorded in part by dyke swarms from the Superior Province in Northern Michigan. Motion of the continent may have been quite rapid during the formation of this loop, and the loop coincides with major orogenesis along the boundaries of North America at this time (Salminen et al., 2009). A similar cusp occurs ca. 600 Ma (Figure 5.1), during the opening of the Iapetus Ocean as the Argentine Precordillera microcontinent rifted from the Wichita embayment on Laurentia's SE margin (Whitmeyer and Karlstrom, 2007; Thomas, 2011). This time period also saw the opening of the Southern Oklahoma Aulacogen (SOA) and Reelfoot Rift (RR), which began spreading as arms of the Iapetus triple junction but ultimately failed to open and remain buried as major failed rifts.

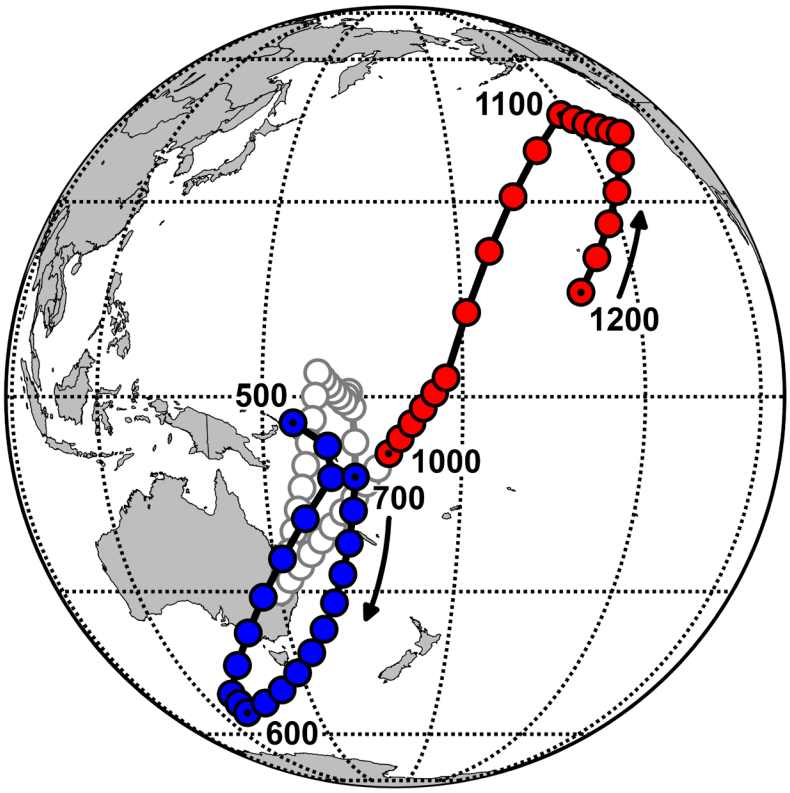

Figure 5.1. Apparent polar wander (APW) path of Laurentia between 1200 and 500 Ma (Elling et al., 2022), plotted with 10-million-year increments in present-day. The red cusp (1200–1000 Ma), sometimes called the Logan Loop is linked to the formation of the Midcontinent Rift (MCR), and the blue cusp (700–500 Ma) is linked to the opening of the Iapetus Ocean off Laurentia's SE margin.

While cusps in Laurentia's APW path have been linked to continental rifts or collisions, many of these instances occur during times of limited paleomagnetic constraints. For example, the change in direction recorded in part by the MCR's volcanic rocks around 1.1 Ga is believed to be related to the rifting of the Amazonian craton from Laurentia between after the Elzeverian and Shawinigan orogenies, but before the onset of the Grenville orogeny (Stein et al., 2018; Elling et al., 2022). However, Amazonia's motion during this time is not well constrained due to limited paleomagnetic data. Likewise, the Ediacaran period of Laurentia's APW path is poorly defined

because paleopoles during this time period are widely scattered (Abrajevitch and Van der Voo, 2010; Meert, 2013). As a result, tectonic arguments are often regarded as poorly constrained and remains contentious.

In the following sections, I present APW paths for thirteen major continental blocks over the last 1.5 Ga that will allow me to test the hypothesis that major tectonic events – such as rifting or collisions – are recorded by changes in the shape of that plate's APW path. I focus on a subset of continental blocks whose relative motions during the Cenozoic and Mesozoic are generally considered well-constrained by hot spot tracks and seafloor spreading isochrons, by the geologic and tectonic histories, and by paleoclimatic and biogeographic information back into the Paleozoic and Precambrian. These continental blocks (and their identification numbers in GPlates) are: Laurentia (101), Amazonia (201), Baltica (301), Siberia (401), India (501), North China (604), South China (611), the Congo craton (701), West Africa (714), Australia (801), Antarctica (802), Rio de la Plata (2011), and the Kalahari craton (7013). The present-day locations of these thirteen cratons and plates are shown in Figure 5.2. Their APW paths, and the analysis of directional changes, are based on a revised global plate model that was created based on a new compilation of paleomagnetic data containing over 13,000 poles ranging from present day to 1.5 billion years ago (Scotese and Elling, 2017).

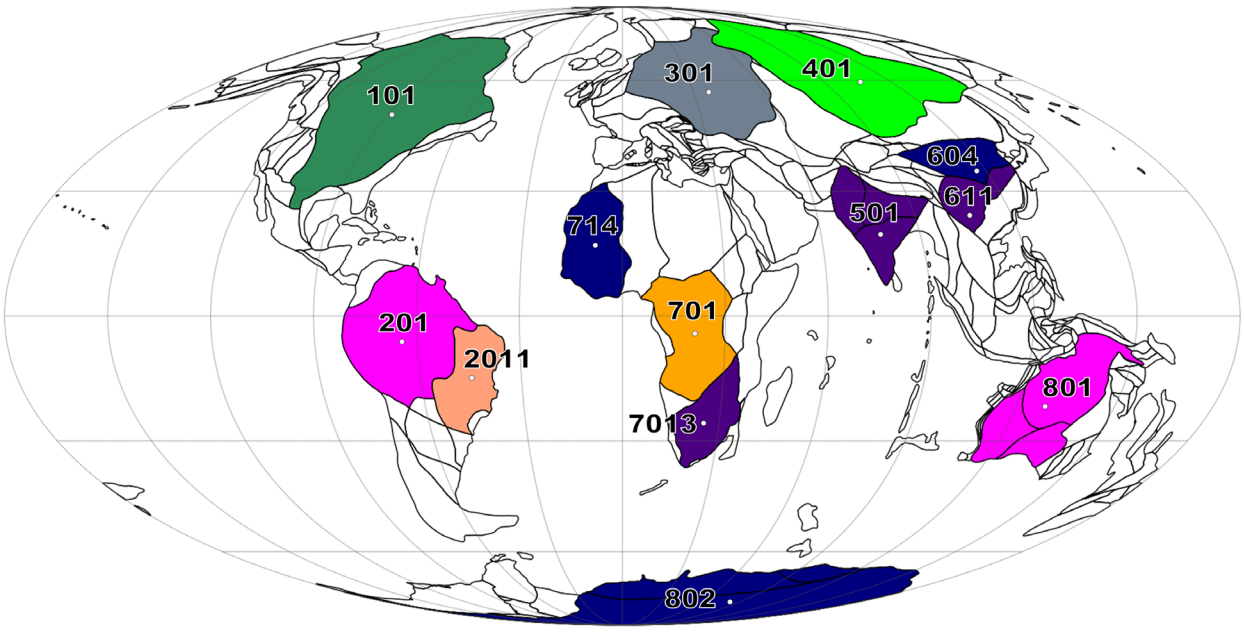

Figure 5.2. Synthetic APW paths were produced for these continental blocks: Laurentia (101), Amazonia (201), Baltica (301), Siberia (401), India (501), North China (604), South China (611), Congo (701), West Africa (714), Australia (801), Antarctica (802), Rio de la Plata (2011), and Kalahari (7013).

5.3. Methodology – Major Tectonic Events and Construction of APW Paths

The "synthetic" APW paths were created by reconstructing the position of the North Pole in the reference frame of each of the continental blocks shown in Figure 5.2. Though each continent has a unique APW path, the APW paths are related because they were produced using the same global plate tectonic model (Scotese and Elling, 2017), which was constrained using the PALEOMAP Paleopole Compilation (PPC) (see Supplemental Material). The number of global paleopoles at each time interval back to 1.5 Ga is shown in Figure 5.3. To test the accuracy of these model dependent APW paths, Global Mean Poles (GMPs) were plotted along the APW path. The GMPs were calculated using standard Fisherian statistics (Fisher, 1953), along with the

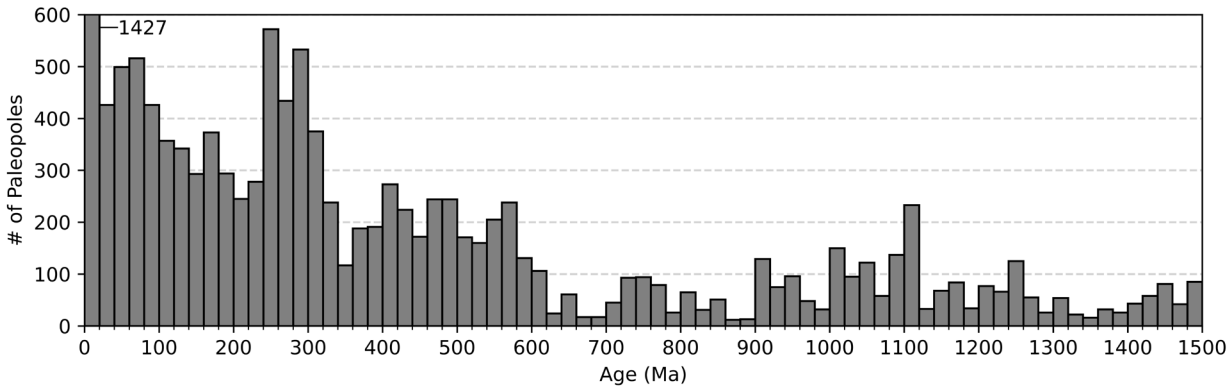

Figure 5.3. Number of paleopoles in the PALEOMAP Paleopole Compilation (PPC) used to constrain the global plate model of Scotese and Elling (2017).

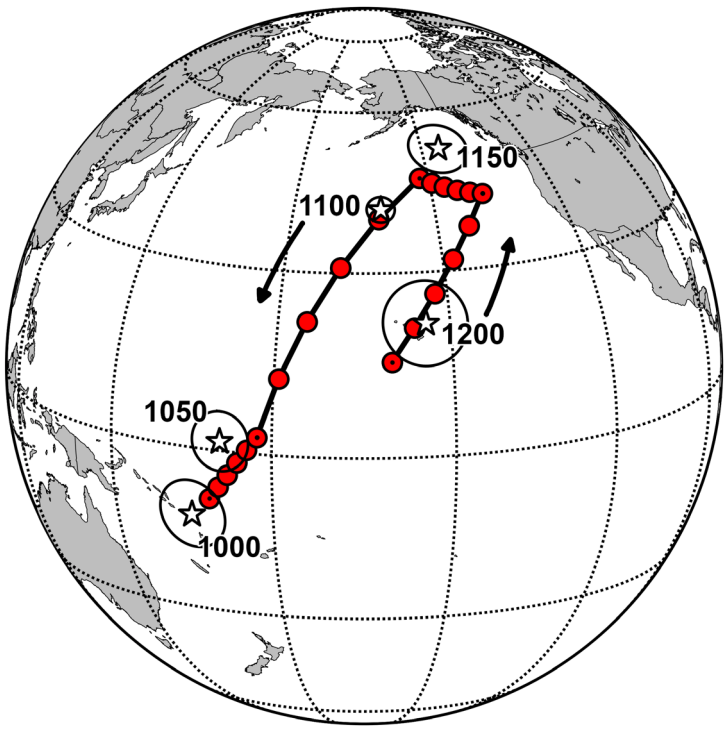

Figure 5.4. Apparent polar wander (APW) path of Laurentia from 1200 Ma to 1000 Ma, plotted in present-day coordinates as red solid circles every 10 million years. Global Mean Poles (GMPs) every 50 million years are plotted as stars with their corresponding A95 confidence circle. A smaller circle represents a more precise grouping of paleopoles. The time intervals on the APW path matching the time of each GMP (1200 Ma, 1150 Ma, 1100 Ma, 1050 Ma, and 1000 Ma) are represented with dots in the center.

associated precision parameters (κ, R) and cone of confidence (A_{95}). The procedure used to calculate the Global Mean Poles is discussed in Chapter 4. A comparison of the GMPs for this time interval (Figure 5.4) shows that Laurentia's synthetic APW path agrees well with the paleomagnetic data. Favorable comparisons were also found for the remaining 12 synthetic APW paths.

To test the hypothesis that tectonic events are directly correlated with changes in plate motion as evidenced by cusps in APW paths, I first built a list of major tectonic collisions and rifting events that occurred during the Mesoproterozoic, Neoproterozoic, Paleozoic, Mesozoic, and Cenozoic (i.e., the last 1.5 billion years) (Table 1). I define major tectonic events as events occurring between adjacent cratons – either as two plates separate during a major rifting event or the breakup of a supercontinent, or the collision between two plates, such as the collisions between Laurentia and Amazonia during the Shawinigan and Rigolet phases of the Grenville orogenic events (Goodge et al., 2002; Rivers, 2008).

I defined 51 major tectonic events, including 21 collisions and 30 rifts over the last 1.5 billion years. For each major tectonic event, I determined a mean (or "peak") age to allow direct comparison with the timing of directional changes in the APW paths. For example, the collisions between Laurentia and Amazonia between 1010–980 Ma that define the Rigolet phase of the Grenville Orogeny (Rivers, 2008) were assigned an age of 1000 Ma. Similarly, the timing of the breakup of Rodinia is considered to have occurred between 800–700 Ma, but the exact dates are not well constrained in the paleomagnetic data (Meert and Torsvik, 2003). For this study, the age of rifting of Rodinia has been assigned a mean age of 750 Ma. I estimate that the average chronological error is ± 5 million years for Phanerozoic tectonic events and ± 25 million years for

Mesoproterozoic and Neoproterozoic tectonic events. The ages and plates involved in the 51 major tectonic events are given in Table 5.1.

Plate motions are primarily driven by forces acting on plate boundaries (Gordon et al., 1984). Hence, not only did I need to consider major rifts and collisions directly impacting a specific plate, but I also needed to determine when each plate was part of a supercontinent configuration and investigate the timing of events that took place for the supercontinent as a whole. Events which occurred at the boundaries of adjacent plates were also included in the history of each plate and plotted as "secondary events" in the analysis of time delay between tectonic events and directional changes – or cusps – in the APW paths.

5.4. Analysis of Apparent Polar Wander Paths

For each plate (e.g., Laurentia, Plate ID = 101), I created synthetic APW paths from the plate model by reconstructing the movement of the North Pole in the reference frame of each continental block (e.g., North America, Figure 5.5A). An APW path is a simple and effective way to visualize a plate's motion throughout Earth's history. The long, straight sections of an APW paths represent time intervals when plate motion was relatively constant. On the other hand, rapid directional changes or cusps represent time intervals when the direction of plate motion changed abruptly.

Plotting the history of tectonic events from Table 1 along the APW paths allows visual comparison of the proposed chronological link between major tectonic events (i.e., rifts and collisions) and directional changes in the APW path. As an example, Laurentia's APW path and the major tectonic events that occurred in the plate's history are plotted in Figure 5.5B. Visually there appears to be a strong correlation. During time periods where rifts (red) or collisions

Table 5.1. Catalog of major tectonic events.

Age (Ma)	Event Type	Primary Plate	Conjugate Plate	Event Name	Reference if applicable
25	Rift	Siberia	Amur?	Baikal Rift Valley	
25	Rift	Congo	Somali/Nubia	East African Rift System	
35	Rift	Baltica	Siberia?	Rhine Graben	
50	Collision	India	Eurasia?	Himalayas	
75	Rift	Antarctica	E/W Antarctica	West Antarctic Rift System	
80	Rift	Laurentia	Baltica	North Atlantic Ocean	Kristoffersen, 1978; Hallam, 1981
100	Rift	Laurentia	Greenland	Canadian Arctic Rift System	
100	Rift	India	Kalahari		
100	Rift	Australia	Antarctica		
120	Rift	Amazonia	W. Africa	South Atlantic Ocean	
120	Rift	Congo	RDLP		
150	Rift	India	Antarctica		
180	Rift	Laurentia	Amazonia	Central Atlantic Ocean	Veevers (2004); Bartolini and Larson (2001)
180	Rift	W. Africa	Laurentia		
180	Rift	Antarctica	Kalahari		
200	Collision	N. China	S. China		
200	Rift	Congo	India		
240	Rift	Laurentia	W. Africa	Fundy Rift Basin	Withjack et al. (1995)
250	Collision	Siberia	N. China		
300	Rift	Baltica	Siberia?	Oslo Rift	
300	Collision	W. Africa	Laurentia		
340	Collision	Baltica	Siberia		
400	Collision	Laurentia	Amazonia	Acadian Orogeny	Ortega-Gutierrez et al. (1999); Dalziel et al. (1994)
440	Collision	Laurentia	Baltica	Gondwana assembly	Torsvik et al. (1996), Meert and Van der Voo (1997)
480	Rift	S. China	Australia		
560	Rift	Laurentia	Amazonia	SOA/RR	Whitmeyer and Karlstrom (2007); Thomas (2011)

580	Rift	Laurentia	Amazonia	Iapetus Ocean	O'Brien and van der Pluijm (2012)
600	Collision	Amazonia	RDLP		
600	Collision	Congo	India		
600	Collision	Antarctica	Kalahari		
750	Rift	Laurentia	Antarctica	Rodinia breakup	Meert and Torsvik (2003)
750	Rift	Siberia	Australia		
750	Collision	India	Aravalli	Aravalli-Delhi Mobile Belt (ADMB)	
900	Collision	Amazonia	Baltica		
1000	Collision	Laurentia	Amazonia	Grenville Orogeny (Rigolet)	Rivers (2008); Goodge et al. (2002)
1000	Collision	Amazonia	Kalahari		
1000	Rift	Amazonia	Kalahari		
1000	Rift	Baltica	Siberia		
1000	Collision	Siberia	Australia		
1000	Collision	Congo	Kalahari		
1000	Collision	W. Africa	RDLP		
1000	Rift	W. Africa	RDLP		
1100	Rift	Laurentia	Amazonia	Midcontinent Rift	Stein et al. (2018)
1150	Collision	Laurentia	Amazonia	Grenville Orogeny (Shawinigan)	Rivers (2008)
1150	Rift	Siberia	Australia		
1150	Rift	N. China	Congo		
1200	Collision	India	Bundelkhand	Central India Tectonic Zone (CITZ)	
1200	Collision	Australia	N. Australia		
1200	Collision	Antarctica	Antarctica		
1450	Rift	Amazonia	India		
1450	Rift	India	W. Africa		

(blue) take place, there are often major changes in the shape of the APW path. To prove or disprove the hypothesis that there is a strong correlation between major tectonic events and the shape of the APW path, I needed to come up with an estimate of "synchroneity" and test whether the observed synchroneity is statistically significant.

To identify directional changes, I calculated the change in azimuth along every 10-million-year step along an APW path. This change in azimuth (Δ azimuth) was plotted for each continental block as shown in part C of Figure 5.5–Figure 5.17. For example, Figure 5.5C shows clearly where Laurentia's plate motion changed abruptly (e.g., 100 Ma, 300 Ma, 360 Ma, 750 Ma, etc.). However, not all directional changes have similar magnitudes. Some changes represent right-angle turns, while others represent more subtle shifts. For the purposes of this study, only direction changes greater than 60° were considered to constitute a major directional change. In Figure 5.5D, solid black lines indicate directional changes greater than 60°.

Dashed red and green lines indicate the "peak" time of each major tectonic event listed in Table 1. I initially compared the average time delay (ΔT, in millions of years) between observed rifts and collisions and determined them to be nearly identical, indicating that the type of tectonic event does not make a difference in whether a cusp occurs in the APW path. Hence, for the purpose of this analysis rifts and collisions were treated equally, yielding average ΔT values for each plate. Red dashed lines are "binary" tectonic events, indicating that the continental block was directly involved in the respective rifting or collisional event. Green dashed lines indicate that the continental block was part of a supercontinent at the time of the tectonic event and was not directly involved in the rifting or collision, as these events would also be expected to affect the motion of plates (Gordon et al., 1984).

The central question now becomes “How synchronous are deflections of the APW path (black lines) and major tectonic events (red and green dashed lines)?”. To make this determination, I used the null hypothesis, “The synchroneity of changes in the shape of an APW path and a given set of known major tectonic events cannot be distinguished from the synchroneity of changes in the shape of an APW path and a simulated set of random tectonic events.” To disprove the null hypothesis it was necessary to: 1) calculate the average time difference (ΔT) between APW shape changes and known ages of the major tectonic events, 2) create a random set of plate tectonic events and calculate the average time difference (ΔT’) between these random events and the changes in the shape of the APW paths, and 3) determine if the ΔT’ was statistically significantly different from the average ΔT. To test this hypothesis, I simulated the history of each plate 200 times with identical APW paths (and thus identical ages of directional changes) but randomized ages for the same number of tectonic events. An example of one of these simulations for each plate is shown in part E of Figure 5.5–Figure 5.17. In these randomized runs, the directional changes occur at the same time I ran these simulations 200 times for the history of each of the 13 tectonic plates defined in this study, with results presented in the following section.

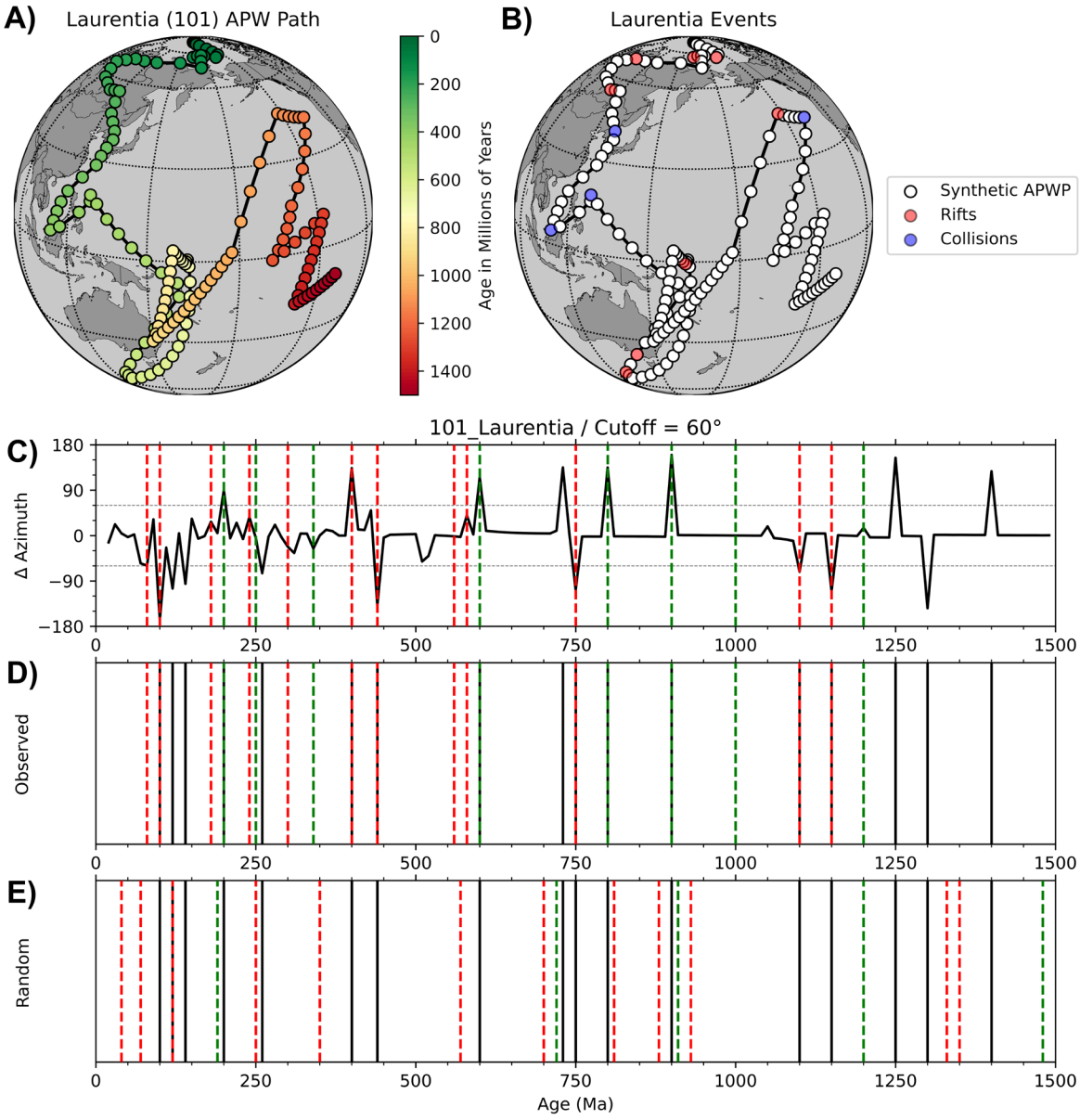

Figure 5.5. (A) Apparent polar wander (APW) path for Laurentia from 1.5 Ga to present day, plotted in present-day coordinates. (B) APW path for Laurentia with major tectonic events from its geologic history plotted. (C) Changes in azimuth calculated every 10 million years. The height of the spikes indicates the angular deflection of the APW path. Red dashed lines are the "peak" ages of events which occurred directly on the boundaries of Laurentia, whereas green dashed lines are the ages of events that took place when Laurentia was part of a supercontinent. (D) Black vertical lines correspond to directional changes in the top plot which are greater than 60°. (E) Example of a single simulation of randomized event ages.

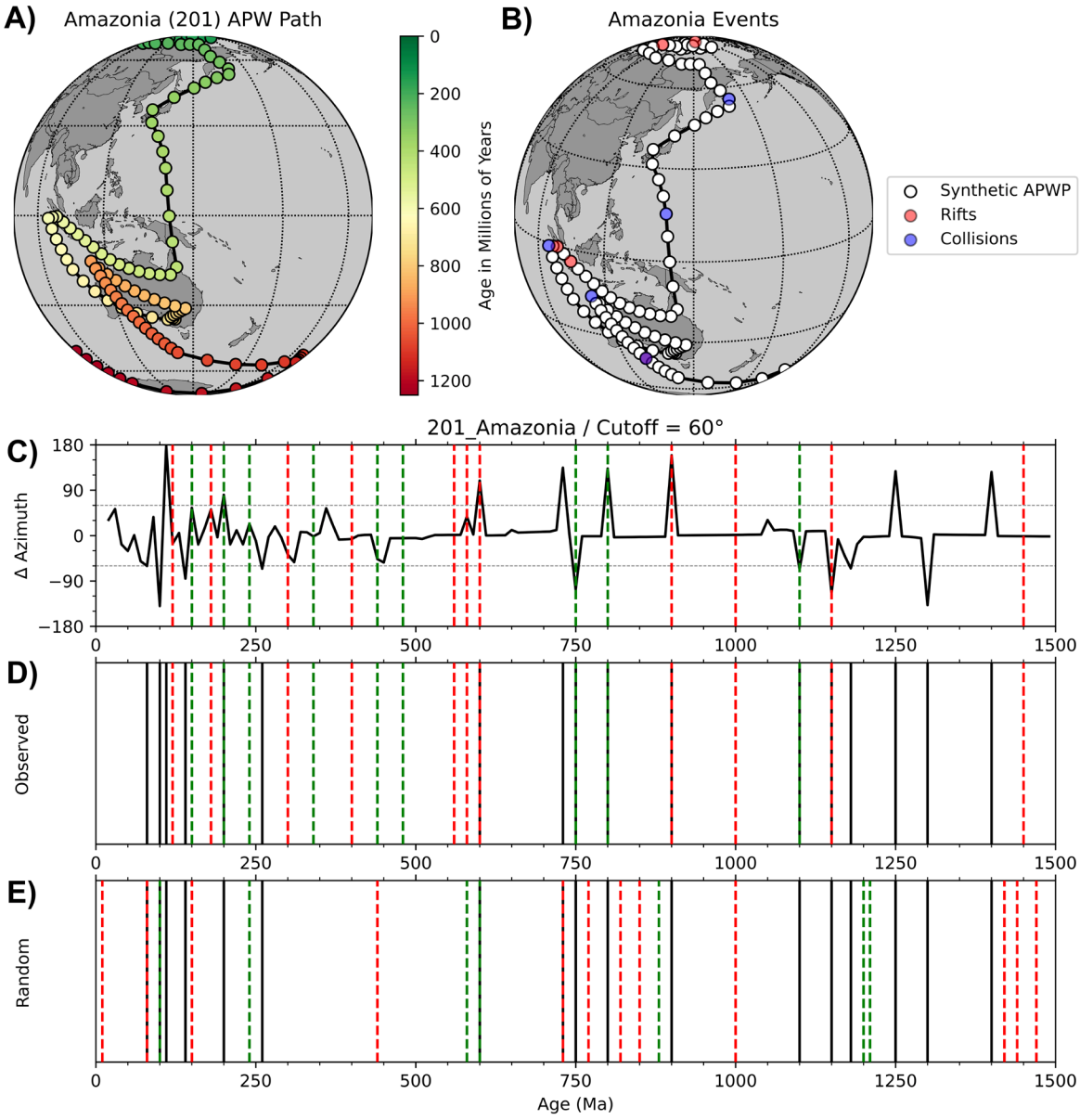

Figure 5.6. (A) Apparent polar wander (APW) path for Amazonia from 1.5 Ga to present day, plotted in present-day coordinates. (B) APW path for Amazonia with major tectonic events from its geologic history plotted. (C) Changes in azimuth calculated every 10 million years. The height of the spikes indicates the angular deflection of the APW path. Red dashed lines are the "peak" ages of events which occurred directly on the boundaries of Amazonia, whereas green dashed lines are the ages of events that took place when Amazonia was part of a supercontinent. (D) Black vertical lines correspond to directional changes in the top plot which are greater than 60°. (E) Example of a single simulation of randomized event ages.

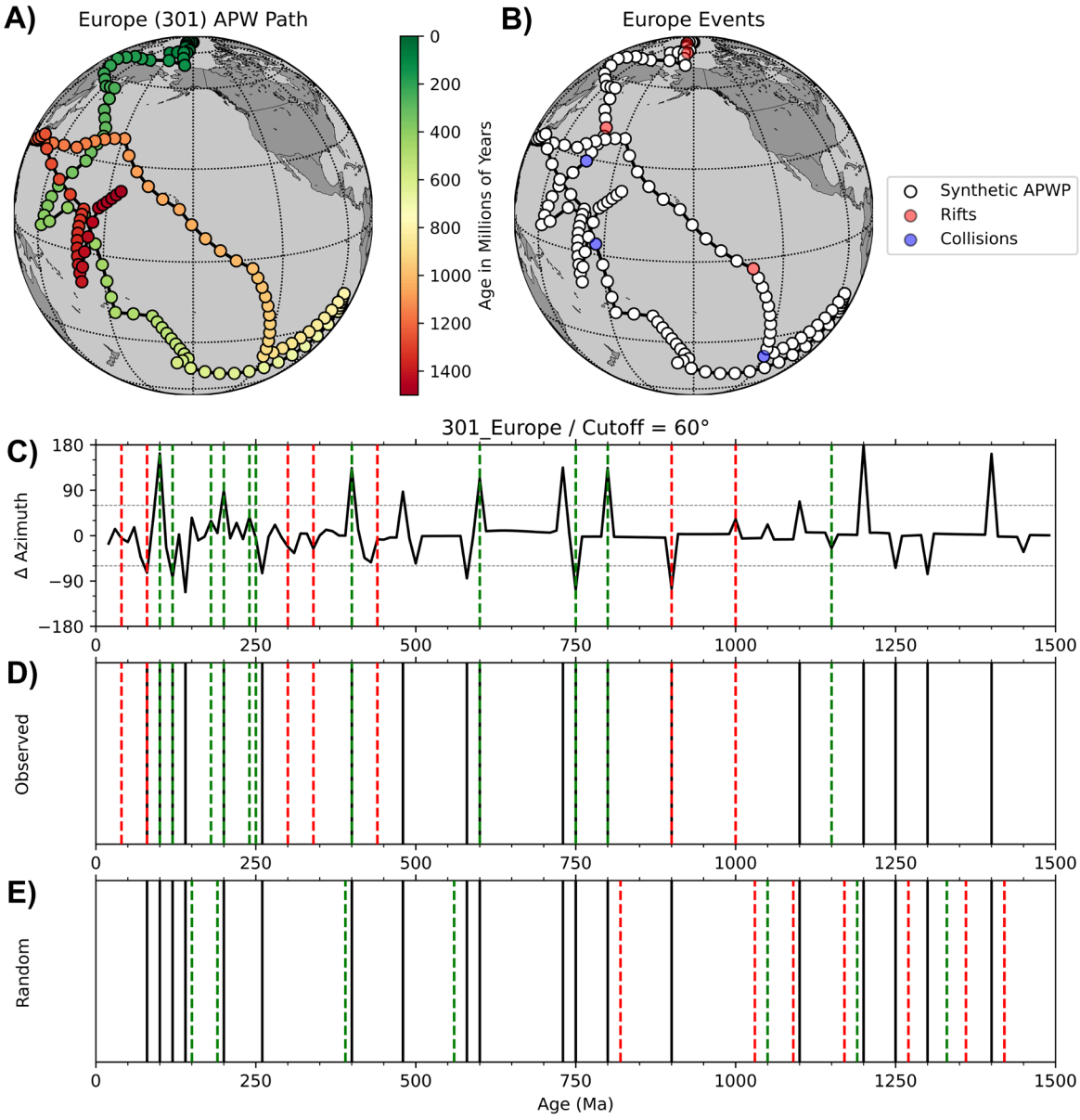

Figure 5.7. (A) Apparent polar wander (APW) path for Baltica from 1.5 Ga to present day, plotted in present-day coordinates. (B) APW path for Baltica with major tectonic events from its geologic history plotted. (C) Changes in azimuth calculated every 10 million years. The height of the spikes indicates the angular deflection of the APW path. Red dashed lines are the "peak" ages of events which occurred directly on the boundaries of Baltica, whereas green dashed lines are the ages of events that took place when Baltica was part of a supercontinent. (D) Black vertical lines correspond to directional changes in the top plot which are greater than 60°. (E) Example of a single simulation of randomized event ages.

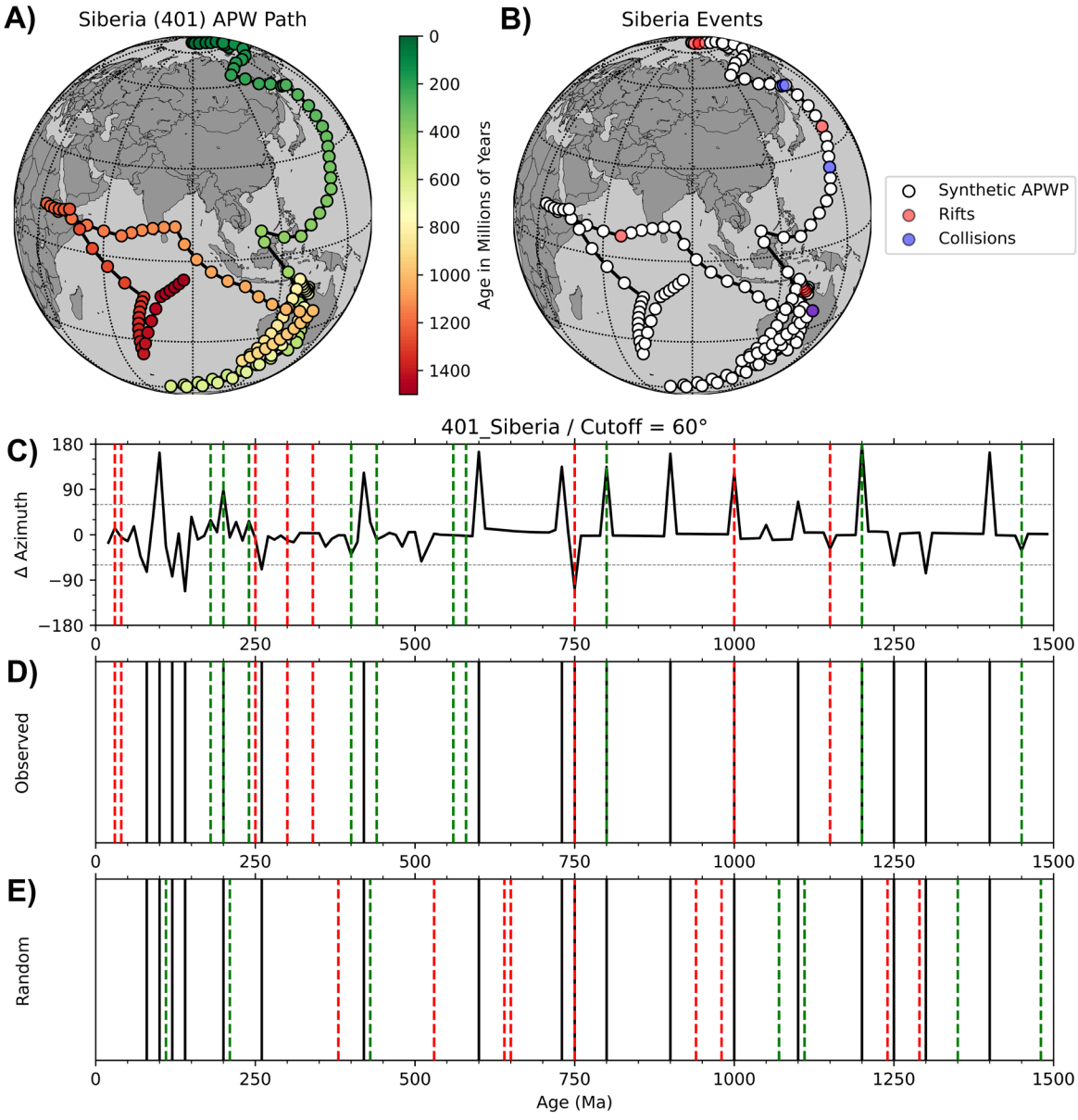

Figure 5.8. (A) Apparent polar wander (APW) path for Siberia from 1.5 Ga to present day, plotted in present-day coordinates. (B) APW path for Siberia with major tectonic events from its geologic history plotted. (C) Changes in azimuth calculated every 10 million years. The height of the spikes indicates the angular deflection of the APW path. Red dashed lines are the "peak" ages of events which occurred directly on the boundaries of Siberia, whereas green dashed lines are the ages of events that took place when Siberia was part of a supercontinent. (D) Black vertical lines correspond to directional changes in the top plot which are greater than 60°. (E) Example of a single simulation of randomized event ages.

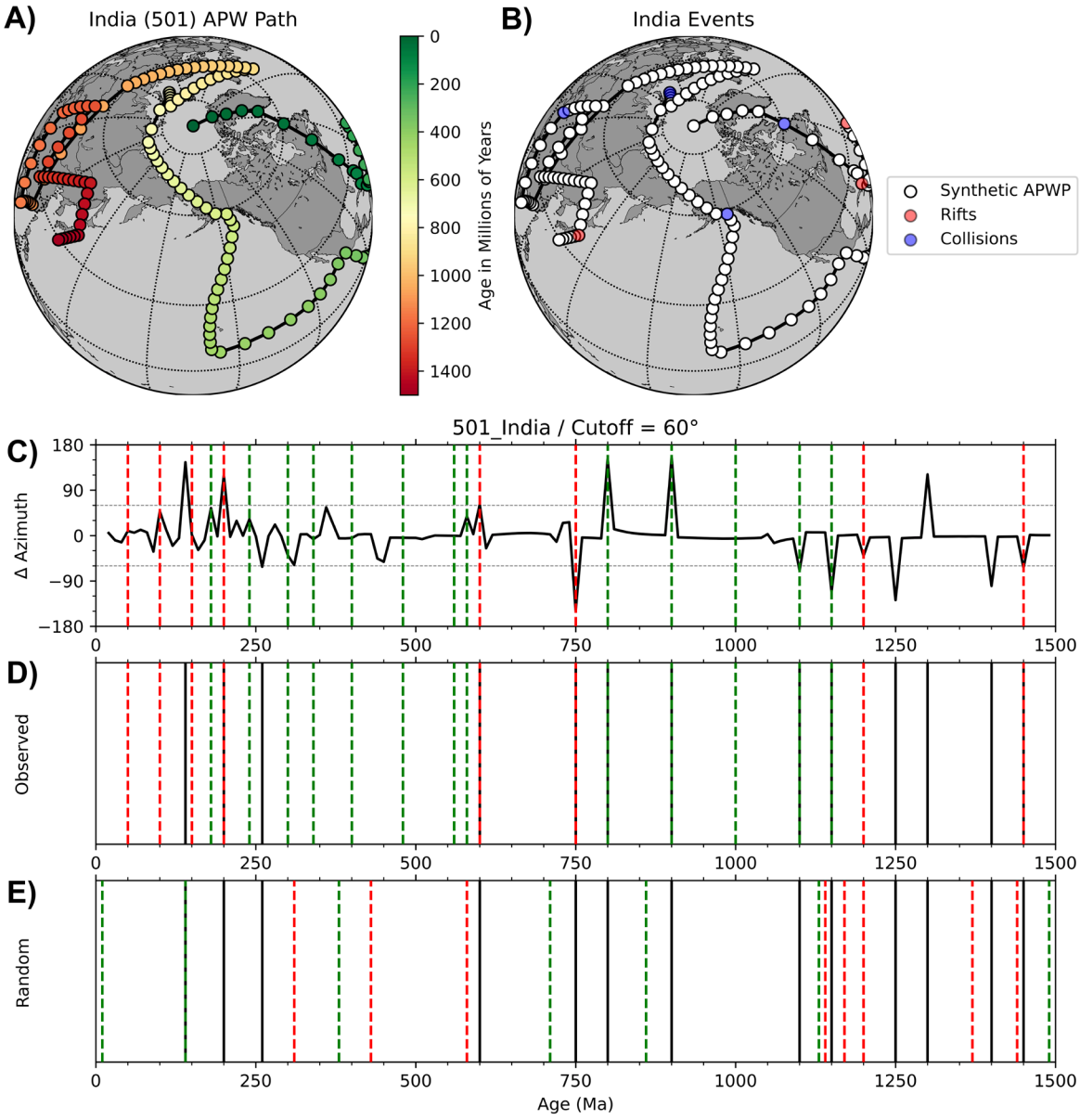

Figure 5.9. (A) Apparent polar wander (APW) path for India from 1.5 Ga to present day, plotted in present-day coordinates. (B) APW path for India with major tectonic events from its geologic history plotted. (C) Changes in azimuth calculated every 10 million years. The height of the spikes indicates the angular deflection of the APW path. Red dashed lines are the "peak" ages of events which occurred directly on the boundaries of India, whereas green dashed lines are the ages of events that took place when India was part of a supercontinent. (D) Black vertical lines correspond to directional changes in the top plot which are greater than 60°. (E) Example of a single simulation of randomized event ages.

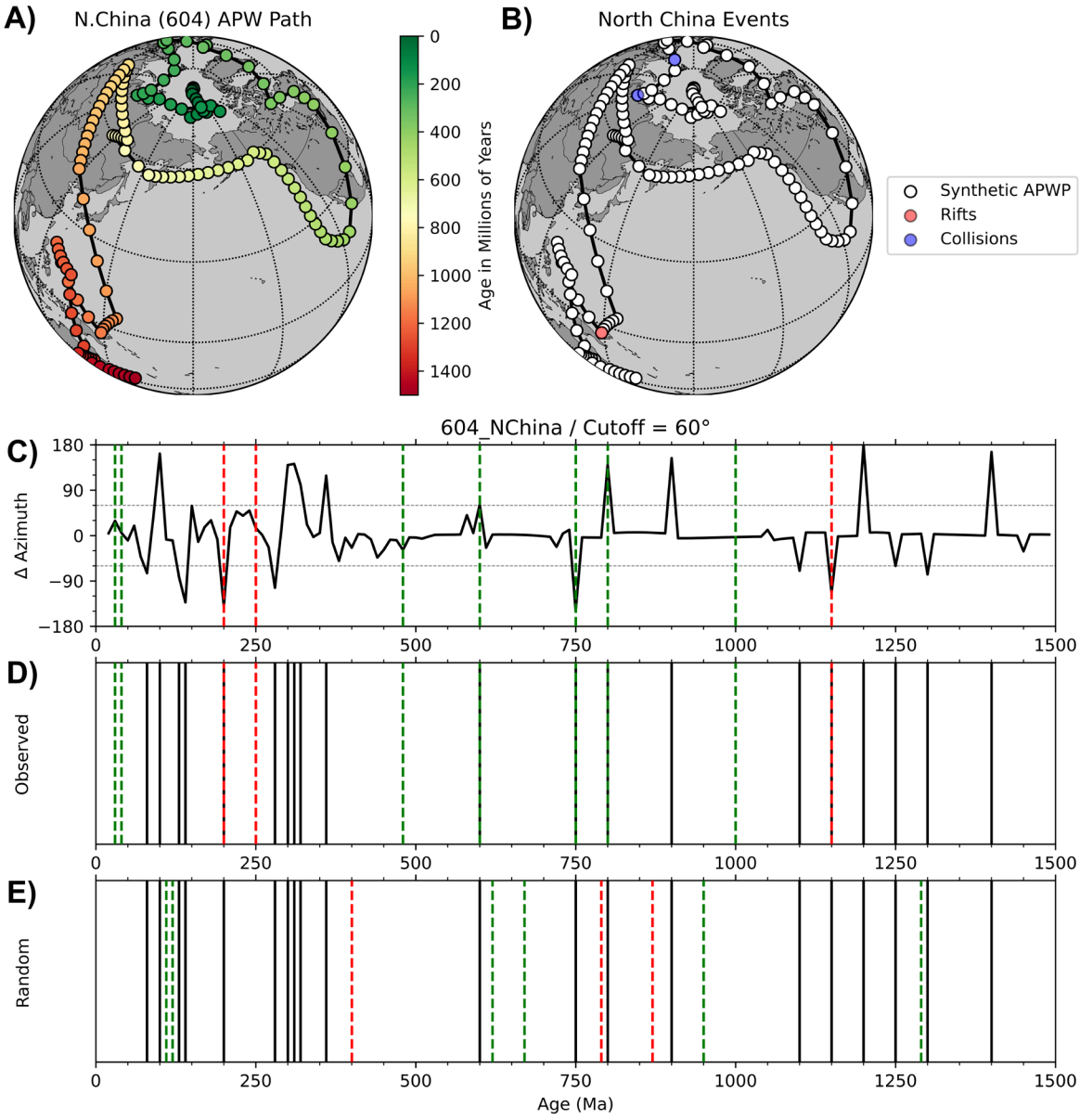

Figure 5.10. (A) Apparent polar wander (APW) path for North China from 1.5 Ga to present day, plotted in present-day coordinates. (B) APW path for North China with major tectonic events from its geologic history plotted. (C) Changes in azimuth calculated every 10 million years. The height of the spikes indicates the angular deflection of the APW path. Red dashed lines are the "peak" ages of events which occurred directly on the boundaries of North China, whereas green dashed lines are the ages of events that took place when North China was part of a supercontinent. (D) Black vertical lines correspond to directional changes in the top plot which are greater than 60°. (E) Example of a single simulation of randomized event ages.

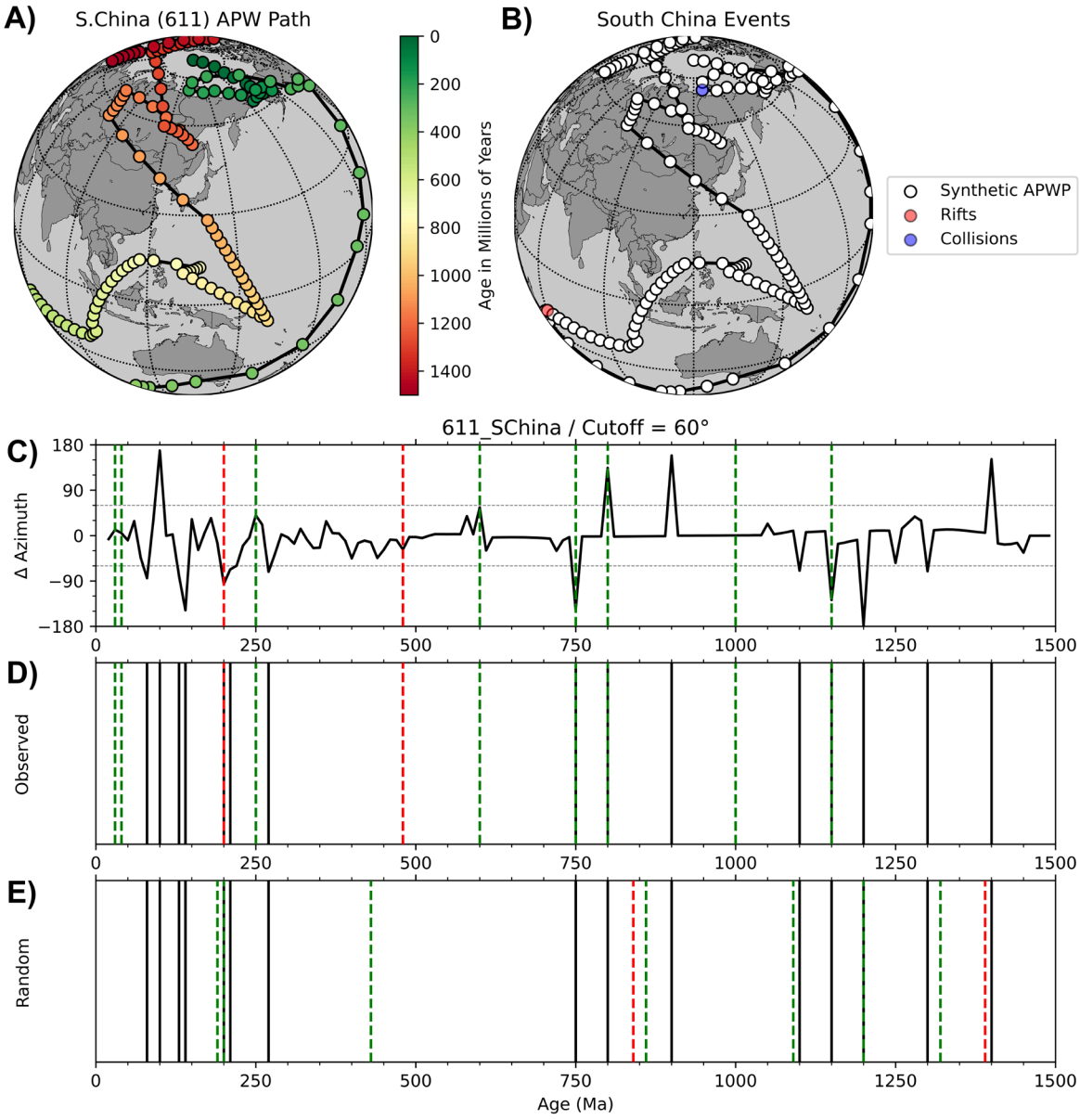

Figure 5.11. (A) Apparent polar wander (APW) path for South China from 1.5 Ga to present day, plotted in present-day coordinates. (B) APW path for South China with major tectonic events from its geologic history plotted. (C) Changes in azimuth calculated every 10 million years. The height of the spikes indicates the angular deflection of the APW path. Red dashed lines are the "peak" ages of events which occurred directly on the boundaries of South China, whereas green dashed lines are the ages of events that took place when South China was part of a supercontinent. (D) Black vertical lines correspond to directional changes in the top plot which are greater than 60°. (E) Example of a single simulation of randomized event ages.

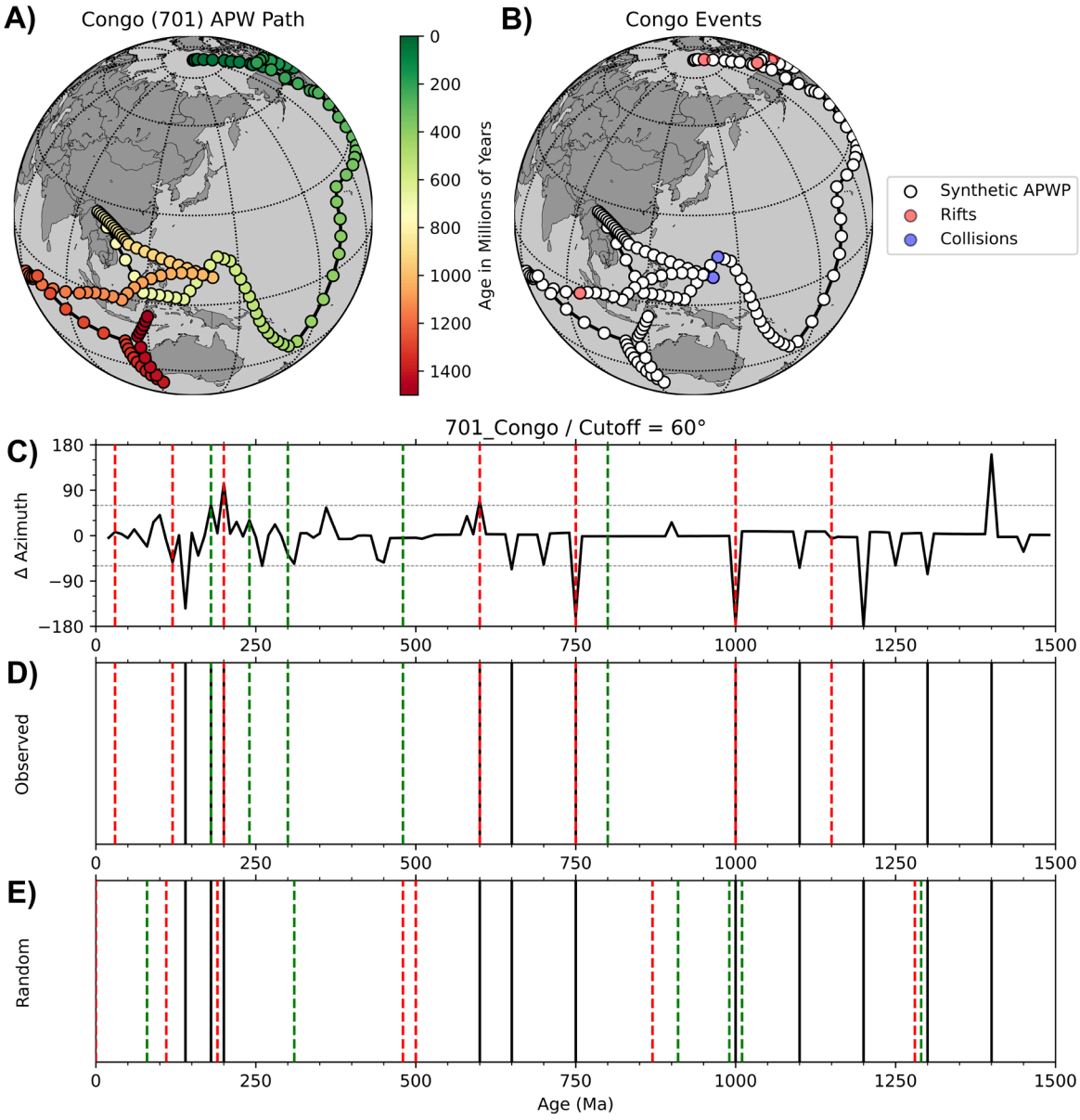

Figure 5.12. (A) Apparent polar wander (APW) path for the Congo craton from 1.5 Ga to present day, plotted in present-day coordinates. (B) APW path for the Congo craton with major tectonic events from its geologic history plotted. (C) Changes in azimuth calculated every 10 million years. The height of the spikes indicates the angular deflection of the APW path. Red dashed lines are the "peak" ages of events which occurred directly on the boundaries of the Congo craton, whereas green dashed lines are the ages of events that took place when the Congo craton was part of a supercontinent. (D) Black vertical lines correspond to directional changes in the top plot which are greater than 60°. (E) Example of a single simulation of randomized event ages.

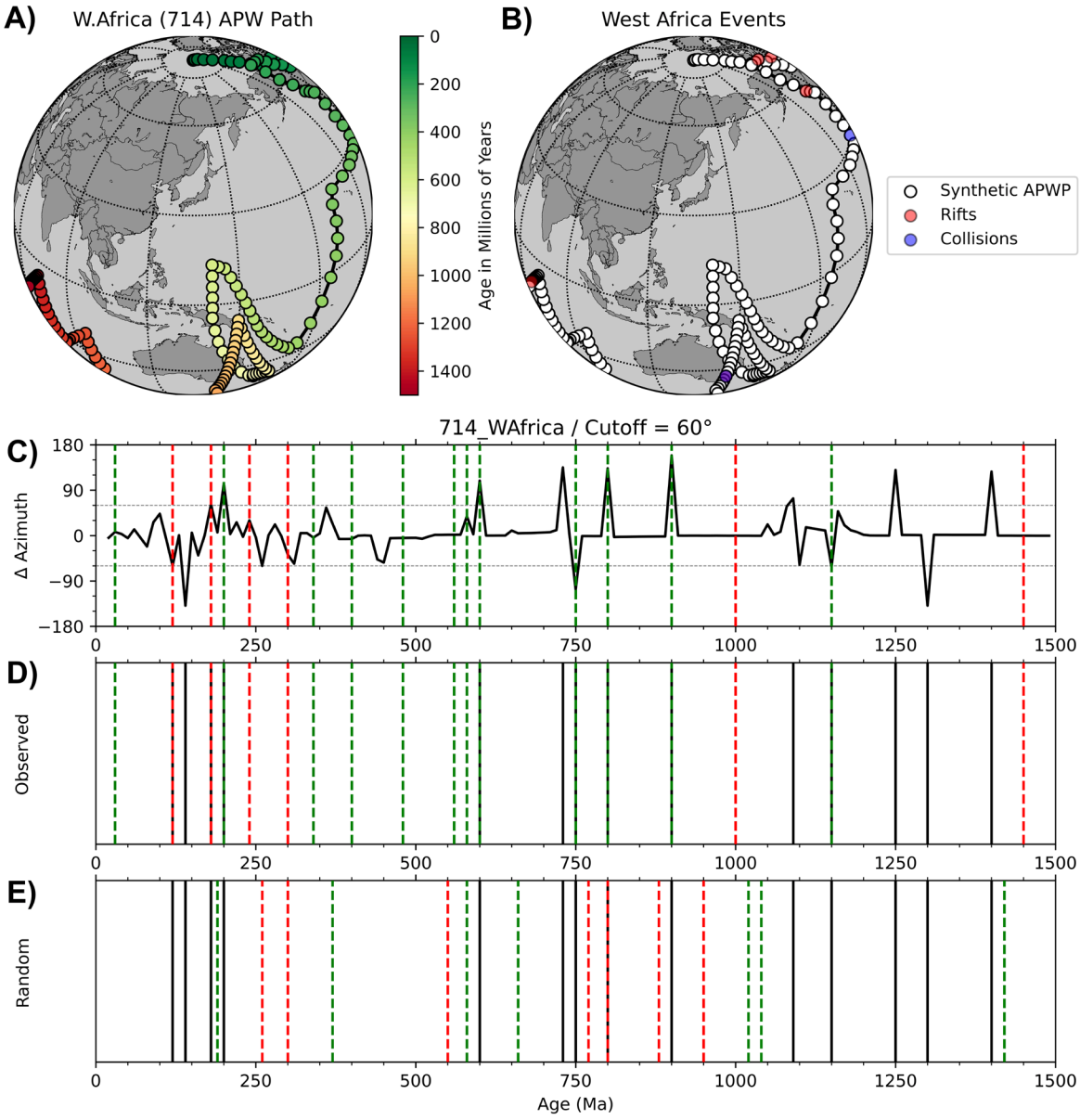

Figure 5.13. (A) Apparent polar wander (APW) path for West Africa from 1.5 Ga to present day, plotted in present-day coordinates. (B) APW path for West Africa with major tectonic events from its geologic history plotted. (C) Changes in azimuth calculated every 10 million years. The height of the spikes indicates the angular deflection of the APW path. Red dashed lines are the "peak" ages of events which occurred directly on the boundaries of West Africa, whereas green dashed lines are the ages of events that took place when West Africa was part of a supercontinent. (D) Black vertical lines correspond to directional changes in the top plot which are greater than 60°. (E) Example of a single simulation of randomized event ages.

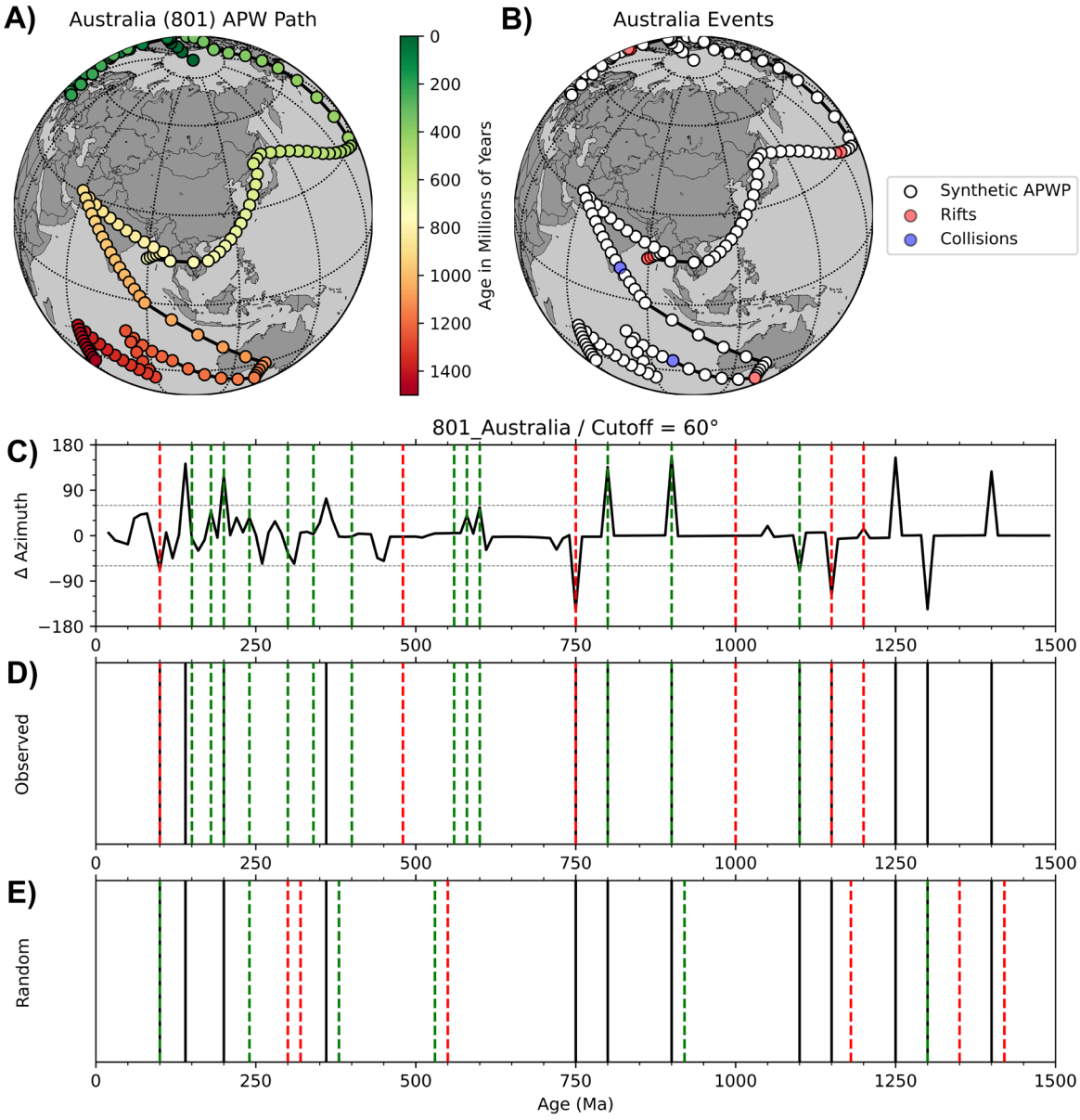

Figure 5.14. (A) Apparent polar wander (APW) path for Australia from 1.5 Ga to present day, plotted in present-day coordinates. (B) APW path for Australia with major tectonic events from its geologic history plotted. (C) Changes in azimuth calculated every 10 million years. The height of the spikes indicates the angular deflection of the APW path. Red dashed lines are the "peak" ages of events which occurred directly on the boundaries of Australia, whereas green dashed lines are the ages of events that took place when Australia was part of a supercontinent. (D) Black vertical lines correspond to directional changes in the top plot which are greater than 60°. (E) Example of a single simulation of randomized event ages.

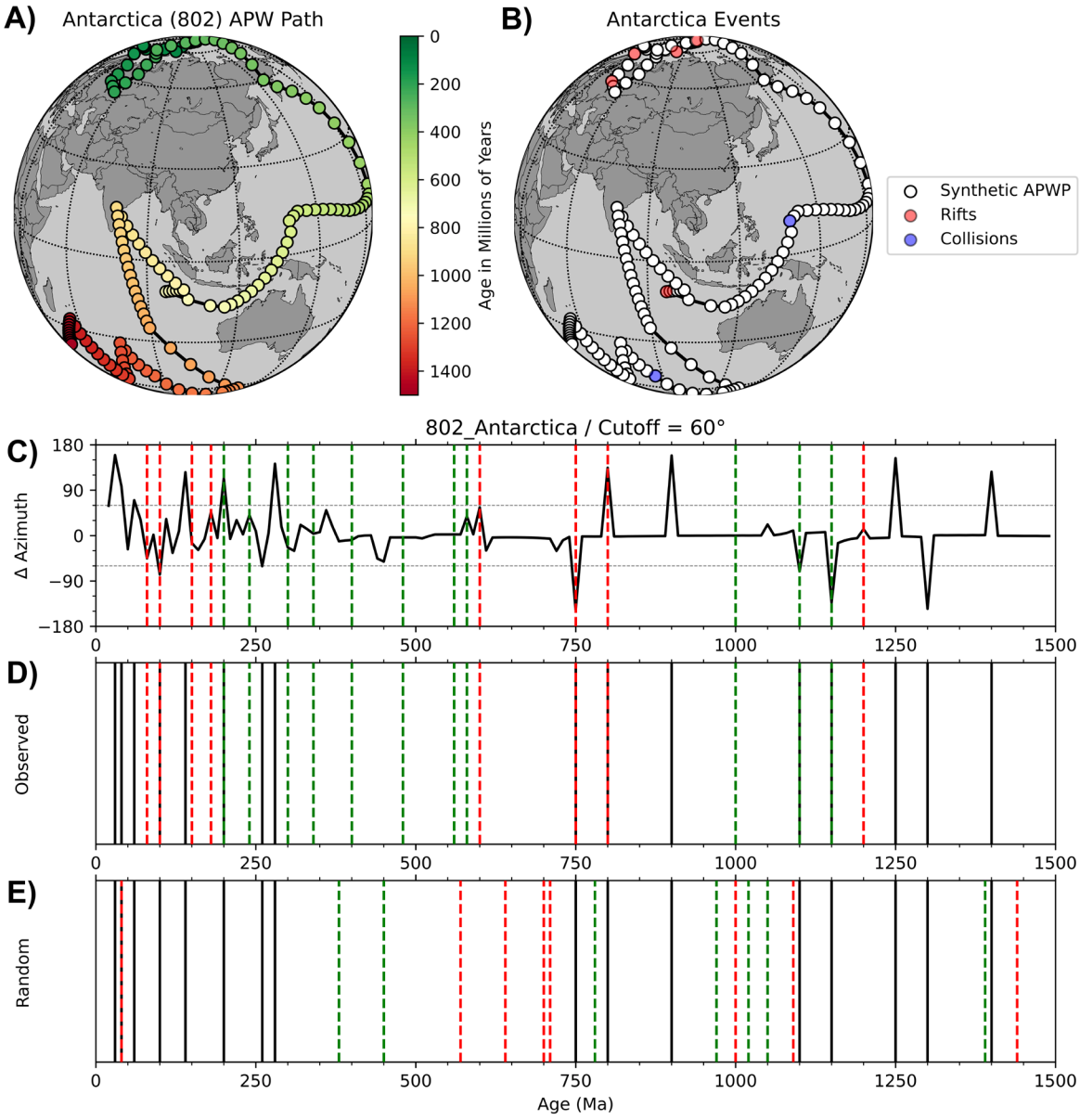

Figure 5.15. (A) Apparent polar wander (APW) path for Antarctica from 1.5 Ga to present day, plotted in present-day coordinates. (B) APW path for Antarctica with major tectonic events from its geologic history plotted. (C) Changes in azimuth calculated every 10 million years. The height of the spikes indicates the angular deflection of the APW path. Red dashed lines are the "peak" ages of events which occurred directly on the boundaries of Antarctica, whereas green dashed lines are the ages of events that took place when Antarctica was part of a supercontinent. (D) Black vertical lines correspond to directional changes in the top plot which are greater than 60°. (E) Example of a single simulation of randomized event ages.

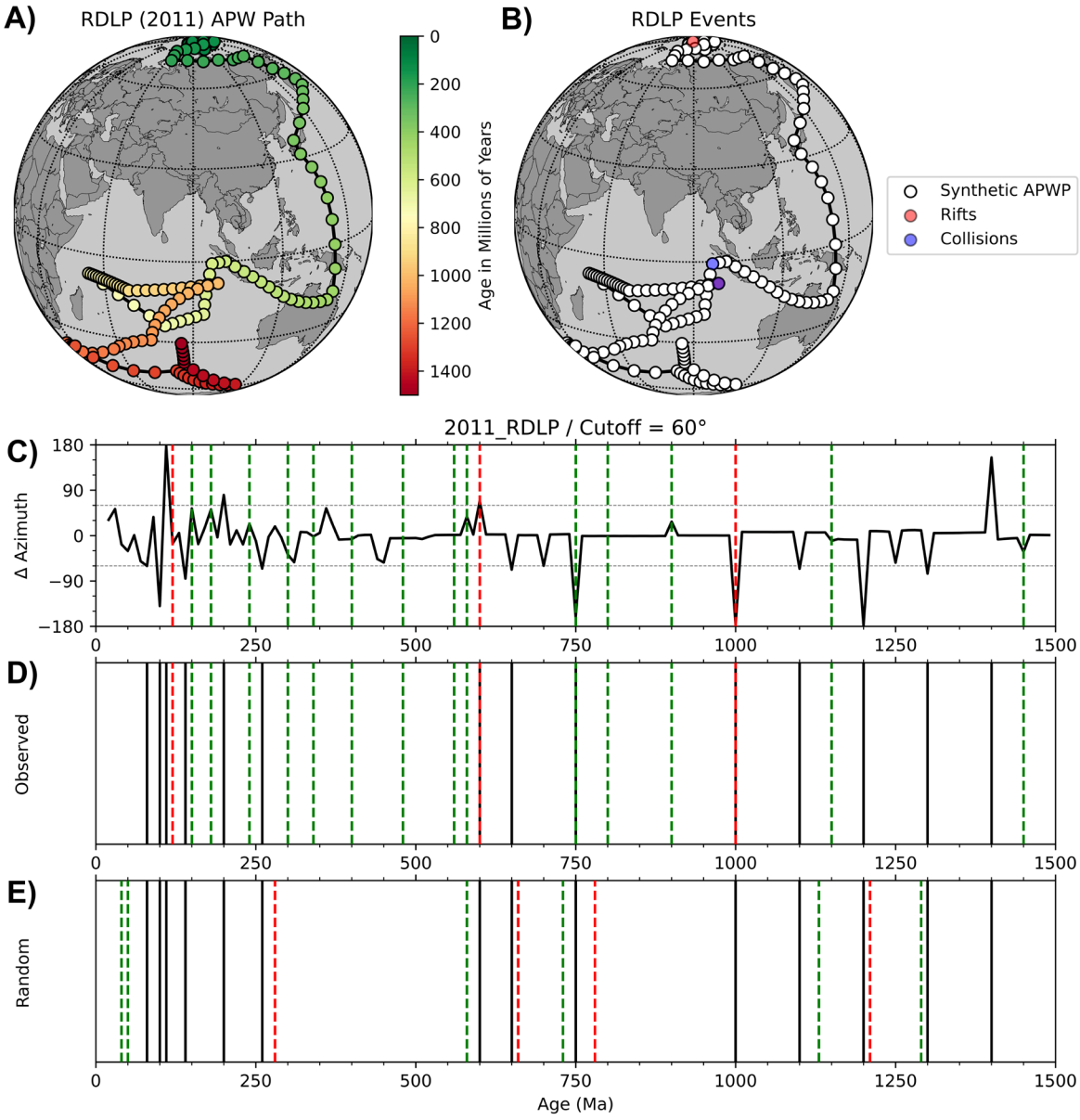

Figure 5.16. (A) Apparent polar wander (APW) path for Rio de la Plata from 1.5 Ga to present day, plotted in present-day coordinates. (B) APW path for Rio de la Plata with major tectonic events from its geologic history plotted. (C) Changes in azimuth calculated every 10 million years. The height of the spikes indicates the angular deflection of the APW path. Red dashed lines are the "peak" ages of events which occurred directly on the boundaries of Rio de la Plata, whereas green dashed lines are the ages of events that took place when Rio de la Plata was part of a supercontinent. (D) Black vertical lines correspond to directional changes in the top plot which are greater than 60°. (E) Example of a single simulation of randomized event ages.

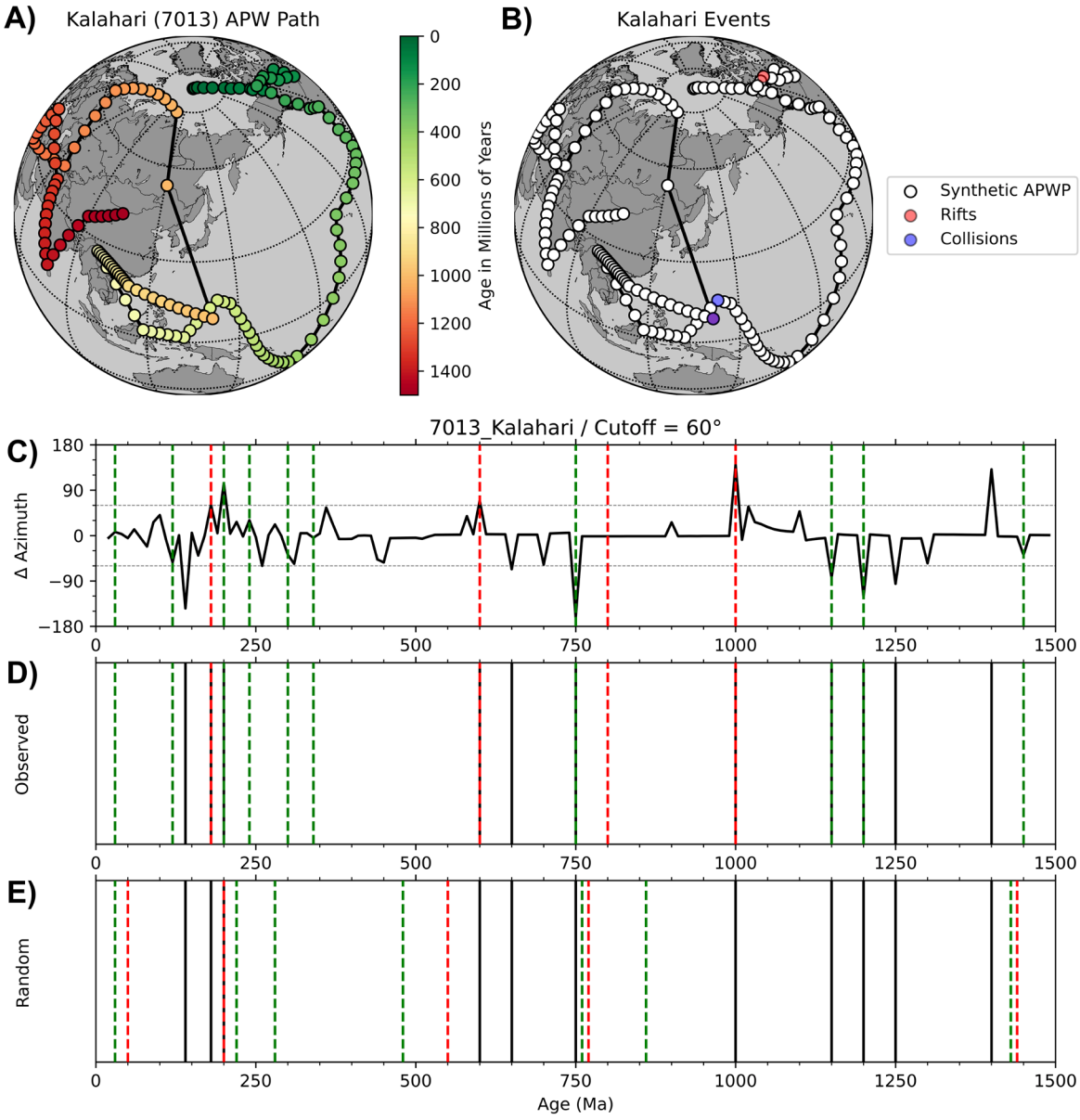

Figure 5.17. (A) Apparent polar wander (APW) path for the Kalahari craton from 1.5 Ga to present day, plotted in present-day coordinates. (B) APW path for the Kalahari craton with major tectonic events from its geologic history plotted. (C) Changes in azimuth calculated every 10 million years. The height of the spikes indicates the angular deflection of the APW path. Red dashed lines are the "peak" ages of events which occurred directly on the boundaries of the Kalahari craton, whereas green dashed lines are the ages of events that took place when the Kalahari craton was part of a supercontinent. (D) Black vertical lines correspond to directional changes in the top plot which are greater than 60°. (E) Example of a single simulation of randomized event ages.

5.5. Results and Implications

I compared changes in the timing of directional changes for each plate to the timing of tectonic events and found significant differences in the average ΔT occurring between the observed history of the plate and the simulations with randomized ages for the tectonic events. First, I determined that the cutoff angle (30°, 45°, 60°, 75°, 90°) was not a significant factor (Figure 5.18). The randomized ΔT' values were nearly identical regardless of the angle, but there was a slight improvement in the ΔT value for large angular deflections of the APW path (i.e., 60°, 75°, 90°). Because there were no significant improvements in ΔT above 60°, I chose 60° as the cutoff angle to compare correlations between multiple plates.

Using Laurentia as an example (Figure 5.18), the observed ΔT for the five cutoff angles ranged from 6.43 to 10.42 million years, with all observed ΔTs being significantly lower than the average (and minimum) of the randomized runs. The observed ΔTs were also consistently below the standard deviation of the randomized runs, indicating a significant correlation. In calculating the observed ΔT for each continent, I decided to not include directional changes older than 1200 million years. It was observed that deflections of the APW path older than 1200 million years occurred at nearly identical times in every plate. This suggests that the timing of these events are likely artifacts of the global plate model itself and not due to the paths of any individual plate. There are also few well-constrained geologic and tectonic events known during this time period. So, for the purposes of this analysis, ΔTs were only calculated and averaged for directional changes between present and 1200 Ma. For all 13 plates, the average ΔT for the observed ages of tectonic events were lower than the ΔT' in the 200 simulations using randomized event ages (Figure 5.19).

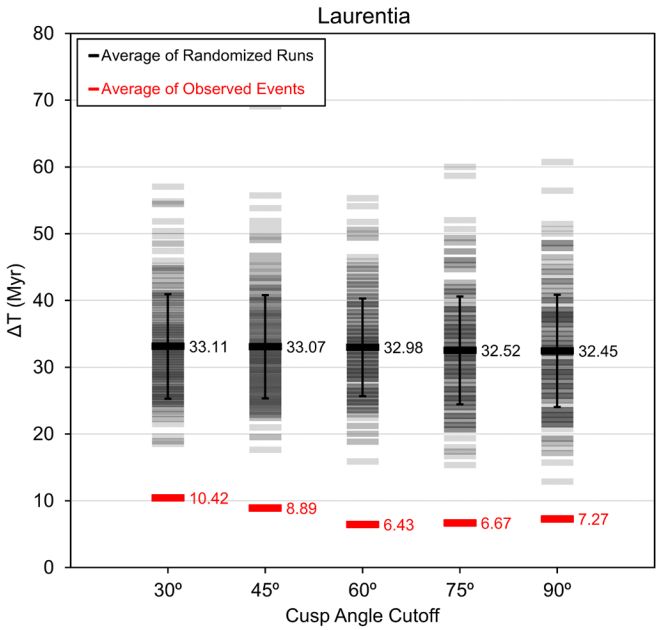

Figure 5.18. Average ΔT for Laurentia for observed and randomized events comparing five cutoff angles between 30° and 90°. The ΔT is nearly the same regardless of the cutoff angle used. All observed averages were significantly lower than the randomized runs.

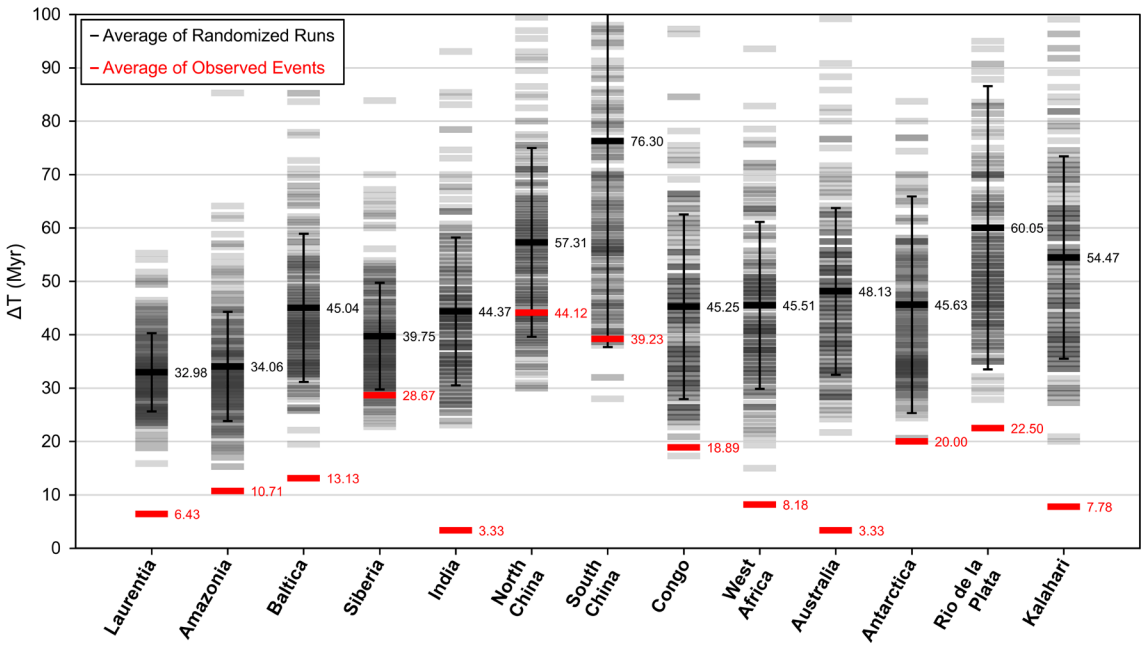

Figure 5.19. Average ΔTs for observed and randomized simulations of each of the 13 tectonic plates, using a cutoff angle of 60°.

11 of the 13 plates had observed ΔTs far below the standard deviation of the 200 simulated runs, indicating a statistically significant difference. Only North and South China fell within the standard deviation, likely due to the fact that few major tectonic events are defined for these plates, and there is great uncertainty regarding their tectonic history. Given that the observed ΔT is significantly lower than the simulated ΔT' for most plates, the null hypothesis can be confidently rejected.

A more extensive analysis of the geologic and tectonic histories of individual plates would likely reveal more tectonic events and lower the average observed ΔT. More tectonic events would also lower the average ΔT of the randomized runs, as they would increase the number of events being randomized, leading to some falling closer in time to the directional changes. These studies have revealed a correlation between tectonic events and cusps or directional changes in APW paths. Tectonic events often occurred at nearly the same time as the directional changes, or within several million years. Events which occurred over longer period of time would be expected to be linked to a wider cusp, as the directional changes would occur over times longer than several million years. This might be why some tectonic plates have average ΔTs greater than others.

5.6. Conclusions

A new and much larger global paleomagnetic dataset allowed me to define the motion of tectonic plates and build synthetic APW paths from a well-defined global plate model (Scotese and Elling, 2017). The analysis linking directional changes in APW paths to global tectonic processes is promising and yields expected results: changes in plate motions result in changes in the shape of APW paths, confirming the long-held hypothesis linking directional changes in APW

paths to major tectonic events. When major episodes of continent-continent collision or major continental rifting events occur, spreading centers and subduction zones are formed and destroyed. These changes in the network of plate boundaries drive the motion of tectonic plates in new directions.

These results justify more in-depth investigations into the geologic and tectonic history of individual plates. Refining the definition of a major tectonic event could change the resulting time delays (ΔT) between them and the cusps. This analysis was done using a specific global plate reconstruction, but time periods with few quality paleomagnetic poles are often reconstructed differently and other global plate models may give different results. Hence, more detailed research into the history of individual plates might yield better defined results. However, this global approach shows considerable correlation between the major tectonic events and the deflection of APW paths and may be useful in recognizing tectonic events during time periods where paleomagnetic data exist, but few geologic or geographic constraints have been discovered.

CHAPTER 6

Conclusion

This dissertation represents my research using gravity modeling and paleomagnetic data to investigate continental rifting and Precambrian tectonics. Chapters 2 and 3 use gravity modeling to learn about the evolution of continental rifting from the failed Midcontinent Rift (MCR) and how it relates to the collisional Grenville Orogeny as well as the two other failed major rifts in central North America: the Southern Oklahoma Aulacogen (SOA) and the Reelfoot Rift (RR). Chapters 4 and 5 use paleomagnetic data to refine our understanding of Precambrian tectonics pertaining to the assembly of Rodinia, which encapsulates the formation of the MCR and collisions related to the Grenville Orogeny.

Modeling the gravity anomalies of the MCR and Grenville Front (GF) where they are confirmed to exist in Michigan and southeast Canada revealed that the positive linear gravity anomalies in the eastern U.S. are consistent with their being part of an extension of the east arm of the MCR and are unlike those on either portion of the GF in Canada. While the northern GF in Canada has a broad, moderately negative anomaly associated with the thickening of an older, less dense, northwestern Laurentian crustal block (Pilkington, 1990; Hynes, 1994; Hynes and Rivers, 2010), the southern GF lacks a significant anomaly where seismic data reveal thrust sheet structures and no crustal thickening (Culotta et al., 1990; Ludden and Hynes, 2000; White et al., 2011). It would be difficult to see how a northern GF-type negative anomaly could exist along the east arm of the MCR, but the gravity data do not exclude southern GF-type thrust sheet structures which would produce only minimal anomalies. Recent seismic data support the existence of southeast-dipping structures east of the MCR's east arm (Long et al., 2019).

In my view, modern high-quality seismic reflection surveys combined with additional geological studies would be the best way to address whether Grenville-age collisions occurred

along the east arm of the MCR. Specifically, new seismic data encompassing both the rift structures of the MCR and any thrust-like features to its east, most likely related to the GF in southern Canada, would be beneficial in further delineating these features in the subsurface.

I also compared the tectonic histories and structures of the three major failed rifts in central North America (the MCR, SOA, and RR) using models derived from gravity, seismic refraction, and magnetic data. All three rifts formed during rifting associated with Laurentia's interactions within the supercontinent Rodinia. The MCR formed as part of rifting of the Amazonia craton from Laurentia, the Precambrian core of North America at 1.1 Ga, after the Elzeverian and Shawinigan orogenies but before the onset of the Grenville Orogeny (C. Stein et al., 2018). Both the SOA and RR formed as failed arms of triple junctions associated with the successful opening of the Iapetus Ocean as the Argentine Precordillera microcontinent rifted from the Wichita embayment on Laurentia's southeast margin (Whitmeyer and Karlstrom, 2007; Thomas, 2011). All three rifts have similar spatial scales and structures that seem to characterize failed rifts: ~60–80 km wide central grabens filled with volcanic and sedimentary rocks that are bounded by faults that presumably had normal fault motion during extension. This supports the idea that failed rifts are consistent with observations that presently spreading rifts had initial widths controlled by crustal thickness rather than the extension history (Allemand and Brun, 1991). However, the RR contains significantly less volcanics than the MCR and SOA and was never subjected to massive inversion commonly seen in rifts that produce positive gravity anomalies. Using hypothetical scenarios for the SOA and RR, I showed that inversion is crucial for a rift to produce a positive gravity anomaly.

The differences between the three rifts, notably the variations in the volumes of underplate material relative to rift-filling volcanics, sparks more questions than answered regarding rift formation. Because there is a relatively constant ratio of the volume of seaward dipping reflectors to high velocity lower crustal bodies in passive margins along the Atlantic Ocean (Gallahue et al., 2020), we would expect a similar ratio to appear early in the evolution of continental rifts. However, the ratio of rift-filling volcanics (which is expected to evolve to seaward dipping reflectors) to underplate material (which would evolve to form the high velocity lower crustal body) in the Midcontinent Rift and Southern Oklahoma Aulacogen is far higher than that of many conjugate passive margins. It also seems that the Reelfoot Rift has a much larger underplate than expected given the few volcanics that fill failed rift basin. One hypothesis explaining these differences is that a high-density upper crustal layer exists above the underplate (Liu et al., 2017), but this is difficult to detect with gravity modeling alone. Seismic reflection surveys above the Reelfoot Rift could determine if igneous material exists in the upper crust. While receiver function data are available to constrain the location of the underplate beneath the MCR's west arm and RR, similar data below the MCR's east arm and the SOA would help define the locations and volumes of their underplates as well. Comparing the ratio of rift-filling volcanics to underplate material at other presently extending and failed rifts around the world would help address questions regarding these observed differences.

Finally, Chapters 4 and 5 presented the revision and compilation of multiple publicly available paleomagnetic pole datasets back into the Precambrian in a consistent format. Consistently compiling multiple datasets allows the calculation of global mean poles using the GPlates software and a recent 1.5 Ga global plate model (Scotese and Elling, 2017). GMPs help constrain accurate

APW paths for 13 tectonic plates, which allowed us to test the long-proposed hypothesis that cusps in APW paths are associated with major rifting or collisional events (Gordon et al., 1984). Evidence for this idea comes from major cusps in Laurentia's APW path. One major cusp, the Logan Loop, is recorded in part by the MCR's volcanic rocks. A similar cusp occurs due to the Ediacaran-Cambrian rifting related to the opening of the Iapetus Ocean and the failed SOA and RR. Analyzing the time-delay (ΔT) between directional changes in APW paths and major tectonic events such as rifts or orogenies revealed significant correlations. This global approach that considers tectonic events and cusps to be related can be useful in identifying tectonic events in time periods where paleomagnetic data exist, but few geologic or geographic constraints have been discovered.

The results of this analysis justify more in-depth investigations into the geologic and tectonic history of individual plates. Refining catalog of major tectonic events (Table 5) could change the resulting time delays (ΔT) between them and the cusps. My analysis was done using a specific global plate reconstruction (Scotese and Elling, 2017), but time periods with few quality paleomagnetic poles are often reconstructed differently and other global plate models may give different results. Hence, more detailed research into the history of individual plates might yield different results. Creating a more comprehensive list of major tectonic events would also change the results slightly. An exception to the general result is that the average ΔT for North and South China fell within the standard deviation of the simulated runs, likely due to the fact that few major tectonic events are defined for these plates, and there is a great uncertainty regarding their tectonic history. A better understanding of their tectonic histories would likely yield more major tectonic events and further support the correlation. Although I show a correlation between the timing of

cusps and the timing of major collisional or rifting events, this begs the question of how this actually happens. APW paths represent the absolute motion of a plate relative to the Earth's spin axis, and in principle should also be useful in determining relative motions between plates. The tectonic events presented in Table 5.1, therefore, should be visible in the difference of the APW paths of each plate involved. A follow-up analysis from this work could involve differencing the APW paths of plates of interest to show changes in relative motion. This could further support the correlation between directional changes in APW paths and major tectonic events.

References

[1] Abrajevitch, A., Van der Voo, R., 2010, Incompatible Ediacaran paleomagnetic directions suggest an equatorial geomagnetic dipole hypothesis: Earth and Planetary Science Letters, v. 293, p. 164–170.

[2] Adams, D.C., Keller, G.R., 1994, Possible extension of the Midcontinental Rift in west Texas and eastern New Mexico: Canadian Journal of Earth Sciences, v. 31, p. 709–720.

[3] Adams, D.C., Keller, G.R., 1996, Precambrian basement geology of the Permian Basin region of West Texas and eastern New Mexico: a geophysical perspective: The American Association of Petroleum Geologists Bulletin, v. 80, p. 410–431.

[4] Allemand, P., Brun, J., 1991, Width of continental rifts and rheological layering of the lithosphere: Tectonophysics, v. 188, p. 63–69.

[5] Aziz Zanjani, A., Zhu, L., Herrmann, R., Liu, Y., Gu, Z., Conder, J., 2019, Crustal structure beneath the Wabash Valley Seismic Zone from joint inversion of receiver functions and surface wave dispersion: Journal of Geophysical Research, v. 124, p. 7028–7039.

[6] Baranoski, M.T., Dean, S.L., Wicks, J.L., Brown, V.M., 2009, Unconformity-bounded seismic reflection sequences define Grenville-age rift system and foreland basins beneath the Phanerozoic in Ohio: Geosphere, v. 5, p. 140–151.

[7] Bartholomew, M.J., Hatcher, R.D., 2010. The Grenville orogenic cycle of southern Laurentia: unraveling sutures, rifts, and shear zones as potential piercing points for Amazonia: Journal of South American Earth Sciences, v. 29, p. 4–20.

[8] Bartolini, A., Larson, R., 2001, Pacific microplate and the Pangea supercontinent in the Early to Middle Jurassic: Geology, v. 29, p. 735–738.

[9] Braile, L., Hinze, W., Keller, G., Lidiak, E., Sexton, J., 1986, Tectonic development of the New Madrid rift complex: Tectonophysics, v. 131, p. 1–21.

[10] Brewer, J., Good, R., Oliver, J., Brown, L., Kaufman, S., 1983, COCORP profiling across the Southern Oklahoma aulacogen: Geology, v. 11, p. 109–114.

[11] Bright, R.M., Amato, J.M., Denyszyn, S.W., Ernst, R.E., 2014, U-Pb geochronology of 1.1 Ga diabase in the southwestern United States: testing models for the origin of a post-Grenville large igneous province: Lithosphere, v. 6, p. 135–156.

[12] Burberry, C., Joeckel, R., Korus, J., 2015, Post-Mississippian tectonics of the Nemaha Tectonic Zone and Mid-Continent Rift System: The Mountain Geologist, v. 52, no. 4, p. 47–73.

[13] Burov, E., Gerya, T., 2014, Asymmetric three-dimensional topography over mantle plumes: Nature, v. 513, p. 85–89.

[14] Calais, E., Freed, A., Van Arsdale, R., Stein, S., 2010, Triggering of New Madrid seismicity by late-Pleistocene erosion: Nature, v. 466, p. 608–611.

[15] Cannon, W.F., et al., 1989, The North American Midcontinent rift beneath Lake Superior from GLIMPCE seismic reflection profiling: Tectonics, v. 8, p. 305–332.

[16] Catchings, R., 1999, Regional Vp, Vs, Vp/Vs, and Poisson's ratios across earthquake source zones from Memphis, Tennessee, to St. Louis, Missouri: Bulletin of the Seismological Society of America, v. 89, p. 1591–1605.

[17] Cawood, P.A., Pisarevsky, S.A., 2017, Laurentia-Baltica-Amazonia relations during Rodinia assembly: Precambrian Research, v. 292, p. 386–397.

[18] Chandler, V.W., McSwiggen, P.L., Morey, G.B., Hinze, W.J., Anderson, R.R., 1989, Interpretation of seismic-reflection, gravity, and magnetic data across middle Proterozoic mid-continent rift system, northwestern Wisconsin, eastern Minnesota, and Central Iowa. American Association of Petroleum Geology Bulletin 73, p. 261–275.

[19] Cox, R., Van Arsdale, R., 2002, The Mississippi embayment: Journal of Geodynamics, v. 34, p. 163–176.

[20] Culotta, R.C., Pratt, T., Oliver, J., 1990, A tale of two sutures: COCORP's deep seismic surveys of the Grenville province in the eastern U.S. midcontinent: Geology, v. 18, p. 646–649.

[21] Dalziel, I., 1991, Pacific margins of Laurentia and Antarctica as a conjugate rift pair: evidence and implications for an Eocambrian supercontinent, Geology, v. 19, p. 598–601.

[22] Dalziel, I., Dalla Salda, L., Gahagan, L., 1994, Paleozoic Laurentia-Gondwana interaction and the origin of the Appalachian-Andean mountain system: Geological Society of America Bulletin, v. 106, p. 243–252.

[23] Davis, W., Collins, M., Rooney, T., Brown, E., Stein, C., Stein, S., Moucha, R., 2021, Geochemical, petrographic, and stratigraphic analyses of the Portage Lake Volcanics of the Keweenawan CFBP, in Srivastava, R.K., et al., eds., Large Igneous Provinces and their Plumbing Systems: Geological Society, London, Special Publication 518, p. 67–100.

[24] Dickas, A.B., Mudrey, M.G., Ojakangas, R.W., Shrake, D.L., 1992, A possible southeastern extension of the Midcontinent Rift System in Ohio: Tectonics, v. 11, p. 1406–1414.

[25] Drahovzal, J.A., 1997, Proterozoic sequences and their implications for Precambrian and Cambrian geologic evolution of western Kentucky: evidence from seismic-reflection data: Seismological Research Letters, v. 68, p. 553–566.

[26] Elling, R., Stein, S., Stein, C., Gefeke, K., 2022, Three major failed rifts in Central North America: Similarities and Differences: GSA Today, v. 32., p. 1–8.

[27] Elling, R., Stein, S., Stein, C., Keller, G., 2020, Tectonic implications of the gravity signatures of the Midcontinent Rift and Grenville Front: Tectonophysics, v. 778, p. 1–6.

[28] Ernst, R., Buchan, K., 1993, Paleomagnetism of the Abitibi dyke swarm, southern Superior Province, and implications for the Logan Loop: Canadian Journal of Earth Sciences, v. 30, p. 1886–1897.

[29] Ervin, C., McGinnis, L., 1975, Reelfoot Rift: Reactivated precursor to the Mississippi Embayment: Geological Society of America Bulletin, v. 86, p. 1287–1295.

[30] Evans, D., and 16 others, 2022, An expanding list of reliable paleomagnetic poles for Precambrian tectonic reconstructions, *in* Pesonen, L., Salminen, J., Elming, S-A., Evans, D., and Veikkolainen, T., eds., 2022, Ancient supercontinents and the paleogeography of Earth: Elsevier, Amsterdam, Netherlands, 646 p.

[31] Fisher, R., 1953, Dispersion on a sphere: Proceedings of the Royal Society of London, Series A, Mathematical and Physical Sciences, v. 217, p. 295–305.

[32] Foulger, G., 2010, Plates vs. Plumes: A Geological Controversy: Chichester, UK, Wiley-Blackwell, 364 p.

[33] Gallahue, M., Stein, S., Stein, C., Jurdy, D., Barklage, M., Rooney, T., 2020, A compilation of igneous rock volumes at volcanic passive continental margins from interpreted seismic profiles: Marine and Petroleum Geology, v. 122, 104635.

[34] Goodge, J., Myrow, P., Williams, I., Bowring, S., 2002, Age and provenance of the Beartmore Group, Antarctica: Constraints on Rodinia supercontinent breakup: The Journal of Geology, v. 110, p. 393–406.

[35] Goodwin, A., 1996, Principles of Precambrian Geology: Academic Press, London, 327 p.

[36] Gordon, R., Cox, A., O'Hare, S., 1984, Paleomagnetic Euler poles and the apparent polar wander and absolute motion of North America since the Carboniferous: Tectonics, v. 3, p. 499–537.

[37] Gordon, R., Van der Voo, R., 1995, Mean paleomagnetic poles for the major continents and the Pacific plate, AGU Global Earth Physics, A Handbook of Physical Constants, AGU Reference Shelf 1.

[38] Green, A.G., Cannon, W.F., Milkereit, B., Hutchinson, D.R., Davidson, A., Behrendt, J.C., Spencer, C., Lee, M.W., Morel-á-LáHuissier, P., Agena, W.F., 1989, A "GLIMPCE" of the deep crust beneath the Great Lakes, *in* Mereu, R.F., Mueller, S., Fountain, D.M., eds, Properties and Processes of Earth's Lower Crust: American Geophysical Union Geophysical Monograph Series, v. 51, p. 65–80.

[39] Green, J.C., 1983, Geologic and geochemical evidence for the nature and development of the Middle Proterozoic (Keweenawan) Midcontinent Rift of North America: Tectonophysics, v. 94, p. 413–437.

[40] Hallam, A., 1981, Mesozoic geology and the opening of the North Atlantic: The Journal of Geology, v. 79, p. 129–157.

[41] Hanson, R.E., Puckett, R.E., Jr., Keller, G.R., Brueseke, M.E., Bulen, C.L., Mertzman, S.A., Finegan, S.A., McCleery, D.A., 2013, Intraplate magmatism related to the opening of the southern Iapetus Ocean: Lithos, v. 174, p. 57–70.

[42] Hildenbrand, T., Hendricks, J., 1995, Geophysical setting of the Reelfoot Rift and relations between rift structures and the New Madrid seismic zone: U.S. Geological Survey Professional Paper 1538-E.

[43] Hinze, W.J., Allen, D., Braile, L., Mariano, J., 1997, The Midcontinent rift system: A major Proterozoic continental rift, *in* Ojakangas, R., Dickas, A., and Green, J., eds., Middle Proterozoic to Cambrian rifting, central North America: Geological Society of America Special Paper 312, p. 7–35.

[44] Hinze, W.J., Allen, D.J., Fox, A.J., Sunwood, D., Woelk, T., Green, A., 1992, Geophysical investigations and crustal structure of the Midcontinent Rift system: Tectonophysics, v. 213, p. 17–32.

[45] Hoffman, P., 1988, United plates of America, the birth of a craton: Early Proterozoic assembly and growth of Laurentia: Annual Review of Earth and Planetary Sciences, v. 16, p. 543–603.

[46] Hoffman, P., 1991, Did the breakout of Laurentia turn Gondwanaland inside out?: Science, v. 252, p. 1409–1412.

[47] Hutchinson, D.R., White, R.S., Cannon, W.F., Schulz, K.J., 1990, Keweenaw hot spot, geophysical evidence for a 1.1 Ga mantle plume beneath the Midcontinent Rift System: Journal of Geophysical Research, v. 95, p. 10869–10884.

[48] Hynes, A., 1994, Gravity, flexure, and the deep structure of the Grenville front, eastern Quebec and Labrador: Canadian Journal of Earth Sciences, v. 31, p. 1002–1011.

[49] Hynes, A., Rivers, T., 2010, Protracted continental collision—Evidence from the Grenville orogen: Canadian Journal of Earth Sciences, v. 47, p. 591–620.

[50] Irving, E., Park, J., 1972, Hairpins and superintervals: Canadian Journal of Earth Sciences, v. 9, p. 1318–1324.

[51] Johnson, K., 2008, Geologic history of Oklahoma. Earth sciences and mineral resources of Oklahoma: Oklahoma Geological Survey Publication 9, p. 3–5.

[52] Keller, G., and 16 others, 2006, A community effort to construct a gravity database for the U.S. and an associated web portal, in Sinha, A., ed., Geoinformatics: Data to Knowledge: Geological Society of America Special Paper 397, p. 21–34.

[53] Keller, G., Baldridge, W., 1995, The Southern Oklahoma aulacogen, in Olsen, K., ed., Continental Rifts: Evolution, Structure, Tectonics: Amsterdam, Elsevier, p. 427–435.

[54] Keller, G., Bland, A.E., Greenberg, J.K., 1982, Evidence for a major Late Precambrian tectonic event (rifting?) in the eastern Midcontinent region, United States: Tectonics, v. 1, p. 213–223.

[55] Keller, G., Lidiak, E., Hinze, W., Braile, L., 1983, The role of rifting in the tectonic development of the midcontinent, U.S.A.: Tectonophysics, v. 94, p. 391–412.

[56] Keller, G., Stephenson, R., 2007, Southern Oklahoma and Dniepr-Donets aulacogens: A comparative analysis, in Hatcher, R., Jr., Carlson, M., McBride, J., and Catalán, M., eds., 4-D Framework of Continental Crust: Geological Society of America Memoir 200., p. 127–143.

[57] King, E., Zietz, I., 1971, Aeromagnetic study of the midcontinent gravity high of central United States: Geological Society of America Bulletin, v. 82, p. 2187–2208.

[58] King, S., 2007, Hotspots and edge-driven convection: Geology, v. 35, p. 223–226.

[59] Kluth, C., Coney, P., 1981, Plate tectonics of the ancestral Rocky Mountains: Geology, v. 9, p. 10–15.

[60] Koptev, A., Calais, E., Burov, E., Leroy, S., Gerya, T., 2015, Dual continental rift systems generated by plume–lithosphere interaction: Nature Geoscience, v. 8, p. 388–392.

[61] Korenaga, J., 2013, Initiation and evolution of plate tectonics on Earth: Annual Review of Earth and Planetary Sciences, v. 41, p. 117–151.

[62] Kristoffersen, Y., 1978, Sea-floor spreading and the early opening of the North Atlantic: Earth and Planetary Science Letters, v. 38, p. 273–290.

[63] Lawton, T., Cashman, P., Trexler, J., Taylor, W., 2017, The late Paleozoic Southwestern Laurentian Borderland: Geology, v. 45, p. 675–678.

[64] Leary, R., Umhoefer, P., Smith, M., Riggs, N., 2017, A three-sided orogen: A new tectonic model for Ancestral Rocky Mountain uplift and basin development: Geology, v. 45, p. 735–738.

[65] Levandowski, W., Zellman, M., Briggs, R., 2017, Gravitational body forces focus North American intraplate earthquakes: Nature Communications, v. 8, 14314.

[66] Li, Z., and 16 others, 2008, Assembly, configuration, and break-up history of Rodinia: A synthesis: Precambrian Research, v. 160, p. 179–210.

[67] Li, Z., Evans, D.D., Halverson, G.P., 2013, Neoproterozoic glaciations in a revised global paleogeography from the breakup of Rodinia to the assembly of Gondwanaland: Sedimentary Geology, v. 294, p. 219–232.

[68] Liu, L., Gao, S., Liu, K., Mickus, K., 2017, Receiver function and gravity constraints on crustal structure and vertical movements of the Upper Mississippi Embayment and Ozark Uplift: Journal of Geophysical Research, v. 122, p. 4572– 4583.

[69] Long, M.D., Benoit, M.H., Aragon, J.C., King, S.D., 2019, Seismic imaging of mid-crustal structure beneath central and eastern North America: possibly the elusive Grenville deformation?: Geology, v. 47, p. 371–374.

[70] Ludden, J., Hynes, A., 2000, The Abitibi-Grenville Lithoprobe project: two billion years of crust formation and recycling in the Precambrian Shield of Canada: Canadian Journal of Earth Sciences, v. 37, p. 459–476.

[71] Lyons, P.L., 1970, Continental and oceanic geophysics, *in* Johnson, H., Smith, B.L., eds, The Megatectonics of Continents and Oceans: Rutgers Press, New Brunswick, New Jersey, p. 147–166.

[72] Malone, D.H., Stein, C.A., Craddock, J.P., Kley, J., Stein, S., Malone, J.E., 2016, Maximum depositional age of the Neoproterozoic Jacobsville Sandstone: implications for the evolution of the Midcontinent Rift: Geosphere, v. 12, p. 1271–1282.

[73] Marshak, S., van der Pluijm, B., 2021, Tectonics of the Continental Interior in the United States, in Alderton, D., and Elias, S., eds., Encyclopedia of Geology (2nd ed.): Oxford, UK, Academic Press, v. 4, p. 173–186.

[74] Mayhew, M., Thomas, H., Wasilewski, P., 1982, Satellite and surface geophysical expression of anomalous crustal structure in Kentucky and Tennessee: Earth and Planetary Science Letters, v. 58, p. 395–405.

[75] McElhinny, M.W., Lock, J., 1996, Iaga paleomagnetic databases with access: Surveys in Geophysics, v. 17, p. 575–591.

[76] McLelland, J.M., Selleck, B.W., Bickford, M.E., 2013, Tectonic evolution of the Adirondack Mountains and Grenville orogen inliers within the USA: Geoscience Canada, v. 40, p. 318–352.

[77] McMenamin, M., and McMenamin, D., 1990, The emergence of animals: the Cambrian breakthrough: Columbia University Press, New York, 217 p.

[78] Meert, J., 2013, Ediacaran-Early Ordovician paleomagnetism of Baltica: A review: Gondwana Research, v. 25, p. 159–169.

[79] Meert, J., Torsvik, T., 2003, The making and unmaking of a supercontinent: Rodinia revisited: Tectonophysics, v. 375, p. 261–288.

[80] Meert, J., Van der Voo, R., 1997, The assembly of Gondwana 800–550 Ma: Journal of Geodynamics, v. 23, p. 223–235.

[81] Merdith, A., and 10 others, 2021, Extending full-plate tectonic models into deep time: Linking the Neoproterozoic and the Phanerozoic: Earth-Science Reviews, v. 213, 44 p.

[82] Merdith, A., and 11 others, 2017, A full-plate global reconstruction of the Neoproterozoic: Gondwana Research, v. 50, p. 84–134.

[83] Merino, M., Keller, G.R., Stein, S., Stein, C., 2013, Variations in Mid-Continent Rift magma volumes consistent with microplate evolution: Geophysical Research Letters, v. 40, p. 1513–1516.

[84] Moecher, D.P., Bowersox, J.R., Hickman, J.B., 2018, Zircon U-Pb geochronology of two basement cores (Kentucky, U.S.A.) and implications for Late Mesoproterozoic sedimentation and tectonics in the eastern Midcontinent: The Journal of Geology, v. 126, p. 25–39.

[85] Mooney, W., Andrews, M.C., Ginzburg, A., Peters, D.A., Hamilton, R.M., 1983, Crustal structure of the Northern Mississippi Embayment and a comparison with other continental rift zones: Tectonophysics, v. 94, p. 327–348.

[86] Moores, E., 1991, Southwest U.S.-East Antarctic (SWEAT) connection: A hypothesis: Geology, v. 19, p. 425–428.

[87] Nelson, K., Zhang, J., 1991, A COCORP deep reflection profile across the buried Reelfoot rift: Tectonophysics, v. 197, p. 271–293.

[88] Nicholson, S., Shirey, S., Schulz, K., Green, J., 1997, Rift-wide correlation of 1.1 Ga Midcontinent rift system basalts: Canadian Journal of Earth Sciences, v. 34, p. 504–520.

[89] O'Brien, T., van der Pluijm, B., 2012, Timing of Iapetus Ocean rifting from Ar geochronology of pseudo-tachylytes in the St. Lawrence rift system of southern Quebec: Geology, v. 40, p. 443–446.

[90] Ojakangas, R., Morey, G., Green, J., 2001, The Mesoproterozoic midcontinent rift system: Sedimentary Geology, v. 141–142, p. 421–442.

[91] Ortega-Gutiérrez, F., Elías-Herrera, M., Reyes-Salas, M., Macías-Romo, C., López, R., 1999, Late Ordovician-Early Silurian continental collisional orogeny in southern Mexico and its bearing on Gondwana-Laurentia connections: Geology, v. 27, p. 719–722.

[92] Pehrsson, S., Eglington, B., Evans, D., Huston, D., Reddy, S., 2016, Metallogeny and its link to orogenic style during the Nuna supercontinent cycle, *in* Li, Z., Evans, D., and Murphy, J., eds., Supercontinent Cycles Through Earth History: Geological Society, London, Special Publications, v. 424, 12 pp.

[93] Perry, W., Jr., 1989, Tectonic evolution of the Anadarko basin region: U.S. Geological Survey Bulletin 1866.

[94] Pesonen, L., 1979, Paleomagnetism of Late Precambrian Keweenawan igneous and baked contact rocks from Thunder Bay District, northern Lake Superior: Geological Society of Finland Bulletin 51, p. 27–44.

[95] Pilkington, M., 1990, Lithospheric flexure and gravity anomalies at Proterozoic plate boundaries in the Canadian Shield: Tectonophysics, v. 176, p. 277–290.

[96] Pisarevsky, S., 2005, New edition of the Global Paleomagnetic Database: Eos, v. 86, 170 pp.

[97] Pisarevsky, S., Elming, S-A., Pesonen, L., Li, Z-X., 2014, Mesoproterozoic paleogeography: Supercontinent and beyond: Precambrian Research, v. 244, p. 207–225.

[98] Richards, M., Duncan, R., Courtillot, V., 1989, Flood basalts and hot-spot tracks: Science, v. 246, p. 103–107.

[99] Rivers, T, Culshaw, N., Hynes, A., Indares, A., Jamieson, R., Matignole, J., 2012, The Grenville Orogen – A post-LITHOPROBE perspective, *in* Percival, J., Cook, F., Clowes, R., eds., Tectonic Styles in Canada: The LITHOPROBE Perspective: Geological Association of Canada Special Paper 49, p. 97–236.

[100] Rivers, T., 2008, Assembly and preservation of lower, mid, and upper orogenic crust in the Grenville Province – Implications for the evolution of large hot long-duration orogens: Precambrian Research, v. 167, p. 237–259.

[101] Rivers, T., 2012, Upper-crustal orogenic lid and mid-crustal core complexes: signature of a collapsed orogenic plateau in the hinterland of the Grenville Province: Canadian Journal of Earth Sciences, v. 49, p. 1–42.

[102] Rivers, T., 2014, Tectonic setting and evolution of the Grenville Orogen: an assessment of progress over the last 40 years: Geoscience Canada, v. 42, p. 77–124.

[103] Robert, B., Domeier, M., Jakob, J., 2021, On the origins of the Iapetus Ocean: Earth-Science Reviews, v. 221, 46 p.

[104] Robertson, W., Fahrig, W., 1971, The great Logan Paleomagnetic Loop – The polar wandering path from Canadian Shield rocks during the Neohelikian Era: Canadian Journal of Earth Sciences, v. 8, p. 1355–1372.

[105] Rooney, T., Lavigne, A., Svoboda, C., Girard, G., Yirgu, G., Ayalew, D., Kappelman, J., 2017, The making of an underplate: Pyroxenites from the Ethiopian lithosphere: Chemical Geology, v. 455, p. 264–281.

[106] Salminen, J., Pesonen, L. J., Mertanen, S., Vuollo, J. Airo, M.-L., 2009. Palaeomagnetism of the Salla Diabase Dyke, northeastern Finland, and its implication for the Baltica-Laurentia entity during the Mesoproterozoic, *in* Reddy, S. M., Mazumder, R., Evans, D., Collins, A. S., eds., Palaeoproterozoic Supercontinents and Global Evolution: Geological Society, London, Special Publications, v. 323, p. 199–217.

[107] Sandwell, D., Garcia, E., Soofi, K., Wessel, P., Chandler, M., Smith, W.H.F., 2013, Towards 1 mGal global marine gravity from CryoSat-2, Envisat, and Jason-1: The Leading Edge, v. 32, p. 892–899.

[108] Schettino, A., Scotese, C. R., 2005, Apparent polar wander paths for the major continents (200 Ma to the present day): a palaeomagnetic reference frame for global plate tectonic reconstructions: Geophysical Journal International, v. 163, p. 727–759.

[109] Schmandt, B., Lin, F.-C., Karlstrom, K.E., 2015, Distinct crustal isostasy trends east and west of the Rocky Mountain Front: Geophysical Research Letters, v. 42, p. 10290–10298.

[110] Scotese, C., Elling, R., 2017, Plate tectonic evolution during the last 1.5 billion years: The Movie, Plate Tectonics at 50, William Smith Meeting, October 3–5, 2017, The Geological Society, Burlington House, London, p. 16–17.

[111] Scotese, C., Van der Voo, R., 2017, A paleomagnetic database for GPlates: Paleopoles, declination arrows, and paleolatitudes: GPlates Tutorial, 52 p.

[112] Serpa, L., Setzer, T., Farmer, H., Brown, L., Oliver, J., Kaufman, S., Sharp, J., Steeples, D.W., 1984, Structure of the southern Keweenawan rift from COCORP surveys across the Midcontinent geophysical anomaly in northeastern Kansas: Tectonics, v. 3, p. 367–384.

[113] Shay, J., Trehu, A., 1993, Crustal structure of the central graben of the Midcontinent Rift beneath Lake Superior: Tectonophysics, v. 225, p. 301–335.

[114] Stein, C.A., Kley, J., Stein, S., Hindle, D., Keller, G., 2015, North America's Midcontinent Rift: When rift met LIP: Geosphere, v. 11, p. 1607–1616.

[115] Stein, C.A., Stein, S., Elling, R., Keller, G., Kley, J., 2018, Is the "Grenville Front" in the central United States really the Midcontinent Rift?: GSA Today, v. 28, p. 4–10.

[116] Stein, C.A., Stein, S., Gallahue, M.M., Elling, R.P., 2022, Revisiting hotspots and continental breakup—Updating the classical three-arm model, in Foulger, G.R., Hamilton, L.C., Jurdy, D.M., Stein, C.A., Howard, K.A., and Stein, S., eds., In the Footsteps of Warren B. Hamilton: New Ideas in Earth Science: Geological Society of America Special Paper 553, p. 41–57.

[117] Stein, C.A., Stein, S., Merino, M., Keller, G., Flesch, L., Jurdy, D., 2014, Was the Midcontinent Rift part of a successful seafloor-spreading episode?: Geophysical Research Letters, v. 41, p. 1465–1470.

[118] Stein, S., et al., 2016, When rift met LIP: new insights about the Midcontinent Rift: Eos, v. 97, p. 10–16.

[119] Stein, S., Stein, C., Elling, R., Kley, J., Keller, R., Wysession, M., Rooney, T., Frederiksen, A., Moucha, R., 2018, Insights from North America's failed Midcontinent Rift into the evolution of continental rifts and passive continental margins: Tectonophysics, v. 744, p. 403–421.

[120] Swanson-Hysell, N., Ramezani, J., Fairchild, L., Rose, I., 2019, Failed rifting and fast drifting: Midcontinent Rift development, Laurentia's rapid motion and the driver of Grenvillian orogenesis: Geological Society of America Bulletin, v. 131, p. 913–940.

[121] Thomas, W., 2011, The Iapetan rifted margin of southern Laurentia: Geosphere, v. 7, p. 97–120.

[122] Thybo, H., Artemieva, I., 2013, Moho and magmatic underplating in continental lithosphere: Tectonophysics, v. 609, p. 605–619.

[123] Tohver, E., D'Agrella-Filho, M., Trindade, R., 2006, Paleomagnetic record of Africa and South America for the 1200–500 Ma interval, and evaluation of Rodinia and Gondwana assemblies: Precambrian Research, v. 147, p. 193–222.

[124] Tohver, E., Teixeira, W., van der Pluijm, B., Geraldes, M., Bettencourt, J., Rizzotto, G., 2006, Restored transect across the exhumed Grenville orogen of Laurentia and Amazonia, with implications for crustal architecture: Geology, v. 34, p. 669–672.

[125] Tohver, E., van der Pluijm, B.A., van der Voo, R., Rizzotto, R.G., Scandolara, J.E., 2002, Paleogeography of the Amazon craton at 1.2 Ga: Early Grenvillian collision with the Llano segment of Laurentia: Earth and Planetary Science Letters, v. 199, p. 185–200.

[126] Torsvik, T., and 12 others, 2012, Phanerozoic polar wander, palaeogeography and dynamics: EarthScience Reviews, v. 114, p. 325–368.

[127] Torsvik, T., Muller, R., Van der Voo, R., and Steinberger, B., 2008, Global plate motion frames: Toward a unified model: Reviews of Geophysics, v. 46, 44 p.

[128] Torsvik, T., Smethurst, M., Meert, J., Van der Voo, R., McKerrow, W., Brasier, M., Sturt, B., Walderhaug, H., 1996, Continental break-up and collision in the Neoproterozoic and Palaeozoic – A tale of Baltica and Laurentia: Earth Science Reviews, v. 40, p. 229–258.

[129] Valentine, J., Moores, E., 1970, Plate-tectonic regulation of faunal diversity and sea level: a model: Nature, v. 228, p. 657–659.

[130] Van der Voo, R., 1990, The reliability of paleomagnetic data: Tectonophysics, v. 184, p. 1–9.

[131] Van der Voo, R., 1993, Paleomagnetism of the Atlantic, Tethys and Iapetus Oceans: Cambridge University Press, Cambridge, 411 p.

[132] van Hinsbergen, D., de Groot, L., van Schaik, S., Spakman, W., Bijl, P., Sluijs, A., Langereis, C., Brinkhuis, H., 2015, A paleolatitude calculator for paleoclimate studies: PLoS ONE, v. 10, 21 p.

[133] Van Schmus, W.R., Hinze, W.J., 1985, The midcontinent rift system: Annual Review of Earth and Planetary Science Letters, v. 13, p. 345–383.

[134] van Wijk, J., Huismans, R., Ter Voorde, M., and Cloetingh, 2001, Melt generation at volcanic continental margins: No need for a mantle plume: Geophysical Research Letters, v. 28, p. 3995–3998.

[135] Veevers, J., 2004, Gondwanaland from 650–500 Ma assembly through 320 Ma merger in Pangea to 185–100 Ma breakup: supercontinental tectonics via stratigraphy and radiometric dating: Earth Science Reviews, v. 68, p. 1–132.

[136] Veikkolainen, T., Biggin, A., Pesonen, L., Evans, D., Jarboe, N., 2017, Advancing Precambrian palaeomagnetism with the PALEOMAGIA and PINT($_{QPI}$) databases: Scientific Data, v. 4, 10 p.

[137] Vervoort, J.D., Wirth, K., Kennedy, B., Sandland, T., Harpp, K.S., 2007, The magmatic evolution of the Midcontinent rift: New geochronologic and geochemical evidence from felsic magmatism: Precambrian Research, v. 157, p. 235–268.

[138] Wall, C., Hanson, R., Schmitz, M., Price, J., Donovan, R., Boro, J., Eschberger, A., Toews, C., 2021, Integrating zircon trace-element geochemistry and high-precision U-Pb zircon geochronology to resolve the timing and petrogenesis of the late Ediacaran–Cambrian Wichita igneous province, Southern Oklahoma Aulacogen: Geology, v. 49, p. 268–272.

[139] Walper, J., 1977, Paleozoic tectonics of the southern margin of North America: Gulf Coast Association of Geological Societies Transactions, v. 27, p. 230–241.

[140] White, D.J., Forsyth, D.A., Aside, I., Carr, S.D., Wu, H., Easton, R.M., Mereu, R.F., 2011, A seismic-based cross-section of the Grenville Orogen in southern Ontario and western Quebec: Canadian Journal of Earth Sciences, v. 37, p. 183–192.

[141] White, R., 1997, Mantle temperature and lithospheric thinning beneath the Midcontinent rift system: Canadian Journal of Earth Sciences, v. 34, p. 464–475.

[142] White, R., McKenzie, D., 1989, Magmatism at rift zones: Journal of Geophysical Research, v. 94, p. 7685–7729.

[143] Whitmeyer, S.J., Karlstrom, K.E., 2007, Tectonic model for the Proterozoic growth of North America: Geosphere, v. 3, p. 220–259.

[144] Withjack, M., Olsen, P., Schlische, R., 1995, Tectonic evolution of the Fundy rift basin, Canada: Evidence of extension and shortening during passive margin development: Tectonics, v. 14, p. 390–405.

[145] Woelk, T.S., Hinze, W.J., 1991, Model of the Midcontinent Rift system in northeastern Kansas: Geology, v. 19, p. 277–280.

[146] Zhang, H., and 11 others, 2016, Distinct crustal structure of the North American Midcontinent Rift from P wave receiver functions: Journal of Geophysical Research, v. 121, p. 8136–8153.

[147] Zietz, I., King, E.R., Geddes, W., Lidiak, E.G., 1966, Crustal study of a continent strip from the Atlantic Ocean to the Rocky Mountains: Geological Society of America Bulletin 77, p. 1427–1448.